AALBORG UNIVERSITY
STUDENT REPORT

Civil Engineering Department
Indoor Environmental and Energy Engineering

MSc Thesis project:

Active Chilled Beams - Air Distribution and Efficiency.

PIV and hot-sphere anemometer measurements, CFD simulations

IE10 Students: Sandijs Vasilevskis 20151294
Bartosz Kozlowski 20151235

Date: 01.06.2017

The School of Engineering and Science
Byggeri og Anlæg
www.byggeri.aau.dk

Title:

Active Chilled Beams - Air Distribution and Efficiency. PIV and hot-sphere anemometer measurements, CFD simulations.

Project period:

September 2016 - June 2017

Authors:

Bartosz Kozlowski
Sandijs Vasilevskis

Supervisors:

Peter V. Nielsen, Professor
Li Liu, Associate Professor
Anders Vorre, Lindab representant

Number of copies: 2
Number of pages: 107
Completed: 01/6/2017

Synopsis:

This paper contains a study and analysis of the draught risk generated by active chilled beam conducted with support of full-scale experiments and CFD simulations. Paper focuses on measuring velocity profiles in beam exit region, gathering velocity distribution patterns for a full-scale test room (the "Cube" facility) and recreation of such conditions with CFD simulations. The "Cube" measurements and simulations are collected as a mid-step to validate and support numerical predictions of Annex 20 room Design Chart.

Preface

This report is created by two IE10 students of the Master's programme Indoor Environmental and Energy Engineering (IEEE) at the School of Civil Engineering at Aalborg University.

The report is a documentation of the experimental work conducted at the laboratory of IEEE and full-scale test room "Cube", and computational fluid dynamics simulations related to these experiments. The main theme of the project is air distribution in the room equipped with an active chilled beam.

The authors would like to express their gratitude to their supervisors - Professor Peter Vilhelm Nielsen and Associate Professor Li Liu for the guidance and assistance. The authors also appreciate the consultancy of Anders Vorre from Lindab regarding the practicalities of use of active chilled beam.

Reading guide

This MSc thesis project document is divided into two parts - main report and appendix. Main report consists of three parts: I Introduction, II Isothermal measurements and III Non-isothermal measurements. Introduction part includes the literature study on active chilled beams, however later in the report another literature study is made regarding the particle image velocimetry measurements.

Throughout the report there will be references to sources which are all listed in the bibliography in the end of the report. The *Harvard-method* is used for references. The source will be referred to as either "[Surname/Organization, Year]" or "Surname/Organization [Year]" and when relevant also with a specific page or section in the source.

Web-pages are listed with author, title, URL and date. Books are listed with author, title, publisher and version, so forth these are available.

The report contains figures and tables which are numbered in relation to the chapter they appear in. Thus, the first figure in chapter 4 will be named figure 4.1, the second figure 4.2 and so on.

In addition to the report there is also an appendix report. Throughout the report there will be references to the appendix, numbered respectively with a letter and a number for parts of the appendix. For example appendix A.1, D.4 and so forth. For references to a whole chapter in the appendix only the letter is used. For example appendix A, B and so forth.

Bartosz Kozlowski　　Sandijs Vasilevskis

Abstract

This project investigates air distribution in an office room with active chilled beam (ACB) system.

Main objective was to evaluate thermal comfort, namely draught risk and air velocity. Therefore Design Chart with regards to air velocity limit of 0,15 m/s was created based on CFD predictions. In order to validate CFD predictions a full-scale test room was used to measure velocity distribution patterns. Based on obtained data, boundary conditions of CFD model were adjusted and best fitting turbulence model selected.

Isothermal measurements were conducted with use of hot-sphere anemometers and PIV system. Non-isothermal experiments (full-scale tests) were done with use of hot-sphere anemometers distributed across the room. Setup of one occupant sitting behind the desk with a computer, PC monitor and desk lamp was used. Four different CFD cases were considered for Annex 20 room: symmetric heat load distribution, asymmetric heat load distribution, personalized ventilation (two active chilled beams, one over each of occupants) and 4 m high room. Each of mentioned cases consisted of two occupants sitting behind the desks with computer, PC monitor and desk lamp located on each of the desks.

Study showed that due to different conditions produced by ACB, it is hard to compare active chilled beam with other previously tested ventilation systems. ACB is unique due to induction phenomenon, where air supplied through the beam consists of two air jets: primary (fresh air) and secondary (induced room air). Due to that, in order to reach indoor air quality limit of 20 l/s of fresh air supply, total volume of diffused air must be over 74 l/s in comparison to 20 l/s for previously tested ventilation systems.

Contents

Part I

Introduction

Introduction 1

Chilled beams were inventeded in Scandinavia in the middle of 80's. Now they are widely used in Europe [Virta et al., 2007] and North America [ASHRAE, 2011]. Active and passive beam (ACB and PCB) systems provide good thermal comfort and energy and space saving advantages with low maintenance requirements [ASHRAE and REHVA, 2015]. Both systems have chilled water circuits and cooling coils that ensure the sensible heat exchange with warm room air. Passive beams operate on the principle of natural convection - warm air moving upwards and cool, more dense air moving downwards. Active chilled beams have an integrated ventilated primary air supply that handles mostly the fresh air requirements and the latent heat loads of the occupied space. Another important characteristic of ACBs is the induction of the room air. The primary air is delivered through special nozzles inside ACB. Due to static nozzle pressure the warm room air is first cooled down as it moves trough the water cooling coil and then entrained and mixed with primary air.

Overall chilled beam systems have specific applications. They are more suitable for places where high sensible heat loads and moderate latent loads, for example, commercial office buildings and schools. These spaces will benefit the most from the water cooling system. They are less suitable for the places like lobby areas, kitchens where high latent heat loads are present and humidity can be hard to control.

Furthermore, many literature sources claim that use of chilled beam systems will decrease the floor height due to smaller ventilation ductwork size. [CIBSE Journal and Tim Dwyer] gives an example that using multi-service chilled beams could save 20 m of height of a 40-storey building, thus increasing the usable building volume for additional 6 floors.

According to ASHRAE [2007] the energy saving potential of chilled beam systems can be achieved in the following ways. Firstly, chilled beam system is considered as a dedicated outdoor air systems (DOAS) where the ventilation air is decoupled from the sensible heat load management. This allows to have lower ventilation air flow rates and thus save on fan energy consumption. Secondly, the chiller for the chilled beam systems operate at higher temperatures (13 °C to 17 °C) than the conventional air-conditioning systems (4 °C to 7 °C), thus a chiller dedicated for chilled beam cooling has lower temperature lift and hence operates at higher efficiency. Also the fact that ACBs induce a lot of warm room air reduces the need for energy-consuming reheating of the cooled air.

Report structure

This project is built around the research of an active chilled beam (ACB) with radial air flow pattern. Main focus thus is the air distribution with regard to thermal comfort parameters, especially air speed and draught, in a single office room with seated occupants.

Figure 1.1 shows the structure of the Master thesis project. It can be seen that the milestone of the project is the Design Chart. Design Chart evaluates draught conditions inside Annex 20 room. It is based on the previous research by Nielsen [2007]. It allows to compare the performance of an ACB with other conventional air distribution systems, such as, mixing ventilation from swirl, slot diffusers, displacement ventilation, textile-based ventilation, and diffuse ceiling ventilation. This can be done because all measurements are made in room with the same dimensions, the Annex 20 Test case B room, with the same heat load distribution and magnitude. *Annex 20: Air Flow Patterns in Buildings* is a project performed by International Energy Agency (IEA) - Energy in Buildings and Communities (EBC) programme.

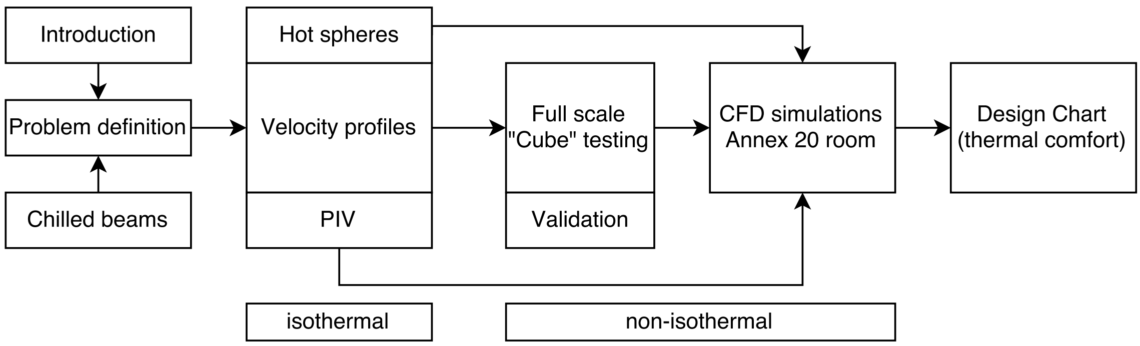

Figure 1.1. Structure of the Master Thesis

After defining the problem, various methods are applied during the process in order to develop and validate ACB model using Computational Fluid Dynamics (CFD). This Master thesis project is divided into 2 parts. Initially, the Lindab ACB is tested at isothermal conditions, where velocity profiles at the wooden board ceiling are measured. Hot-sphere draught probes (anemometers) and Particle Image Velocimetry (PIV) are the methods used to evaluate the air speed. Afterwards the chilled beam is tested in full-scale testing facility, named "Cube" where the air distribution and velocity profiles are evaluated in non-isothermal conditions. "Cube" has different dimensions than the previously mentioned Annex 20 room. Therefore CFD model for Annex 20 room is created in order to create Design Chart as the last step.

Literature review - Chilled Beam Systems 2

In this chapter basic principles of an active and passive chilled beam systems, their application and design procedure is shortly introduced. Induction ratio measurement methods, indoor environmental quality, air distribution pattern, and conclusions regarding these topics is described from the other researches involving active chilled beams.

2.1 Basic principles - chilled beam types

Currently for most of the buildings process of cooling takes place before delivering air to a given space. Newly constructed office building often combine big glazed areas with good insulation properties. Such conditions generate high solar heat gains in addition to internal gains from people, and equipment such as computers, copiers, tvs, fridges etc.

Improvement of indoor climate conditions results in better indoor climate conditions result in high comfort of occupants and as such it results higher efficiency. Chilled beams is a good solution of an issue of overheating in modern office buildings.

Basic difference of active chilled beams (ACBs) from other cooling systems available on the market is cooling inside the chilled beam with use of water pipes instead of cooling with central unit. Temperature of water used for cooling should not drop below 13°C due to condensation issues. Additionally, heat is primarily transferred due to convection instead of radiation [ASHRAE, 2007]. Chilled beams can be divided to two types: passive and active chilled beams (PCB and ACB). Main differences can be observed in figure 2.1. As a result to forced convection, ACBs reach twice as high cooling capacity in comparison to PCBs [ASHRAE, 2007].

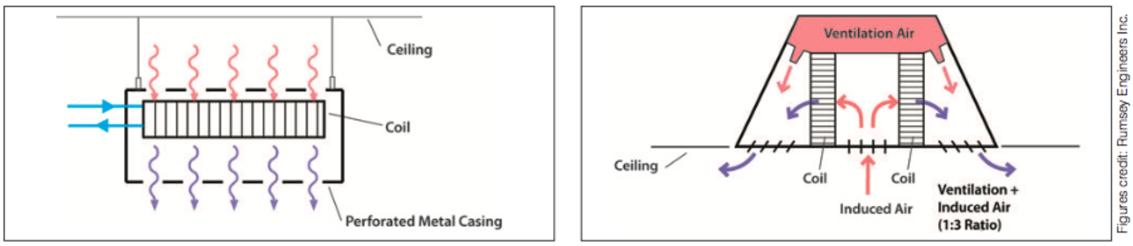

Figure 2.1. ACB vs PCB, [ASHRAE, 2007]

Surface of active chilled beam can be divided into two parts:

- induction area
- diffusion area

Induced warm room air is sucked inside the beam due to static nozzle pressure and mixed with primary ventilation air. Later, the mixture is introduced back into space through diffuser surfaces. Figure 2.2 represents this phenomenon.

Chilled beam can work as both air conditioner and heating unit depending on a certain model selected.

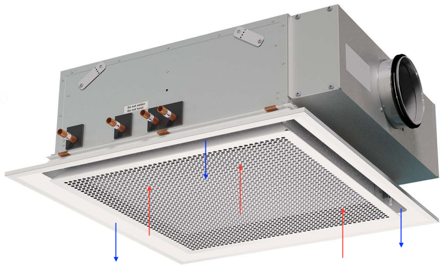

Figure 2.2. Induction area trough perforated plate (red) and diffusing area (blue), Lindab Plexus S60

2.2 Induction ratio measurement methods

Filipsson et al. [2016] summarize the methods used for the evaluation of the induction ratio (IR), 3 measuring methods and their influencing parameters are described.

1. a) *Capacity method* uses an energy balance over the chilled coil. By measuring the flow and the temperature rise of the chilled water, $t_{w,out} - t_{w,in}$, and the temperature drop of the induced air, $t_{room} - t_{ind}$, the flow of induced air can be determined by eq. 2.1.

$$IR = \frac{\dot{m_a} \cdot c_{pw}(t_{w,out} - t_{w,in})}{\dot{m_w} \cdot c_{pa}(t_{room} - t_{ind})} \tag{2.1}$$

1. b) *Modified capacity method*, see eq. 2.2.

$$IR = \frac{t_{mix} - t_p}{t_{room} - t_{mix}} + \frac{\dot{m_a} \cdot c_{pw}(t_{w,out} - t_{w,in})}{\dot{m_w} \cdot c_{pa}(t_{room} - t_{mix})} \tag{2.2}$$

2. *Temperature method* is based on the temperature measurements of the mixed air temperature, t_{mix}, after the induced air, t_{ind}, and primary air, t_p, is mixed. The IR can be calculated by eq. 2.3.

$$IR = \frac{t_p - t_{mix}}{t_{mix} - t_{ind}} \tag{2.3}$$

3. *Velocity method*

   1. Chen et al. [2015] calculated IR by traversing a hot-wire anemometer in a dense grid with 90 measurement points over a quarter of the induction area of ACB. Creating 3D and 2D velocity map from which the induced air flow rate, Q_i, could be calculated.

2. Guan and Wen [2016] used an external hood at the exit region of an ACB. Thus the mixed air at the exit of the hood had much smaller turbulence and its speed became more uniform, which was then be measured with 19 velocity transducer on each side.
3. Filipsson et al. [2016] conclude that the IR is influenced by the chilled water temperature due to buoyant forces. Novel methods of determining the IR are presented and it is concluded that current methods may lead to overestimation.

2.3 Thermal comfort

Dréau et al. [2014] in AAU full-scale testing facility with one thermal manikin compared the energy performance and thermal comfort conditions between active chilled beam and radiant wall. The latter one performed better regarding the heat removal from the room. Both systems met the thermal comfort and local discomfort requirements in the simulated single cell scenario both under steady-state and dynamic conditions.

Mustakallio et al. [2016] evaluated thermal environment in simulated offices with convective and radiant cooling systems under cooling mode. Active chilled beam system with convective cooling was able to provide good thermal environment.

Rhee et al. [2015] evaluated thermal comfort in an open-plan office building conditions with multiple ACB. Air diffusion performance index (ADPI), air velocity for the local discomfort, and vertical air temperature difference was measured. Results proved that ACB system can provide acceptable thermal comfort, even with less air flow rate than other conventional air distribution systems (CAV system with overhead mixing ventilation and an underfloor air distribution (UFAD) system).

2.4 Air distribution

Koskela et al. [2010] evaluated the air distribution in mock-up office with asymmetric workstation layout using chilled beams. It was concluded that the risk of draught was caused by the downfall of colliding inlet jets and large recirculation due to asymmetric heat load distribution.

Cao et al. [2009] and Cao et al. [2010] used PIV measurement system to evaluate airflow pattern next to the exit region of active chilled beam.

Another important area that affect the air distribution in rooms is the ventilation airflow interaction with convection flows from heat sources. Kosonen et al. [2007b] from full-scale measurements with ACBs state that convection flow opposing the supplied flow should be avoided because it can cause wall jet detachment and cause the cool ventilation air to entry the occupied zone. Kosonen et al. [2007a] with the physical measurements and the performed smoke visualization investigated various heat load strengths in a room with length-wise installed ACB. Results showed that the flow from the ACBs was not disturbed with the heat load of $56\,\mathrm{W/m^2}$. However higher loads depicted significant impact of the convective flow and thus increased the draught risk and local velocities in the occupied zone.

One of the Mustakallio et al. [2016] conclusions from full-scale measurements with various chilled beam system arrangements was that the heat load distribution affect the airflow pattern significantly. Research reports that due to the interaction of the strong upward buoyancy flow generated by the heat sources near the window the supplied ventilation air was pushed toward the opposite wall.

2.5 Predictions with CFD

In order to utilize computational fluid dynamic (CFD) simulation advantages it is important to compare the developed chilled beam models with measured results. Modelling of the secondary airflow induced in the ACB is one of difficulties that has to be resolved. Summary of the researches that try to simulate indoor climate conditions in rooms with ACB is shortly introduced.

2.5.1 CFD models for ACB

Guan and Wen [2016] created geometrically detailed ACB terminal unit including nozzles, see figure 2.3. The pressure drop, $\triangle P_{loss}$, eq. 2.4, across the cooling grilles and water circuit was evaluated by means of separate simulation which estimated the loss coefficient, f, see figure 2.4 and eq. 2.5. In this way the pressure drop across ACB and grille is only calculated once, instead of in every simulation.

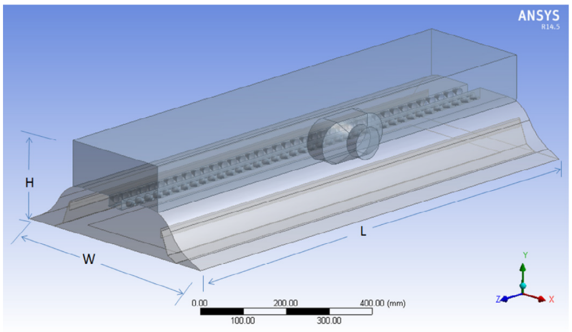

Figure 2.3. CFD model, Guan and Wen [2016]

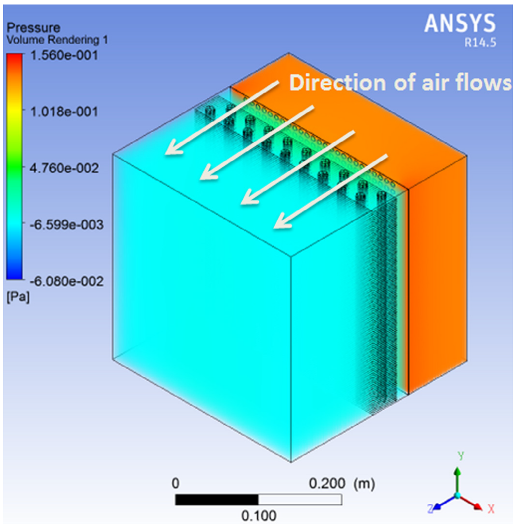

Figure 2.4. CFD model, Guan and Wen [2016]

Guan and Wen [2016] the turbulence of the flow is modelled by the standard $k - \epsilon$ model. Boundary conditions of primary inlet air defined by the pressure, inlet to room and mixing chamber by the mass-flow including the f. Comparing with air velocity transducer readings readings, the deviation of CFD results was kept within +/- 5%.

$$\triangle P_{loss} = \frac{1}{2} f \rho U_n^2 \tag{2.4}$$

$$f = \frac{2(\widehat{P_{out}} - \widehat{P_{in}})}{\rho \widehat{U_n}} \tag{2.5}$$

2.5.2 Turbulence models

REHVA guidebook by Müller et al. [2013] mentions that the use of Reynolds averaged Navier-Stokes (RANS) in CFD modelling fail to predict the interaction of thermal plumes and ventilation air. Therefore for each research it is important to choose the most suitable turbulence model.

Sadrizadeh and Holmberg [2006] tested 9 turbulence models by CFD with a focus on accuracy and computing cost. These models cover RANS modelling, including both turbulent-viscosity and Reynolds-stress. Their experimental set-up consisted of thermal manikin in a box-shaped wind tunnel. From the results RNG $k-\epsilon$ and $V2F$ proved to have the best performance. Also it was concluded that the Realizable $k-\epsilon$ model is the most robust and with easy convergence; however, convergence didn't not equate with accuracy.

Zhang et al. [2007] compared 8 turbulence models in enclosed environments with experimental data. Similarly, among the RANS models studied, the RNG $k-\epsilon$ and $V2F$ turbulence models performed the best overall in terms of accuracy, computing efficiency, and robustness. The $k-\omega$ SST model did improve the accuracy in a strong buoyant flow scenario without significantly increasing computing time, compared to the RNG model.

In chapter 7. Computational Fluid Dynamics the selection of the turbulence model is made.

2.6 Summary of literature study

2.6.1 IR measurement methods

In this project the *velocity method* was regarded as the most suitable method due to available equipment, mostly omni-directional anemometers. Also the literature source study shown that this method was applied in more researches than the other two methods. Also both *capacity method* and *temperature method* suffer from difficulty to measure induced air temperature as it is non-uniform and varies both along and across the coil. Induced air also is mixed with the primary air very soon after the cooling coil.

2.6.2 Thermal comfort

Thermal environment of the room is influenced by the factors like metabolic rate, clothing insulation, air temperature, mean radiant temperature, air speed and relative humidity.

From the literature analysis of the thermal comfort in rooms with ACBs, it can be summarized that the general thermal comfort criteria defined by ASHRAE Standard 55 and EN 7730 are fulfilled in rooms with active chilled beam systems.

However, some of the researches indicate possible problems with local discomfort, specially draught risk that is caused by high air movement generated by ACB terminal units. Therefore in this project the air movement is investigated in more detail then other thermal comfort criteria.

2.6.3 Air distribution

From this review the regions of higher draught risk in rooms with active chilled beams is estimated. The previous studies show that under the ACB, were the induction of room air occur, there is a higher risk of local discomfort due to higher air velocities.

Regarding the heat load distribution in room with chilled beams installed, it is important to locate the heat sources evenly distributed because asymmetric layout may cause opposing upward buoyancy flow that deflects the ventilation air into the occupied zone, or large recirculation that creates draught risk at the ankle level. CFD simulations regarding the heat load and air distribution for this project are presented in chapter 8. Heat load distribution.

2.6.4 CFD models

Following, review of the available CFD model descriptions is summarized. During the recent years computational power is increasing significantly and the use of CFD predictions in ventilation system design is getting more common, therefore detailed geometries of diffuser terminals are modelled.

The perforated part of chilled beam, the induction area, in many cases is simplified, for example by adding pressure loss.

Exit region of the terminal unit determines the airflow distribution and therefore has to be modelled precisely.

RNG k-ϵ is the most commonly used turbulence model in reviewed research papers.

2.7 Active Chilled Beams - Lindab

In general ACBs are operating based on the induction principle. Ventilation air with a certain dynamic pressure is supplied through special nozzles, which creates a low static pressure. This low pressure causes room air to be induced towards the cooling battery and afterwards mixed with the primary air.

2.7.1 System description - Lindab Plexus 60

In this project the experiments are performed with ACB terminal device from Lindab, model Plexus 60, Type S (standard), see figure 2.5. Plexus provides radial, 360 ° air spread pattern according to [Lindab, a]. It results in short air throws and indoor environment without draught. Plexus fits to all types of false 600x600 ceilings. It can be used for both cooling, heating and ventilation. In this project, however, the use is limited to the cooling. Cooling capacity of Plexus 60 will vary with respect to room, water, and air temperature, air and water flow, and induction ratio.

Figure 2.5. ACB - Plexus 60, Type S, horizontal air connection. [Lindab, a]

The flexibility regarding the air volume for Plexus 60 can be adjusted by ordering 4 different types of beams: S (standard), L(low), M(medium) and H(high). Each type has different air volume operating range. Type M and H gives higher air volumes. Ventilation with variable air volume of Type S is Lindab's standard configuration that covers most common demands. Plexus ACB model has the perforation pattern Dotx2 50%, see figure 2.5.

The researched ACB is provided with standard Ø12 mm water and Ø125 vertical air connection. See figure 2.6 for the geometry of the Plexus 60 chilled beam.

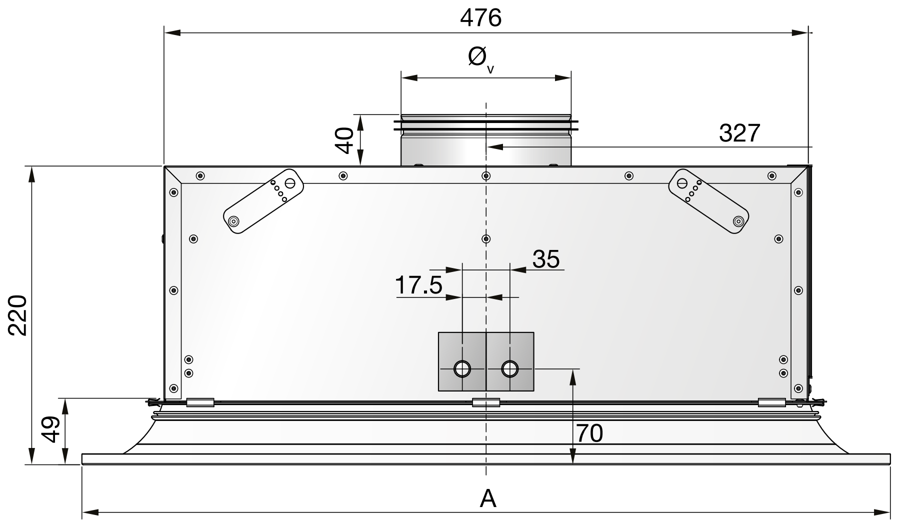

Figure 2.6. Dimensions of Plexus 60 (cooling model). Vertical air connection. [Lindab, a]

2.7.2 Induction ratio

Lindab's Plexus chilled beam is based on the induction principle. Main difference from conventional air diffusers is that ACB are capable of inducing the room air. The induced air is thus cooled down by the water flow in the cooling unit. Further it is mixed with the primary ventilation air.

The efficiency of the ACB can be characterized by the amount of the room air that is induced and thus also cooled down in the mixing chamber. This entrainment ratio (ER) or efficiency of the system can be thus described by eq. 2.6.
Induction ratio (IR) of an ACB is the mixed air volume or mass flow rate divided by the primary air flow rate. Mixed air flow rate is, $Q_3 = Q_1 + Q_2$. Then IR can be calculated with the following equation, eq. 2.7.

$$ER = \frac{Q_2}{Q_1} \tag{2.6}$$

$$IR = \frac{Q_3}{Q_1} = \frac{Q_1 + Q_2}{Q_1} \tag{2.7}$$

where

Q_1	Primary, supply air flow rate	m^3/h
Q_2	Secondary, induced room air flow rate	m^3/h

The more of the warm indoor air is entrained and cooled down, the more efficient the use of the cooling power is achieved. Thus IR/ER is one of the parameters that evaluates performance of an ACB. The volume of the induced room indoor air is 4 to 5 times that of the ventilation air. [Lindab, a]

Static nozzle pressure (SNP) is important factor that determines how much of the room air is entrained into the chilled beam. Figures 2.7 and 2.8 show that by increasing the SNP the secondary airflow rate, Q_2, and ER are increasing.

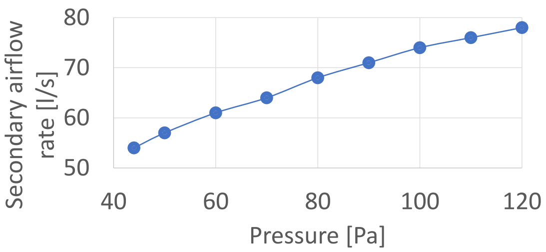

Figure 2.7. Secondary airflow rate versus static nozzle pressure.

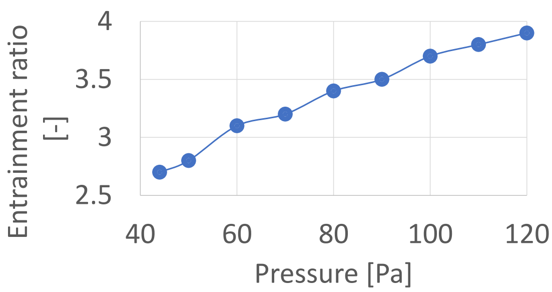

Figure 2.8. Entrainment ratio versus static nozzle pressure.

2.7.3 Cooling capacity

In this research the total cooling demand in s single-cell office room is 240 W. It is combined from PC, desktop, table lamp and a thermal manikin.

The cooling capacity of Plexus 60 ACB is a combined effect of:

- Cooling capacity air, Pa
- Cooling capacity water, Pw

Primary supply air generally is supplied with lower temperature, cooled down by the cooling coil in the ventilation system. Cooling capacity of ventilation air, Pa, of Plexus can be calculated by the eq. 2.8:

$$P_a = q_{ma} \cdot c_{pa} \cdot \triangle t_{ra} \tag{2.8}$$

where

q_{ma}	air mass flow rate	kg/s
c_{pa}	specific heat capacity air	1,004 kJ/kgK
$\triangle t_{ra}$	Temp. diff., room air and primary air	K

The rest of cooling capacity, which is not covered by the ventilation air, is provided by the water cooling circuit. Certain water flow is recommended depending on the pipe size and required cooling capacity. Exceeding the nominal flow-rate, q_{wnom}, in the water circuit will not provide significant cooling capacity gains. Therefore the water flow-rates are kept within the range presented in table 2.1.

Flow-rate	[l/s]	[m^3/h]
Minimal, q_{wmin}	0,025	0,090
Nominal, q_{wnom}	0,038	0,137

Table 2.1. Recommended minimal and nominal water flow in 12 mm pipe for Plexus 60 [Lindab, a]

In order to calculate Pw the temperature difference between room air, t_r, and mean water temperature, $\triangle t_w$, must be registered. The value is denoted as $\triangle t_w$, see eq. 2.9 for the calculation:

$$\triangle t_{rw} = t_r - \triangle t_w = t_r - (t_{wi} + t_{wo})/2 \tag{2.9}$$

where

t_{wi}	water inlet temp.	°C
t_{wo}	water outlet temp.	°C

Temperature difference in water circuit, $\triangle t_w$, is the first indicator of the cooling system efficiency. Cooling capacity by water flow, Pw, is estimated by eq. 2.10:

$$P_w = P_t \cdot \triangle t_{rw} \cdot \epsilon_{\triangle t_{rw}} \cdot \epsilon_{qw} \tag{2.10}$$

where

P_t	Specific cooling capacity	W/K
$\epsilon_{\triangle t_{rw}}$	capacity correction factor for temperature	–
ϵ_{qw}	capacity correction factor for water flow	–

Specific cooling capacity depending on the static pressure and primary air flow rate, $\epsilon_{\triangle t_{rw}}$, and ϵ_{qw} can be found in the manual [Lindab, a].

Water-borne calculator at from Lindab QST, [Lindab, c], can be used to calculate cooling capacity of the Plexus S60 chilled beam. Cooling capacity will vary according to the room air temperature, primary air and water flow rate and temperature. The cooling capacity thus is also adjustable to an extent. Figure 2.9 shows the relationship of ER versus total cooling capacity. These results are made for the ventilation with Q_1 of 20 l/s. It shows that the cooling capacity at this specific airflow rate can be adjusted from 460 W to 510 W just by varying ER (via changing SNP from 40 Pa to 120 Pa).

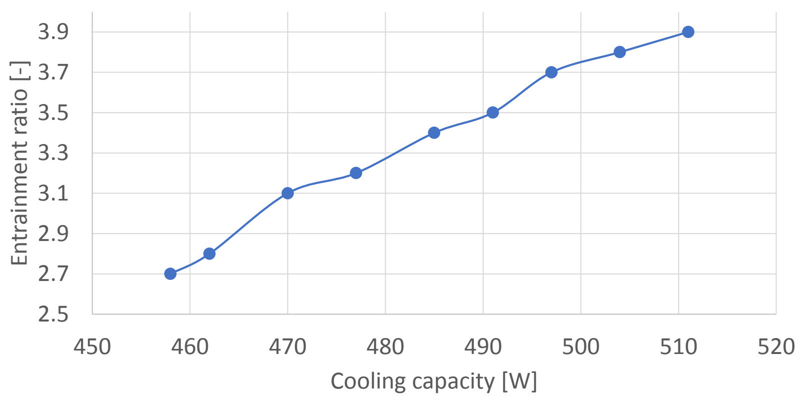

Figure 2.9. Entrainment ratio versus cooling capacity.

An example from [Lindab, c] is presented in appendix A. Total cooling capacity of Plexus S60 is 293 W, from which cooling with water consist of 245 W and with air - 48 W. Thus this ACB model with such settings (nominal water flow, t_{ra} = 22,0 °C, t_{pa} = 18,0 °C, and t_w = 14,0 °C), will be able to satisfy the cooling demand of 240 W in an investigated single-cell scenario.

2.7.4 Air distribution - JetCone adjustment system

The air volume can be easily adjusted with Lindab's JetCone system. JetCone allows adjusting air diffusion, air volume and air pressure. It gives also a flexibility to adjust the throw length at each side of the ACB. This allows to create an asymmetrical distribution pattern and direct air in the desired direction.

Figure 2.10 and figure 2.11 shows the jet cones. In each corner of ACB there is an adjustment pin that can be set to a specific position from 0 to 9.

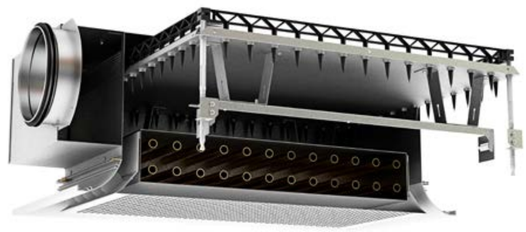

Figure 2.10. Plexus S60 JetCone adjustment system. [Lindab, a]

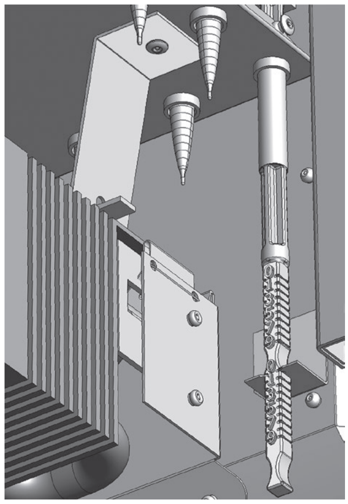

Figure 2.11. Plexus S60 JetCone adjustment pin. Position 0. [Lindab, b]

Position of JetCone adjustment pins allows to easily adjust necessary volume flow rate. Therefore Plexus S60 ACB can be adjusted for various occupation scenarios. In figure 2.12 it is shown how to read the actual flow rate after the static nozzle pressure (SNP) is

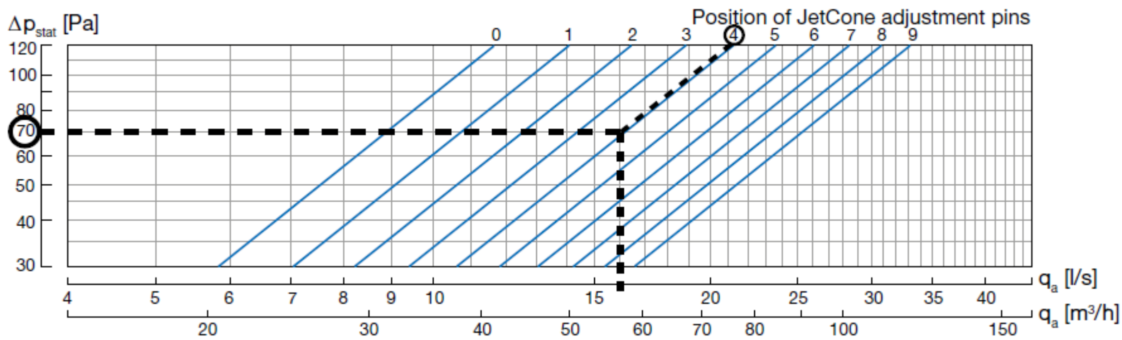

Figure 2.12. JetCone Adjustment diagram for airflow rate and SNP. Plexus S60. [Lindab, b]

It can be seen that each JetCone position is limited within a specific range of volumetric flow-rate. For example, JetCones in pos.: 4-4-4-4 will have flow-rate from 11 l/s to 21 l/s. Overall Plexus S60 model ACB can be adjusted approximately from 5 l/s to 32 l/s by changing JetCones from pos. 0 to 9.

Problem definition 3

In this chapter the research objective and the procedure of reaching it is introduced. Moreover, the Design Chart method to evaluate thermal comfort and compare different ventilation systems is described.

3.1 Design Chart

Design Chart is a tool developed by [Nielsen, 2007]. Based on it user may compare various ventilation systems and select most suitable unit that will fulfill requirements.

Design Chart is based on two variables ΔT (difference between inlet and outlet temperatures) and q_0 (allowable flow rate in the room). Sketch of Design Chart is shown in figure 3.1.

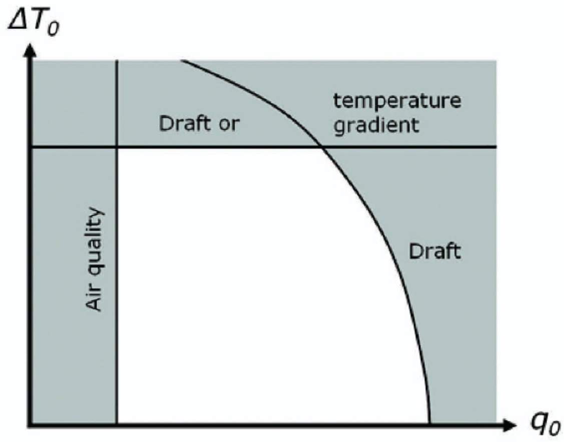

Figure 3.1. Sketch of Design Chart with included IAQ limitation. [Nielsen, 2007, figure 2]

From figure 3.1 it may be observed that the chart is divided into two areas: white (zone of thermal comfort) and grey (zone of draft and/or insufficient ventilation rate). White area illustrates draft-free conditions with conservation of Indoor Air Quality (IAQ) requirements. Any conditions within the white area of the graph should produce draft-free and air cleanliness-satisfactory conditions within the room's occupied zone.

Design limitations used for developing the Design Chart were as follows: maximum air velocity within occupied zone: 0,15 m/s, maximum vertical gradient: 2.5 K, minimum flow rate per person in the room: 10 l/s.

Figure 3.2 shows previous experimental research on various ventilation systems with constant heat load conducted by [Nielsen, 2007]. Design Chart show capability of different ventilation systems to remove heat, conserving comfort conditions within occupied zone. In presented graph the IAQ limit is set to 20 l/s (72 m^3/h).

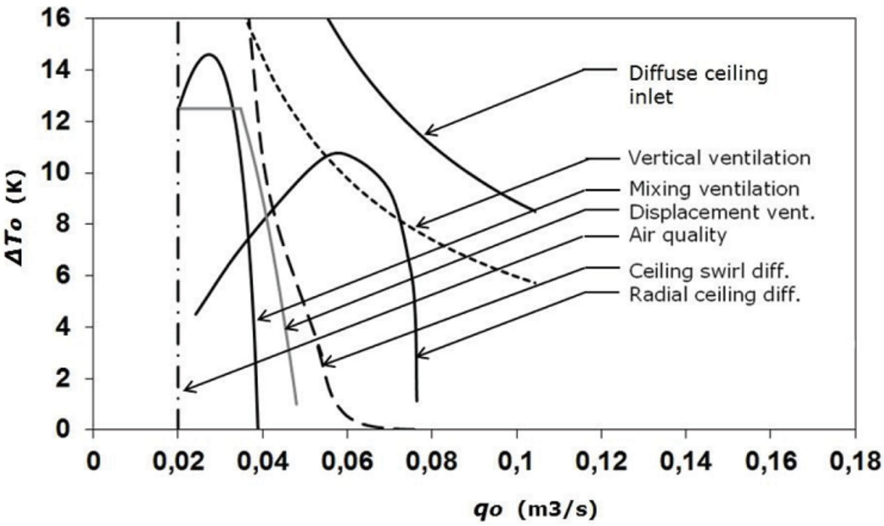

Figure 3.2. Design Chart for different ventilation systems. [Nielsen, 2007].

3.2 Problem definition

After literature review of previous researches regarding thermal comfort in the rooms with ACBs. Possible research areas that can influence the performance and efficiency of ACB are summarized:

- induction ratio - influence on the cooling efficiency, air distribution pattern
- cooling Capacity - air and water circuit - energy efficiency
- jetCone position - influence on air distribution pattern
- air movement and thermal comfort in a single-cell room - various heat load distributions

In this project, after evaluating the available test facilities, describing active chilled beams, and the previous research, the research aims are limited to few. The following thesis objectives are selected in this order:

- determine velocity profiles of an active chilled beam
- develop and validate CFD-model for an active chilled beam system
- evaluate thermal comfort in a full-scale test room
- create Design Chart for Annex 20 room based on the full-scale and CFD results, compare results with [Nielsen, 2007]
- investigate chilled beam performance with various heat load distributions

3.3 Procedure

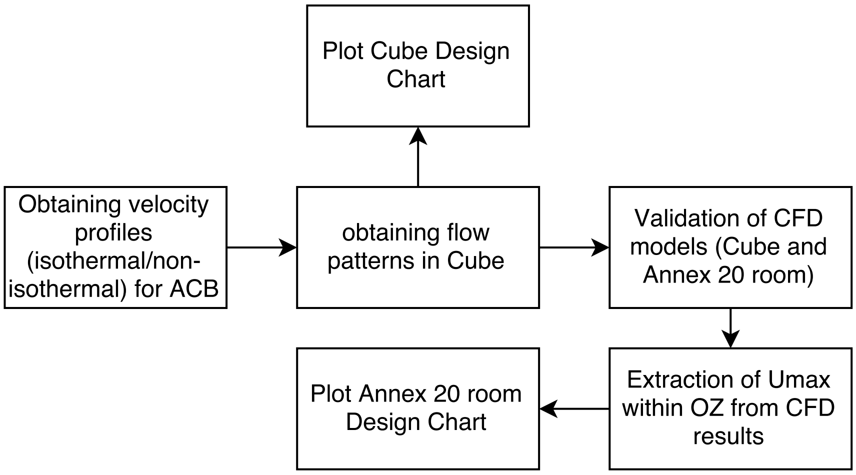

Figure 3.3. Procedure of obtaining Design Chart

Obtaining final Design Chart consisted of few steps. First, velocity profiles in isothermal conditions were measured. After acquiring results for beam-close region (PIV and hot-sphere anemometer measurements), flow patterns in test room, the "Cube" were obtained.

"Cube" setup consisted of one centrally positioned manikin sitting behind the desk with computer, PC and lamp. "Cube" measurements were later used for CFD validation of beam and turbulence models.

After validation, Annex 20 room CFD simulations were conducted. Annex 20 room consists of two manikins sitting behind two desks with one PC, monitor and a lamp at each of the desks.

Obtained data was later statistically treated (maximum velocities within head and feet heights in region close to manikin were extracted) and used for Design Chart creation. Additionally, secondary Design Chart for "Cube" was created at the same time.

Part II

Isothermal measurements

In this part, the velocity profiles at the exit region of an active chilled beam (ACB) are measured. Velocity magnitudes are estimated with hot-sphere anemometers. Particle Image Velocimetry (PIV) is used to validate the whole flow field at different flow rates. In addition to the experiment, a CFD simulation of the experiment will be presented.

Velocity profile measurements 4

In this chapter velocity profiles of active chilled beam are measured in isothermal conditions. The measurement method and results are presented.

4.1 Isothermal measurements

It is important to know air distribution generated by the active chilled beam terminal. Airflow jet development was analysed using Dantec hot-sphere draught probes. These probes can measure omnidirectional air speed, turbulence and temperature. Isothermal measurements were conducted at the false wooden ceiling with ACB reversed.

Main aim of both isothermal and non-isothermal velocity profile measurements is validation of CFD exit region model.

4.1.1 System description

Velocity profile measurements are conducted at fixed distances from beam (0, 15, 30 cm for middle position, 0, 15 cm for corner position, see figure 4.2). Measurements were made with JetCones set at position 9 in all 4 corners.

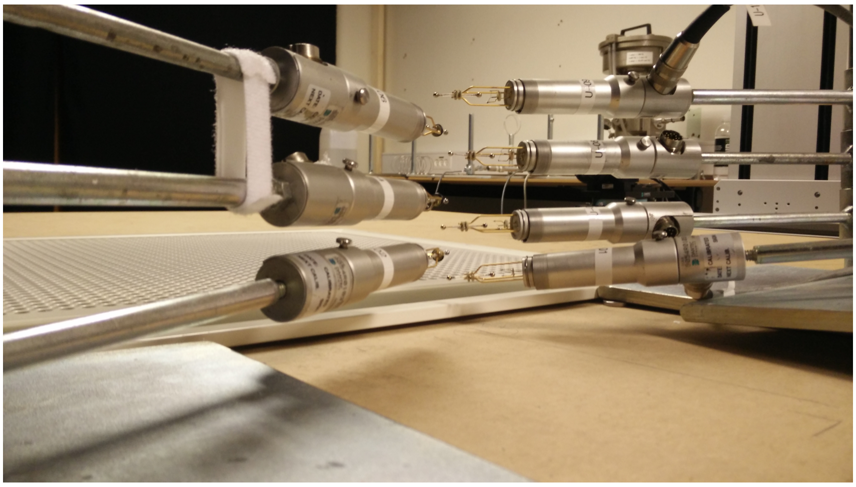

Figure 4.1. Example anemometer setup layout for the velocity profile measurements.

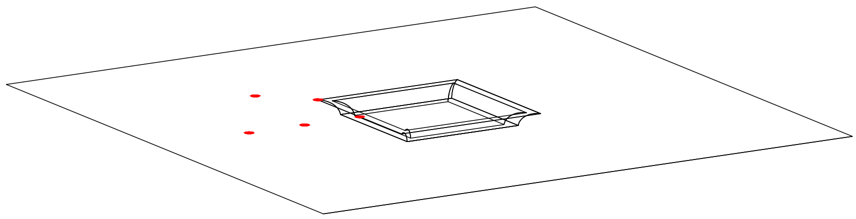

Figure 4.2. Measurement positions distribution.

Beam was supplied by fan coupled with power transducer. Measurements were conducted in range of 15 l/s to 40 l/s with 5 l/s step. Setup was equipped with orifice for pressure drop (and flowrate) readings as well as pipe stuffed with plastic straws to limit turbulence.

4.1.2 Resultant velocity profiles

Obtained velocity profiles are presented in figures 4.3 - 4.7. Main conclusion that can be drawn from the graphs is that velocity profile shape does not change with velocity. All profiles conserve identical form with only visible magnitude change. Thus Plexus 60 has radial air distribution pattern.

Measurements at the center of the ACB:

Maximum air velocity is obtained at 20 mm to 40 mm height. Velocity profile show a decay in the magnitudes as the measurement position is moved further from the beam exit. Maximum air speed decreases approx. 2 times comparing the value next to the beam with value at 15 cm distance. For example, from 3,0 m/s to 1,4 m/s at flow rate of 40 l/s.

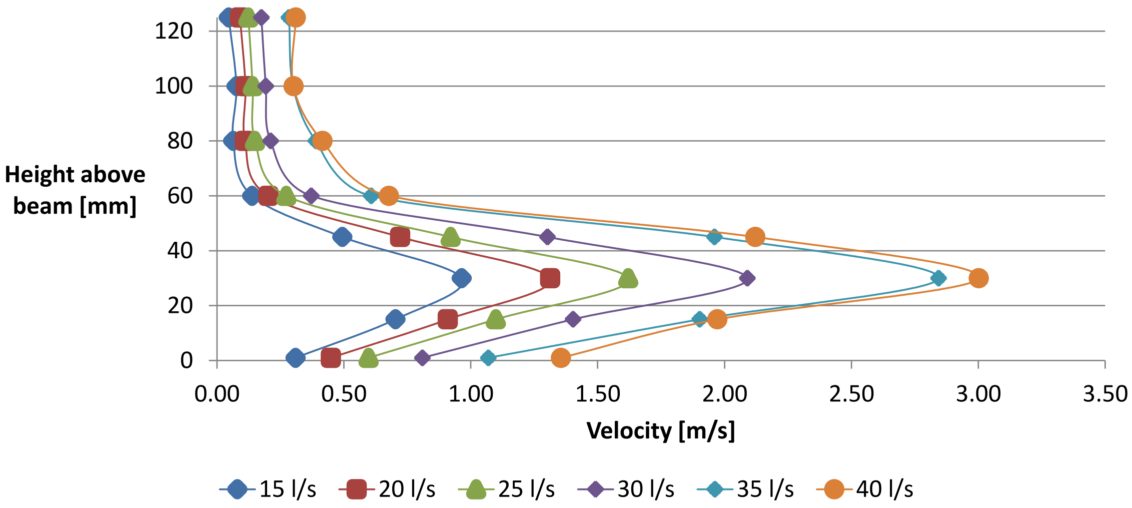

Figure 4.3. Velocity profile, 0 cm distance from the beam.

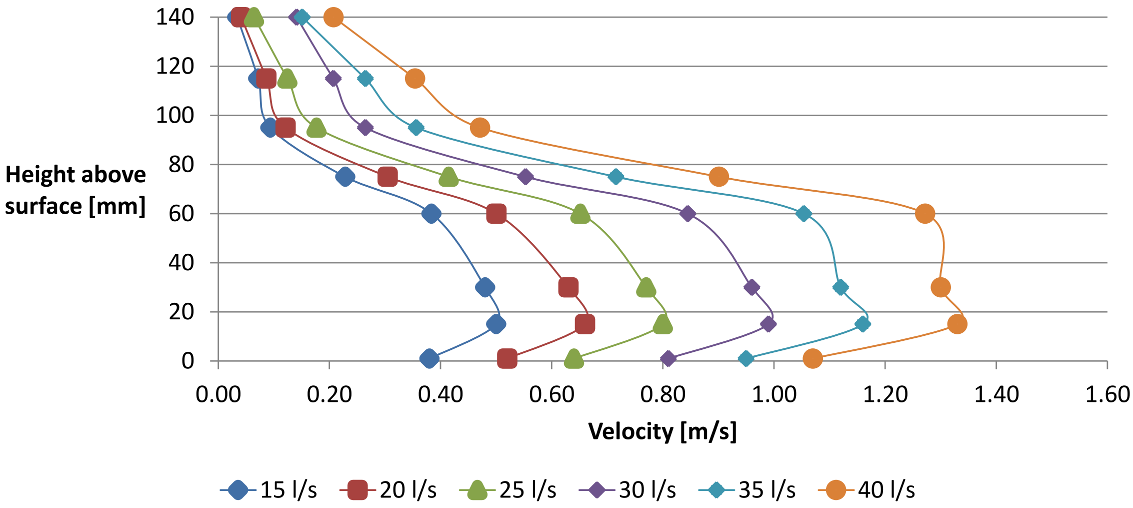

Figure 4.4. Velocity profile, 15 cm distance from the beam.

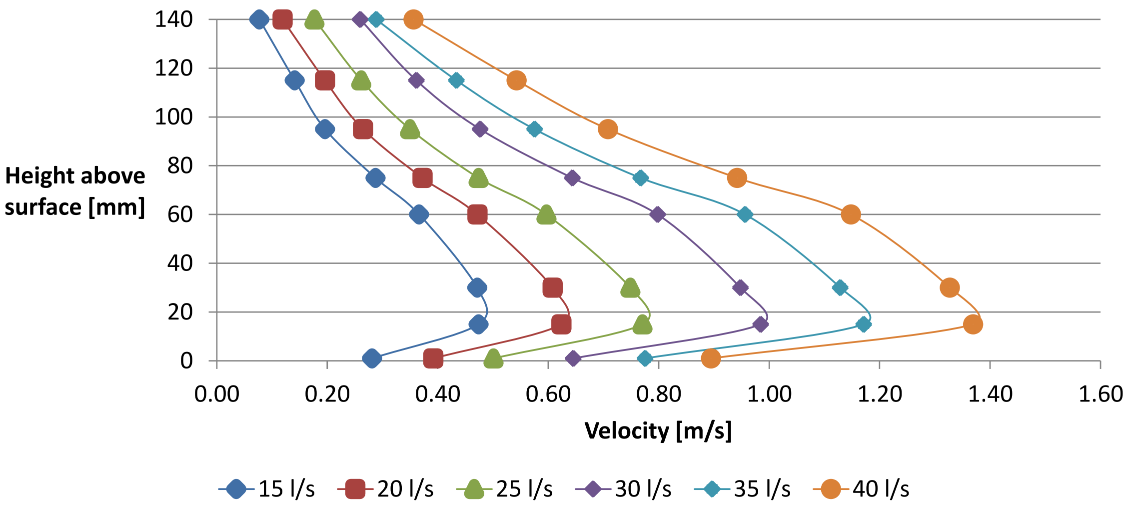

Figure 4.5. Velocity profile, 30 cm distance from the beam.

Measurements at the corner of the ACB:

Maximum air speed is obtained at 20 mm height. Maximum air speed decreases approx. 2 times comparing the value next to the beam with value at 15 cm distance. For example, from 2,6 m/s to 1,3 m/s at flow rate of 40 l/s.

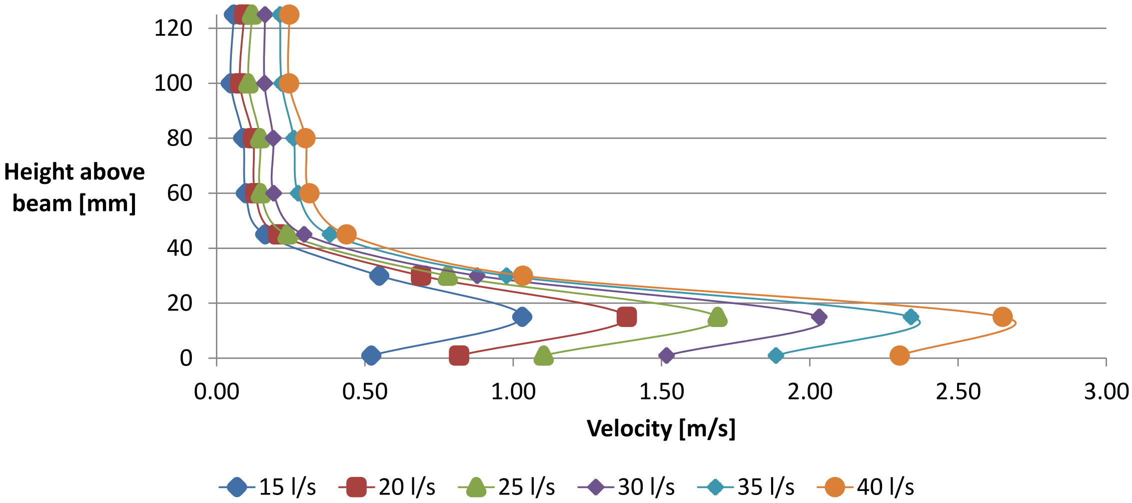

Figure 4.6. Velocity profile, 0 cm distance from the beam.

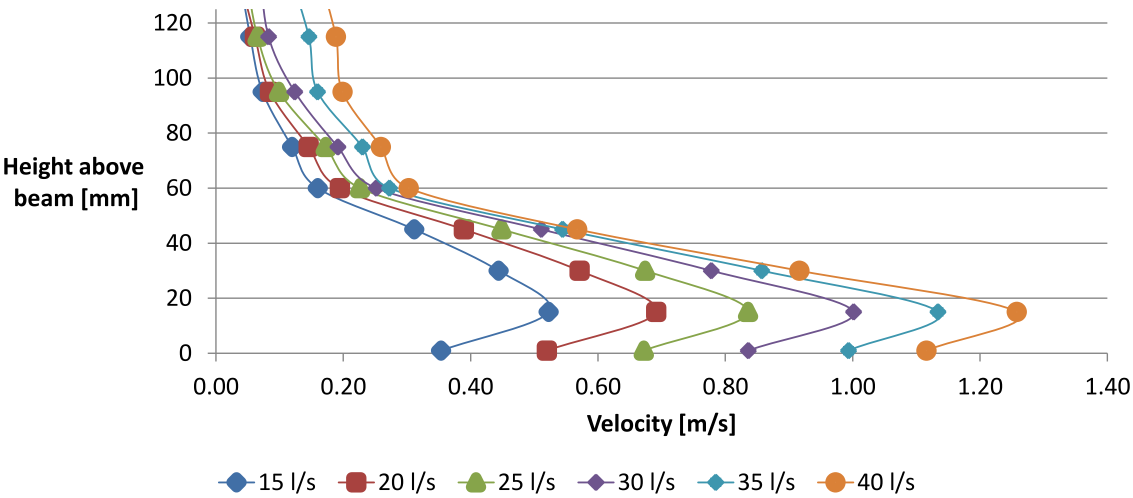

Figure 4.7. Velocity profile, 15 cm distance from the beam.

Velocity in both corner and middle points present very similar magnitudes at the same distances - with a bit lower values in the corner position. It means that jet generated by Lindab Plexus 60 creates radial air distribution.

4.2 Induction rate

Induction rate is a volume of air being inducted into the beam. Sum of primary air and secondary (inducted) air volumes are later supplied to the room. As inducted air volume mainly depends on primary air supply and is it's relation to primary air is non-linear, it can be determined experimentally. LindQST (Annex A) has been used as as source of data for induction rate estimation.

4.3 Summary of Hot-sphere anemometer measurements

Results from the HSA measurements are used further to analyse exit region of the CFD-model simulations. See chapter 7 and figure 7.10 on page 54 for the visualization.

Velocity magnitudes close to the chilled beam outlet by the CFD model were estimated to be higher than the ones measured with the hot-sphere draught probes with the same volumetric flow-rate.

It was decided that later for the full-scale CFD model the inlet velocity of a beam will be adjusted to match the measured velocity magnitudes further away from the

Particle Image Velocimetry 5

In this chapter basic the principles of particle image velocimetry are introduced. Previous research results and concerns regarding accurate measurements are shortly reviewed. Measurement setup is described, and results are presented.

5.1 Background - basic principles

Particle Image Velocimetry (PIV) is a measuring technique that can determine whole-flow field instantaneously. Other measurement methods like hot-sphere anemometers, Laser-Doppler Anemometry (LDA) can measure the velocity at specific locations and thus cannot reflect air distribution in a cross-section simultaneously. PIV air velocity vector measurements can be compared with CFD predictions in order to validate the developed active chilled beam CFD-models.

PIV velocity vector, $\overline{V}$, measurements are based on photo imaging of a particle motion - displacement, $\overline{X}$, over a known time interval - time between two laser pulses, $\triangle t$, see eq. 5.1:

$$\overline{V} = \frac{\triangle \overline{X}}{\triangle t} \tag{5.1}$$

Basic principles of a PIV measurement process are represented in a figure 5.5. Two particle image frames are registered with digital CCD-cameras. The smoke particles are illuminated by the light sheet of a double-pulsed laser with known $\triangle t$. Image is subdivided into small parts called interrogation areas (IA). IA's from each image frame are analysed by applying cross-correlation procedure which results in a velocity vector map.

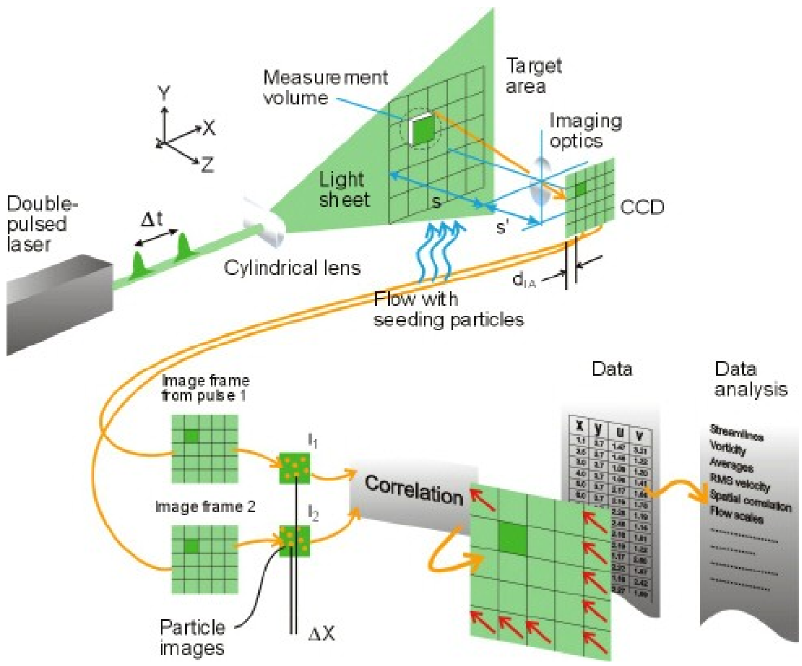

Figure 5.1. PIV principles. [DantecDynamics]

5.1.1 Digital Image Recording

Most popular digital cameras used for PIV measurements are based on a charge-coupled device (CCD) sensor technology with high resolution and high sensitivity. Frame rates of CCD-imaging can match the high pulse energies and repetition rates of flash lamp pumped double oscillator Nd:YAG-lasers. This allows to make two images with the same camera with few microseconds difference. Another advantage of using CCD technology is the increased spatial resolution (Markus Raffel and Christian E.Willert and Steve T.Wereley and Jürgen Kompenhans [2007]).

In general, CCD is an electronic sensor that can convert illuminated light from the moving particles into electric charge. CCD sensor technology is shifting between exposed and non-exposed pixels, in other words - first and second frame. In order to capture the second frame, first the accumulated charge from the first frame is shifted down into the masked-off area, where it cannot be further exposed to light. This electric charge from the first frame has to be also transferred into the storage area. Whereas further it is converted to the voltage.

Besides digital cameras and laser, the crucial element of a PIV system is the the synchronizer or timer box. It is the external link that triggers the laser and digital camera in order to capture qualitative PIV image. Timing diagram is presented in figure 5.2. It shows a way how the particles must be illuminated in order to produce single exposed PIV images.

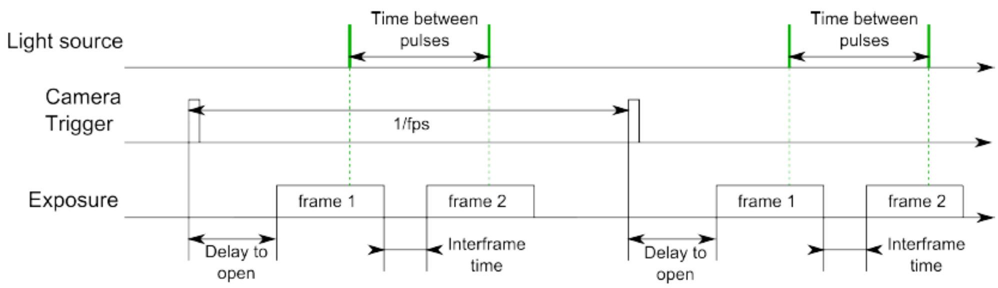

Figure 5.2. Timing diagrams with laser pulsing and camera frame rate. [Dynamics, 2015]

5.1.2 Cross-Correlation

After acquiring two subsequent images with digital camera, this data is post-processed using correlation procedure to estimate the velocity vector map. Auto-correlation is used when a single frame mode is used to acquire PIV images and cross-correlation for the double-frame mode. Data processing procedure using Fast Fourier transform (FFT) algorithm is shown in figure 5.3.

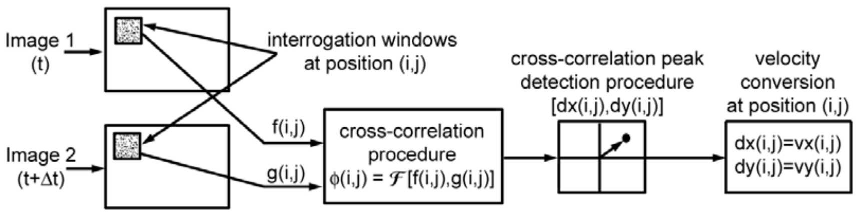

Figure 5.3. Cross-correlation data processing procedure using FFT algorithm.

The two subsequent IA are cross-correlated. The correlation produces a signal peak, identifying the common particle displacement, $\overline{X}$. An accurate measure of $\overline{X}$ - and thus also the velocity - is achieved with sub-pixel interpolation. Normalized cross-correlation map of a given IA within the image can be seen in figure 5.4.

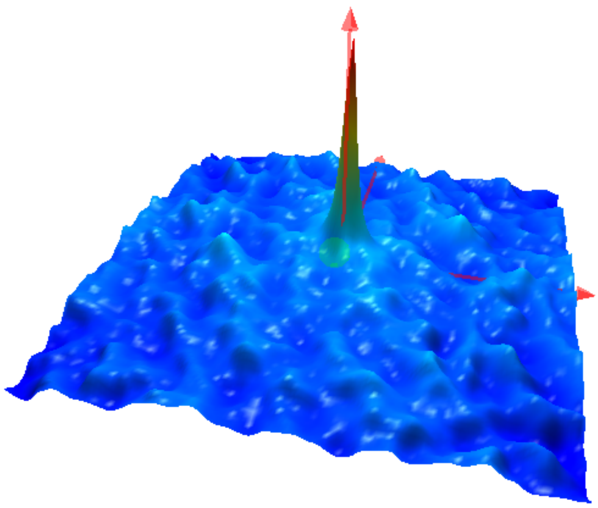

Figure 5.4. Normalized cross-correlation map. [Dynamics, 2015]

Regarding IA, there are some limitations for correct velocity evaluation. With regards to velocity gradient, see eq. 5.2, it is important to evaluate the image magnification, $\frac{s}{s'}$ and length of IA, d_{IA}. Therefore velocity gradient with the IA has to be smaller than 5%.

Also loss of velocity information can be attributed to the fact that the particle can move outside the second image frame before the $\triangle t$ has finished. Therefore it is important to limit how big the $\overline{X}$ is compared to the IA size, d_{IA}, eq. 5.3, the limitation here is 25%.

$$\frac{\frac{s}{s'} \cdot \mid V_{max} - V_{min} \mid_{IA} \cdot \triangle t}{d_{IA}} < 5\% \quad (5.2)$$

$$\frac{\frac{s}{s'} \cdot V \cdot \triangle t}{d_{IA}} < 25\% \quad (5.3)$$

5.2 Background - previous research

5.2.1 Applications

This section summarizes the previous applications of PIV measurements. Cao et al. [2013] have reviewed the PIV measurements in enclosed environment testing facilities. They summarize that PIV method is more used for small-scale models and not so much in large-scale testing facilities. The most fitting work regarding this project is performed by Cao et al. [2009] and Cao et al. [2010]. Both research papers describe the exit region of an active chilled beam in a full-scale testing chamber. For example, Cao et al. [2009] results show a clear structure of the turbulent attached plane jet in the entrainment process after exiting the chilled beam. The study proves that the jet will attach to the ceiling and become fully turbulent very close to the ACB exit region.

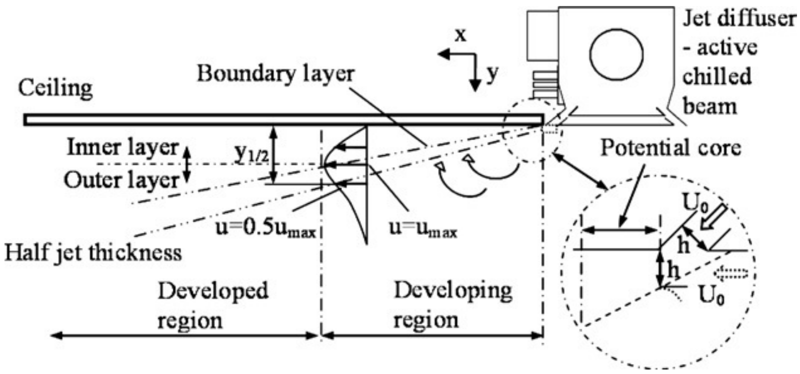

Figure 5.5. Schematics of jet velocity field. [Cao et al., 2010]

Sattari [2015] firstly used PIV measurements to investigate effects of pulsating ventilation, namely the effects of air mixing and stagnation regions, in a small-scale model. Second experiment included analysis of an air flow over a wall-mounted radiator in a full-scale room model. The latter experiment was of interest because the author used the same particle seeding technique and fog generating liquid as in this project.

5.2.2 PIV measurements - accuracy and uncertainties

PIV measurements are rather complex and involve many difficulties because there are many parameters that can be influenced and adjusted by the operator. To mention some: the time between laser pulses, digital camera configuration like lens number, particle seeding technique and density, post-processing settings like interrogation window size, and so on.

Sandberg [2007] review the whole-flow field measuring methods in ventilated rooms. Author mentions that PIV method is dependant on the uncertainty in particle displacement and the uncertainty in the 'time between pulses'. However the uncertainty in 'time between pulses' can be neglected due to low air velocities in the room relative to the error in displacement. Thus PIV has a relative accuracy of about 1%–2%.

Similarly, Cao et al. [2010] outline the problems of performing PIV measurements, namely difficulties of applying appropriate particle seeding and estimating the 'time between pulses' value. Cao et al. [2009] compared the PIV measurements with hot-wire anemometer (HWA) readings. The inaccuracy comparing with instantaneous PIV results was estimated at 20 % for the attached jet flow at Reynolds number of 960 and 1680, respectively and ± 11% if compared with time averaged PIV velocity vector map.

Gericke and Scholz [2014] compared 2D and 3D PIV measurements with hot-wire anemometry measurements in the wake region of an air outlet. Both PIV methods were in good agreement with velocity results in the free stream region and slightly different in convex region of an air outlet. The latter deviation is explained with the relatively steep calibration curve of HWA system at high velocities. Also for PIV measurements it suggested to perform interrogation window size study due to the increased averaging effect over the IA.

5.2.3 Difficulties using PIV system

In order to perform good PIV measurements, operator has to take care to provide:

- appropriate seeding of the particles
- accurate time between pulses

Particle seeding density

The number of particles in the flow is of some importance in obtaining a good signal peak in the cross-correlation. According to DantecDynamics 10 to 25 particles should be detected in each interrogation area.

In indoor climate studies mostly various smoke types are used as a particle seeding material. Cao et al. [2009] evaluated and suggested appropriate particle seeding density based on the acquired images and their color schemes, see figure 5.6. These observations relates well with the results achieved in the experiments performed in this project.

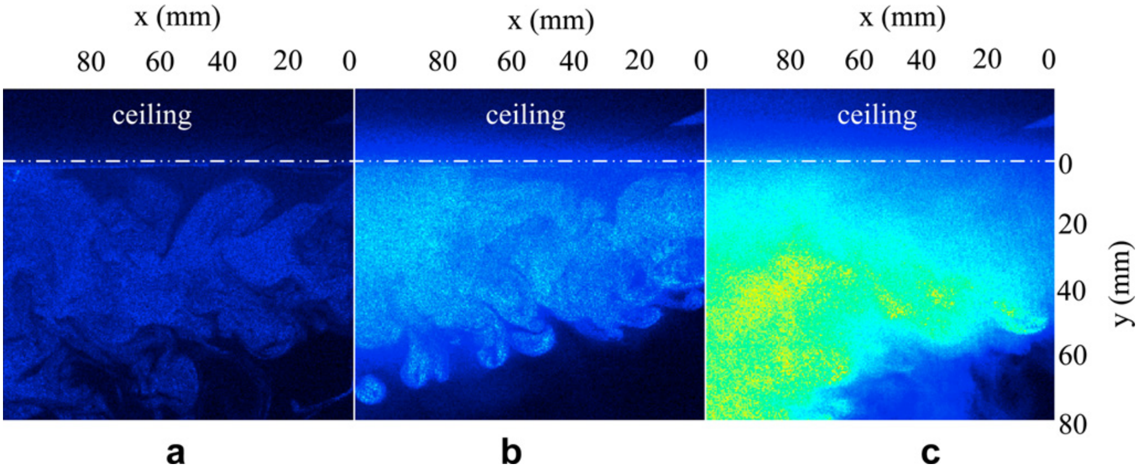

Figure 5.6. Smoke density: a) unacceptable - with insufficient seeding b) acceptable - with sufficient seeding c) unacceptable - with excess of seeding particles.[Cao et al., 2009]

Time between pulses

In practice time between pulses is crucial to validate PIV measurement results. In order to set correct 'time between pulses' value it is important to know the in-plane velocity of the moving particles. For example, in this project hot-sphere anemometers were used to validate this value. In order to estimate 'time between pulses' the following values from figure B.1, in appendix B were used. This is an example with an in-plane velocity of 1,0 m/s which estimates value of 1036,0μs.

Laser light

Furthermore, Sattari [2015] encountered problems in the near wall PIV measurements: the generation of a homogeneous global seeding and optical problems in form of strong laser reflections from the wall surface. This was limiting the research area of the heated airflow, both for the plume and the surrounding entrainment region.

5.2.4 Summary of literature study on PIV measurements

Regarding the practical applications of PIV system, suggestions for better measurement quality from previous research was taken into account when building the actual setup. The considerations regarding the PIV system use are listed below:

1. For example, the problem of near-surface laser light reflection mentioned by Sattari [2015] was encountered in this project as well. This effect was minimized to some extent by colouring the chilled beam surface and false ceiling black. However, the laser-reflection in the PIV-images was still strongly visible and thus limited the research area.
2. In this project different ways of seeding particle injection were tested. Initially, the smoke generator was placed in a box and thus smoke particles were injected in ventilation duct before mixing chamber of ACB. Another idea from Sattari [2015] to utilize global smoke seeding in the room was applied, however it didn't give the expected result, as the smoke was too dispersed. Better PIV-image quality was achieved when the smoke-generator was placed next to the induction area of active chilled beam. This method was used by Cao et al. [2009]. This method gave the best results and was used throughout the following measuring session.

In order to validate PIV measurement accuracy, suggestion of using another air speed technique was taken into account. Gericke and Scholz [2014] and Cao et al. [2009] used hot-wire anemometry. In this project the hot-sphere anemometers (HSA) with same velocity estimation principle were used.

5.3 Isothermal measurements

Velocity profiles were measured with PIV system as a supplementary method to hot-sphere anemometer method presented earlier. As results obtained with PIV measurements are vectors, it is not only possible to observe magnitude but also direction of flow. As such PIV measurements show supremacy over more simple, hot-sphere anemometer method. Knowing the direction of flow may be very helpful for validation of CFD simulations.

5.3.1 PIV Setup

Active chilled beam was placed upside down, in the middle of a room, centrally positioned to avoid influence of walls. In order to avoid laser reflection from white walls, they were covered with black cloth. Digital CCD-camera was installed on a traverse (figure 5.7).

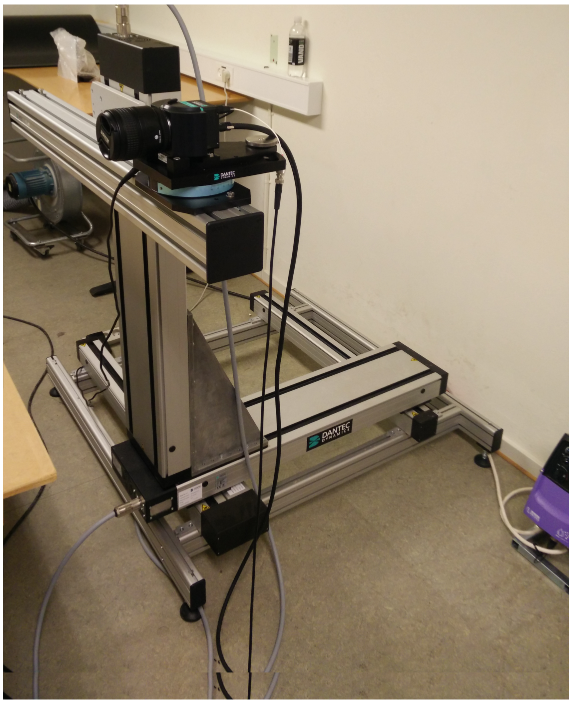

Figure 5.7. Traverse with a camera mounted

A laser guiding arm (Dantec Light Guide, figure 5.8) was used to deliver the laser beam. Before taking measurements the CCD camera was calibrated with use of Dantec 200x200 mm calibration target.

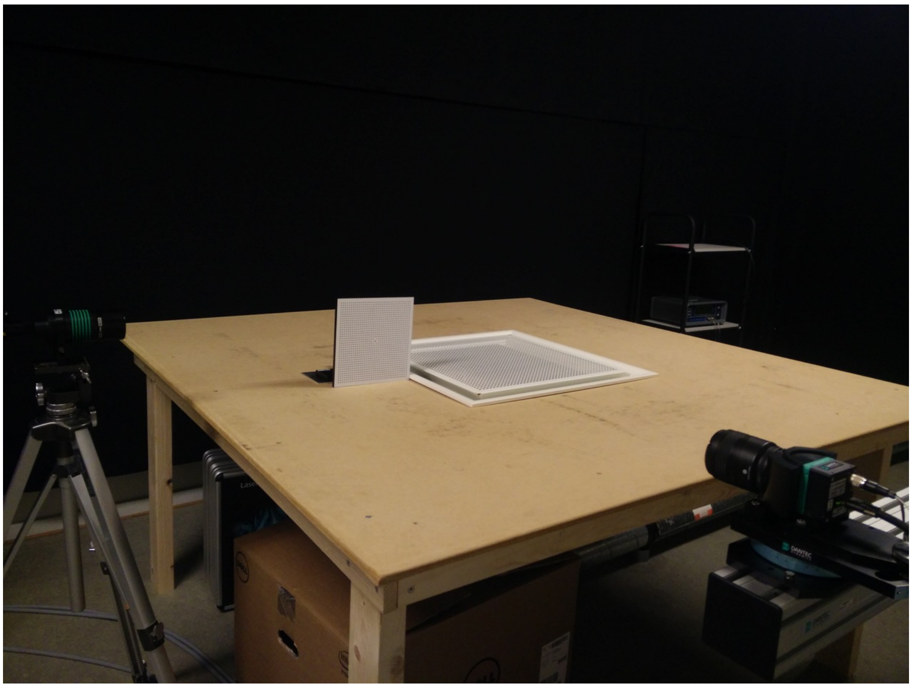

Figure 5.8. PIV setup - ACB mounted on false ceiling with calibration plate, laser sheet and CCD-camera.

Two methods of seed feed were tested during experiments. First - box method where supply air is mixed with smoke inside the box (figure 5.9) and induced into the beam. Second method consisted of seed feed by supplying smoke in the induction area. Second method was used for measurements as it gave better results and more control over amount of smoke released (PIV system is very dependent on density of smoke, if seeding is too dense or too thin, pictures obtained from acquisition cannot be properly post-processed. Seed was illuminated in the measured plane twice within a short time interval and two pictures by CCD camera are taken. The difference between particle photos is used afterwards to calculate the velocity vectors.

Figure 5.9. Seeding, box method.

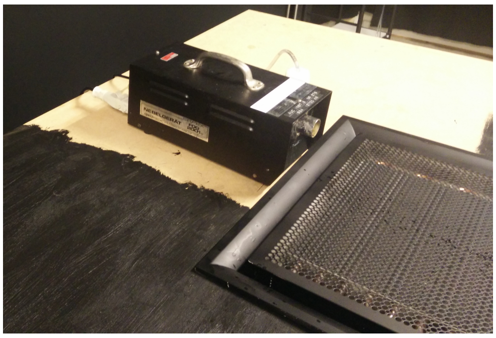

Figure 5.10. Seeding, direct introduction through induction surface

The trigger signals are synchronized with Timer Box (model 80N77) from Dantec Dynamics with use of computer with DynamicStudio software installed. Mentioned software also post-process pictures taken by CCD cameras and calculate vector field. Camera is based on a Charge-Coupled Device sensor with high sensitivity and resolution. During measurements, the power of the laser has to be increased gradually in order to prevent overexposure (white spot with no visible smoke particles).

Laser beam was dispersed with use of Dantec Light Sheet positioned in such way that emitted laser beam is aligned with target plate (beam touches the surface of target plate) used for calibration of a camera.

Air flow rate supplied to a beam was measured by an orifice coupled with a manometer. In order to limit turbulence produced by fan, metal duct was stuffed with plastic straws. Additionally, length of ten times a diameter of orifice pipe an orifice before and five times a diameter after an orifice was ensured.

Experiments were taken under isothermal conditions. The primary air supply is provided through circular inlet of 125 mm diameter with a powering fan in the other end of a system. Ambient air is induced through perforated plate at the top of a beam. Sampling of 200 pictures is recorded with frequency of 8 Hz. Double frame picture acquisition was taken with time delays between lasers dependant on expected in plane velocity, using PIV Assistant Tool as a reference.

5.3.2 PIV Analysis

Adaptive PIV was used as a method for analysis (one of methods available in Dantec Studio 2015). Grid step size was set to 32x32 px, minimum and maximum interrogation area sizes were set at 32x32 and 192x192 px respectively. Each picture from acquisition was validated with peak size of 0,25, interrogation area adaptivity was set to 5 for both particle detection limit and desired number of particles/IA as recommended in Dantec Studio manual. As adaptive PIV analyze each acquired picture separately, in order to obtain one final result, ensemble was treated with vector statistics tool afterwards.

5.3.3 PIV Results

In general obtained profiles show the same pattern in every measured case and only differ by a magnitude. As such, only one example profile is presented. All calculated velocity profiles can be found in page 83. Due to technical limitations (the camera can only capture the picture size of 20 cm in used distance), measurements were only conducted in distance up to 20 cm from beam. Difference between instantaneous vector flow field and averaged vector flow field can be observed in figures 5.11 - 5.14.

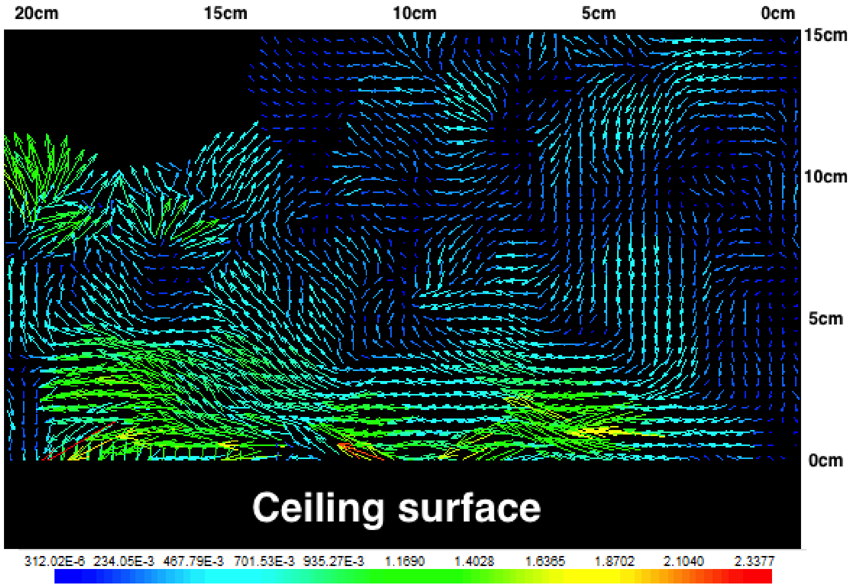

Figure 5.11. Instantenous velocity profile (single picture), 15 l/s.

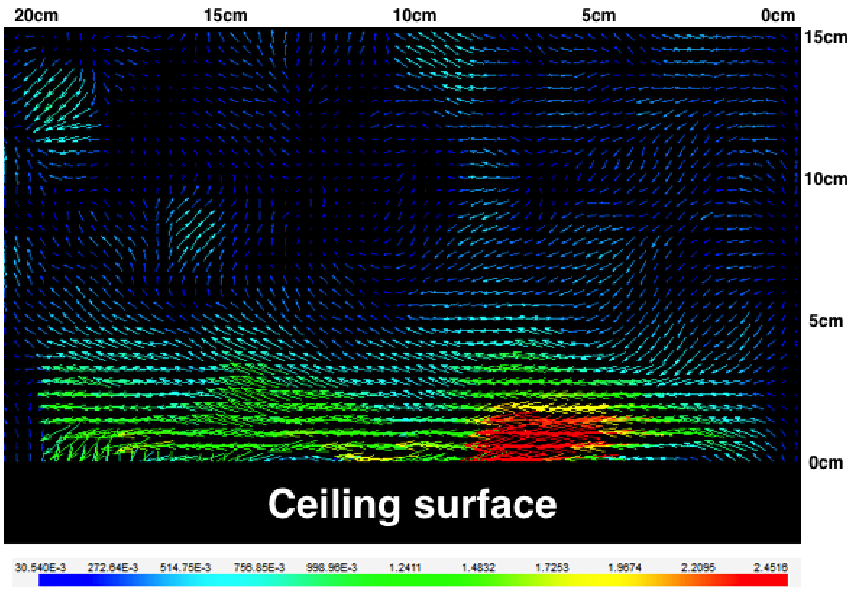

Figure 5.12. Averaged velocity profile (6,25 s acquisition, 50 pictures) 15 l/s.

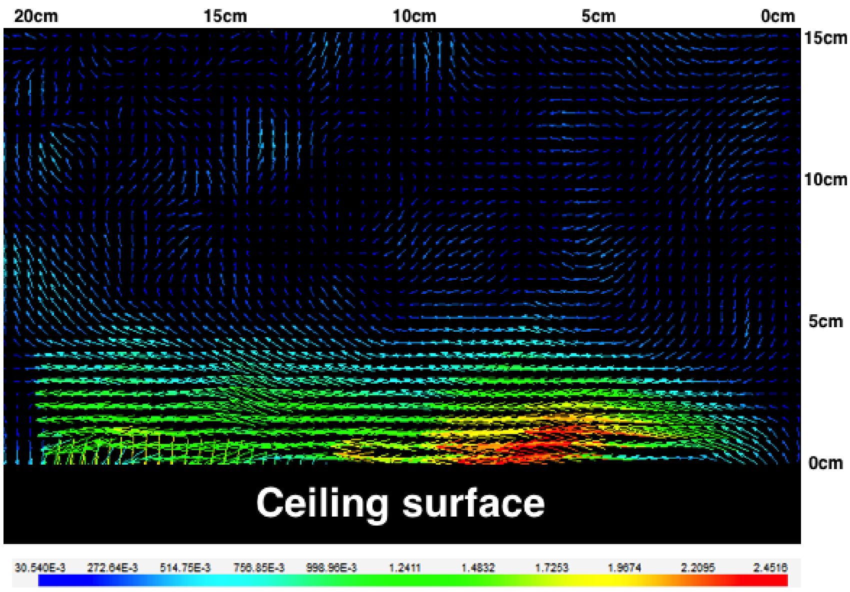

Figure 5.13. Averaged velocity profile (12,5 s acquisition, 100 pictures) 15 l/s.

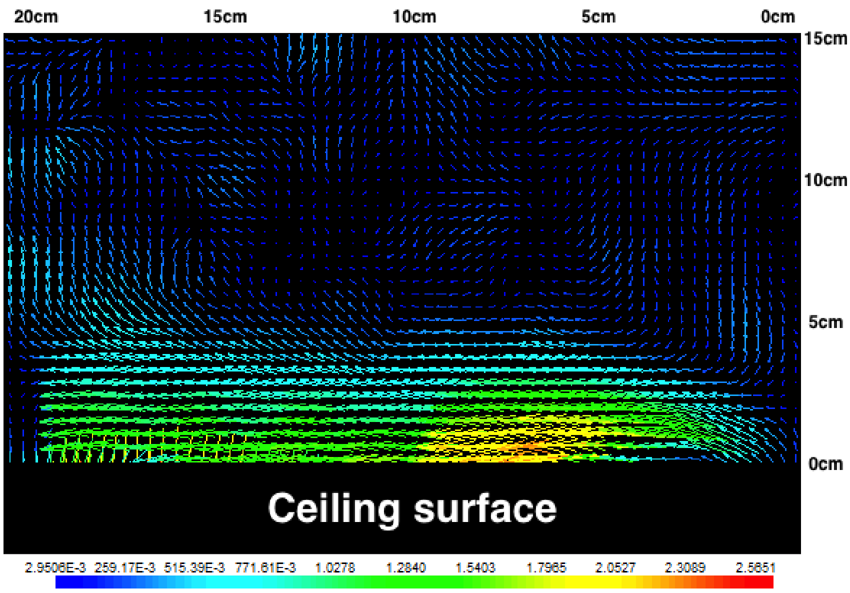

Figure 5.14. Averaged velocity profile (25 s acquisition, 200 pictures) 15 l/s.

Figure of instantaneous vector flow field, 5.11, shows the entrainment of the room air in the outer part of the jet.

Figure of averaged vector flow field, 5.11, clearly shows the Coanda effect - the air jet is bending towards the ceiling surface - reaching the maximum air velocity few centimetres above the surface - similarly as measured with hot-sphere anemometers.

However the reflectance of the laser light from the table and beam surface limits the measurement area next to the ceiling and chilled beam exit surfaces.

5.4 Summary of PIV measurements

Analysing the wall jet flow from chilled beam in isothermal conditions, PIV measurements show an air distribution pattern that is similar to one that was predicted with CFD. Especially comparing them with the time-averaged PIV images. See chapter 7 and figure 7.10 on page 54 for the wall jet visualization produced by simplified CFD-model simulation.

Furthermore, comparing the PIV results with anemometer readings, the PIV measurements show higher magnitudes, therefore PIV results are only used to validate the beam exit region in terms of shape of jet.

Part III

Non-isothermal measurements

In this part, the velocity profiles at the exit region of an active chilled beam (ACB) are measured in a full-scale testing facility with working water cooling circuit. Thermal comfort and air speed are estimated with hot-sphere anemometers. In addition to the experiment, a CFD simulation of the experiment is presented. The purpose of this part is to create a CFD model of ACB and validate it for the further use in an Annex 20 room model. Furthermore, CFD model of the Annex 20 room will be used to create thermal comfort Design Chart to compare the performance of ACB with other conventional air distribution systems.

Full-scale measurements 6

In this chapter it is described how the active chilled beam performs in a full-scale testing room. Thermal comfort and air velocity distribution at the exit region of the active chilled beam.

Full-scale testing is a mid step taken to validate the researched active chilled beam CFD model. Combining CFD simulation with measurements obtained from full-scale measurements makes CFD model more accurate. Data collected in multiple locations within test room is later compared with CFD results and boundary conditions are adjusted in order to obtain identical velocity patterns in both CFD simulation and full-scale test.

6.1 Testing facility "Cube" overview

Full-scale experiments have been done in the "Cube", an outdoor full-scale test room located in Aalborg, Denmark (57.02°N, 10.0°E). Test room was constructed with use of wood and 160 mm EPS insulation. Additionally, 22 mm of plywood is added to the floor as well as 13 mm plasterboards to side walls. Internal dimensions of test room are 2,75x3,6x2,76 m. Test room is exposed with three sides to a guarded zone with possibility of temperature control and exposed to outdoors with fourth wall. Schematics of "Cube" can be seen in figure 6.1.

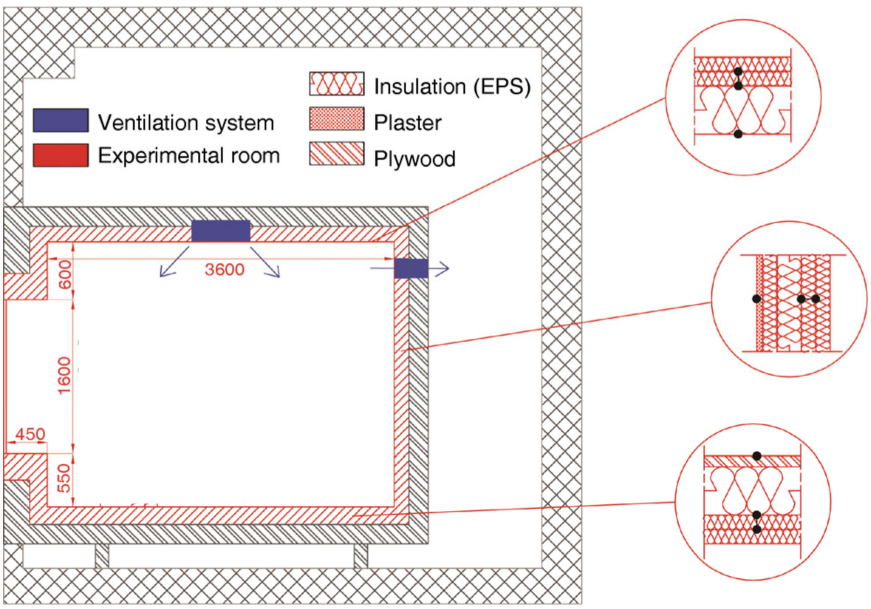

Figure 6.1. Schematics of "Cube", [Dréau et al., 2014].

As originally "Cube" is equipped with a double-pane window, in order to eliminate heat transmission between test room and outdoors, it has been additionally insulated with EPS insulation.

6.2 Ventilation and Cooling

Temperature inside test facility can be controlled with a chiller operating in range of temperatures with a lowest possible value of from 6 degrees Celsius. "Cube" is equipped with several water circuits that can be independently controlled, however only one, common temperature can be set in a chiller (for all water circuits coolant temperature is the same). As set point of chiller does not fully reflect temperature of coolant that is received in water circuits (chiller generates a lot of heat and slightly heats up coolant), set point for a chiller had to be adjusted by observation of actual temperature in fluid circuits in the facility. As aim of experiments is to obtain measurements in certain conditions and range, (temperature is measured at inlet and outlet and range should cover approximately 10 K difference between those two) temperature of coolant was varied suitably to needs of selected measurement conditions.

Desired temperature inside guarded zone has been achieved with use of high power fan and cooling coil mounted at the top of guarded zone. Cold coolant flows through the cooling coil and fan blows the air through it eventually causing the temperature of ambient air to drop.

Test room is cooled with use of Lindab Plexus S60 active chilled beam. Volumetric flowrate as well as flow of coolant in cooling coil of the beam was manually controlled and adjusted according to needs. As mentioned before, both guarded zone and and chilled beam share the same chiller. As such, the set-point had to be carefully controlled to obtain reasonable thermal conditions inside the test room. Schematic presentation of room ventilation is shown in figure 6.2.

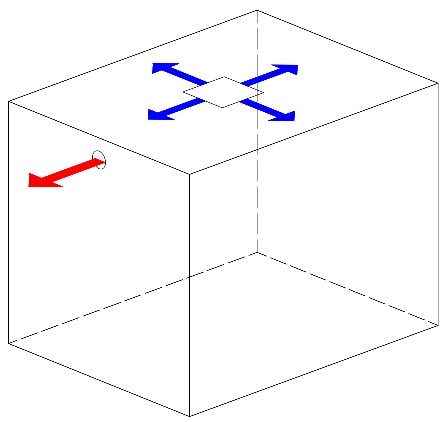

Figure 6.2. Supply and exhaust location of ventilation in full-scale test room "Cube".

6.3 Measurement procedure

Single seated occupant (thermal manikin) was positioned in the middle of room behind a workstation consisting of a desk, desk lamp, PC and monitor as shown in figure 6.4. For exact dimensions of equipment and distribution across the desk refer to appendix H. All conducted measurements were taken maintaining the same procedure. Measurements were taken within range of 0,01 to 0,021 m^3/s. Stable conditions were determined based on surface temperatures measured with use of Fluke Helios Plus 2287A coupled with ice point reference and compensation box. Volumetric flow rate (primary air flow) rate was controlled with voltage-controlled fan. In order to determine flow rate, electronic pressure transducer (PSIDAC AB FlowGuard 6280) was coupled with beam static nozzle pressure measurement system. Knowing pressure drop inside the beam and using graph provided by Lindab [b], it was possible to read primary air flow rate with certain JetCone setup. Each heat source was regulated with separate vario-transformer. Power outputs of heat sources were measured with kWh Power Detective.

After securing steady state conditions, measurements were conducted for 15 minutes (velocity and surface temperature measurements). Each obtained acquisition was later statistically treated.

6.4 Sensors distribution

Two sets of measurements, each with different hot-sphere anemometers location, are performed:

- Thermal comfort measurements
- Aerodynamic measurements.

6.4.1 Thermal comfort measurements

Walls, floor and ceiling was equipped with two thermocouples each, positioned centrally. Thermocouples were also placed inside outlet and inlet pipes (two per each pipe). Velocity magnitude measurements were conducted with use of 26 hot-sphere anemometers distributed around manikin and occupied zone as well as region close to the beam at heights as shown in figure 6.3. Experiments taken in "Cube" are divided into two parts. First part focusing on thermal comfort (Design Chart) and second focusing on aerodynamics later used for Annex 20 room CFD validation procedure. Figure 6.4 presents pole distribution for first part of measurements.

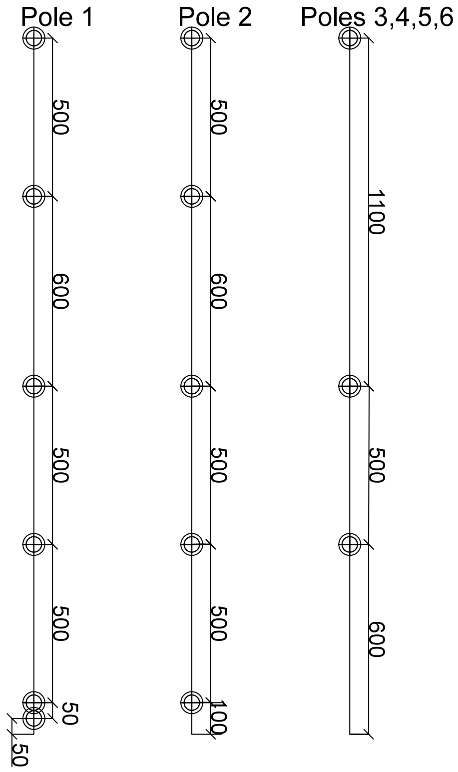

Figure 6.3. Thermal comfort measurements. Hot-sphere anemometers distribution on poles.

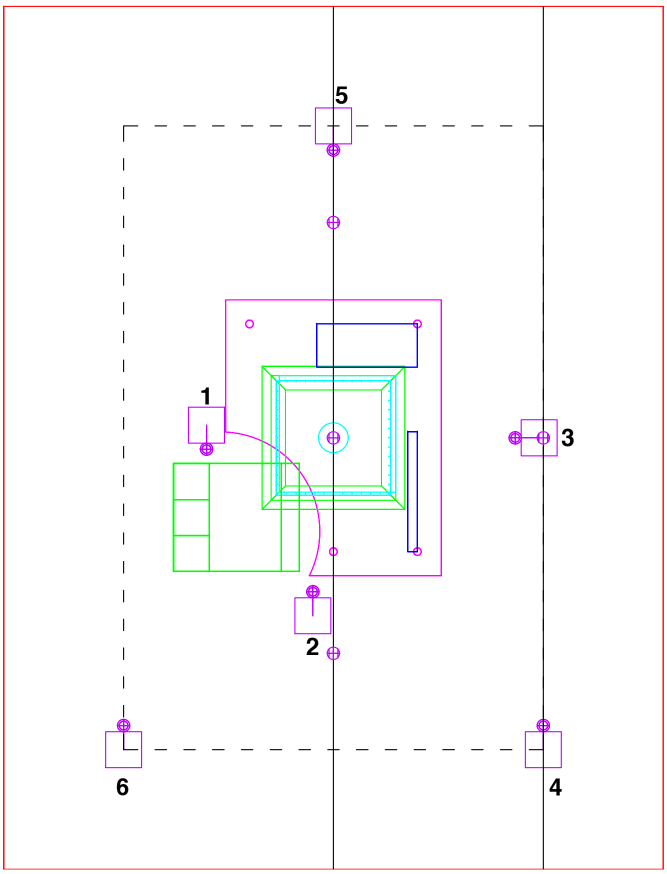

Figure 6.4. Thermal comfort measurements. Pole distribution, top view, dashed line indicate occupied zone borders.

Results

All previously analysed systems, in the research made by Nielsen and Jakubowska [2009], could be considered as diffusers. In such case cool air is simply introduced into test room and velocity magnitudes can be measured within occupied zone. Such procedure can be applied for both momentum and buoyancy driven flows. Active chilled beam utilizes active cooling system, and is based on the induction principle. Low static nozzle pressure in the ACB entrains the warm room air. As such, the system requires special considerations in terms of what approach should be used to obtain comparable results with previously tested system with regards to the supplied airflow rate. Four approaches were analysed in terms of creating thermal comfort graph ($q_0/\Delta T$). Considered solutions were:

- $q_{primary}/\Delta T$(outlet-beam)
- $q_{mixed}/\Delta T$(outlet-beam)
- $q_{primary}/\Delta T$(outlet-inlet)
- $q_{mixed}/\Delta T$(outlet-inlet)

where

$q_{primary}$	is the fresh air supply rate
q_{mixed}	is the sum of fresh and recirculated air
outlet	is the surface temperature of outlet
inlet	is the surface temperatures of inlet
beam	is the surface temperatures of beam
outlet-beam	is the difference between surface temperatures
outlet-inlet	is the difference between surface temperatures

Active chilled beam is not only a diffuser. Warm room air (secondary air) is induced into the beam and mixed with fresh cold air (primary air). At the same time secondary air is cooled by cooling coil. After the process, mixed air volume consisting of both induced and primary air volumes is diffused back into the room. As such, selected approach to thermal comfort graph was $q_{mixed}/\Delta T$(outlet-beam) graph which was believed to be most comparable with regular diffuser ventilation systems. Obtained solution is presented in figure 6.5. All previously mentioned approaches to the graph are presented in appendix F.

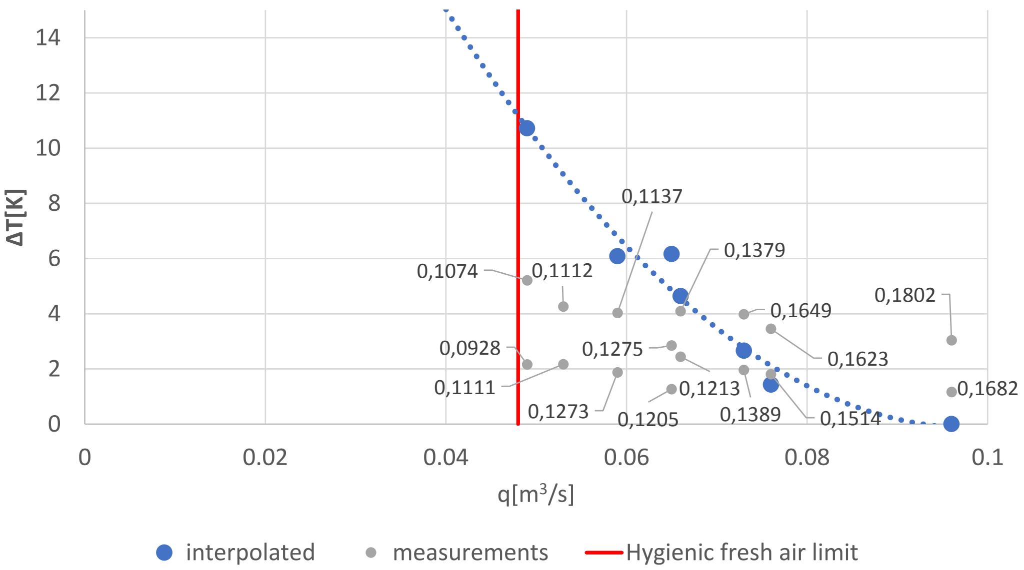

Figure 6.5. Design Chart - q/ΔT graph, full-scale test room "Cube".

The graph shows ability of ACB to remove heat mantaining comfortable conditions for occupants inside. Area for which ventilation flow rates and heat load can provide sufficiently good thermal comfort - namely the air velocity lower than 0.15 m/s is located under the curve. Results from the graph cannot be compared to other ventilation systems, as there were no measurements performed for other ventilation systems in the "Cube" facility except from an ACB.

6.4.2 Aerodynamic measurements

As mentioned before, second part of experiments is focused on aerodynamics research. In order to validate CFD models, 21 anemometers were distributed across occupied zone of the room in order to obtain full picture of velocity distribution. Figure 6.6 presents the distribution in detail. Poles were distributed in front and behind manikin and across the ceiling. Two additional anemometers were placed over manikin's head to validate velocity magnitudes affected by thermal plume.

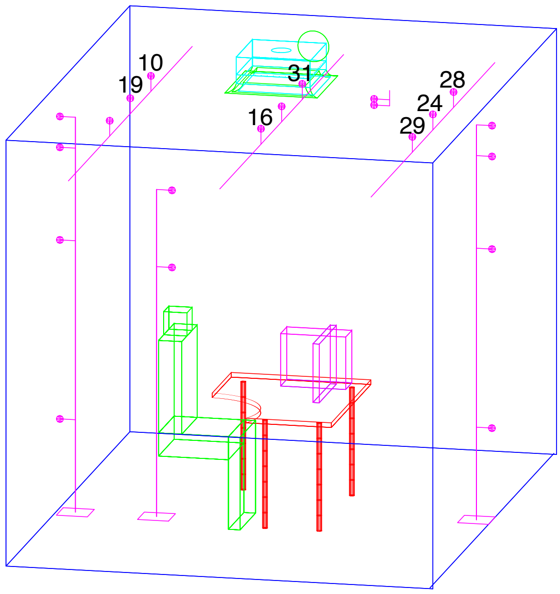

Figure 6.6. Aerodynamic measurements. Full scale set-up used for CFD validation.

Results

The obtained aerodynamics measurement results are shown in figure 6.7, 6.8 and 6.9. Airflow rate is varied from 10 l/s to 20 l/s.

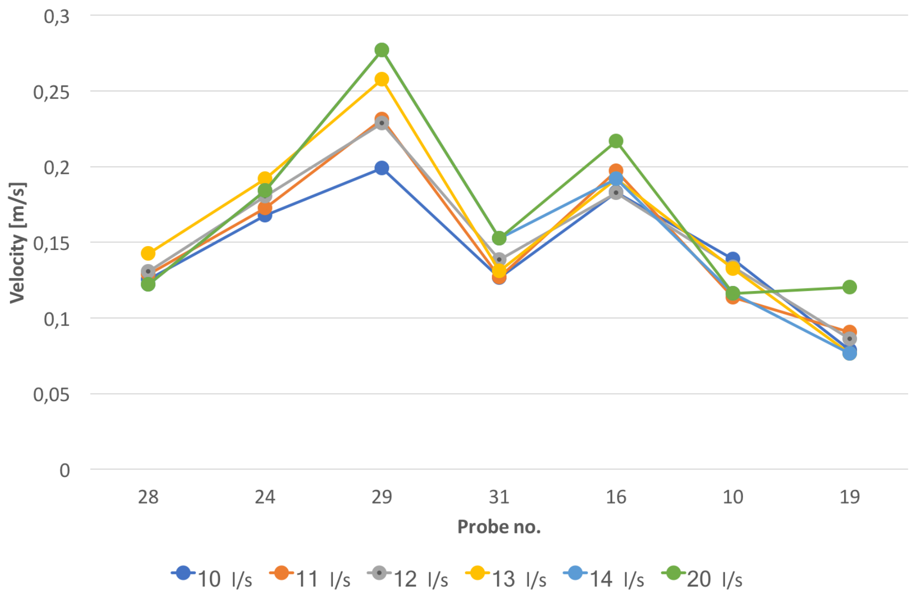

Figure 6.7. Ceiling grid velocity distribution at 2,64 m (12 cm below ceiling), primary air volume flow rate. Refer to figure 6.6 for anemometer placement.

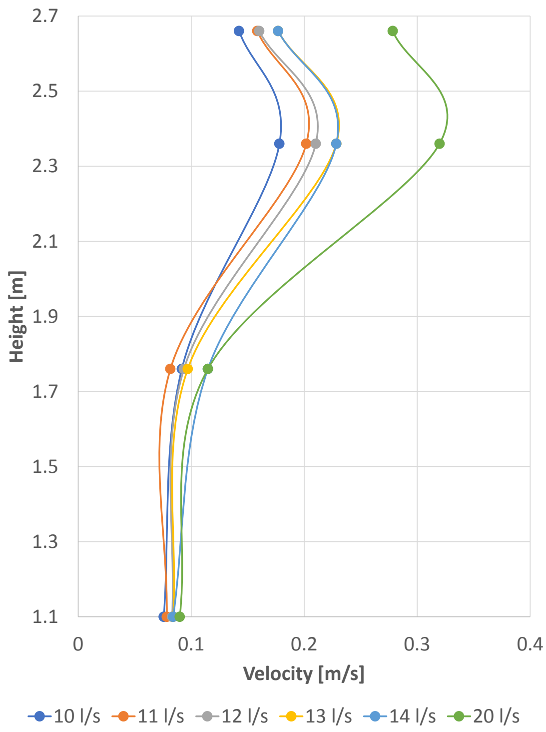

Figure 6.8. Pole in front of the manikin.

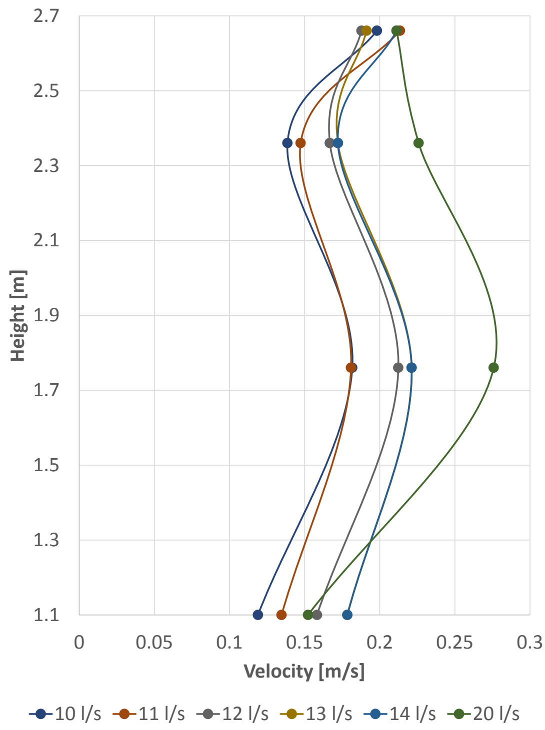

Figure 6.9. Pole behind the manikin.

The comparison of this data with CFD simulation results is shown in table 7.15 on page 57.

Computational Fluid Dynamics 7

CFD simulations aim to obtain flow patterns inside the room as well representing real phenomena as possible. Annex 20 room simulation requires validation and as such, supplementary geometry ("Cube") has been created as an intermediate step. Results obtained as a result of measurements in "Cube" were later compared with "Cube" CFD simulation in order to validate boundary conditions for Annex 20 room.

7.1 Geometries

In the following subsections all geometries (models) used for CFD are presented. For additional data concerning dimensions of work stations, heat sources, heat sources location around the work station as well as position of work stations in the room, refer to Annex H.

7.1.1 "Cube"

First geometry is created for "Cube" dimensions, with one person sitting next to desk with a computer, computer display and a lamp. Internal room dimensions are 3,6x2,75x2,76 m (width, length, height respectively). Beam (Lindab Plexus) is centrally positioned at the top of ceiling, above the heat sources. Air is supplied through inlet surface of the beam (refer to section7.1.3 for beam details). Outlet is positioned close to the ceiling, in the middle of northern wall. Model used for simulations is presented in figure 7.1.

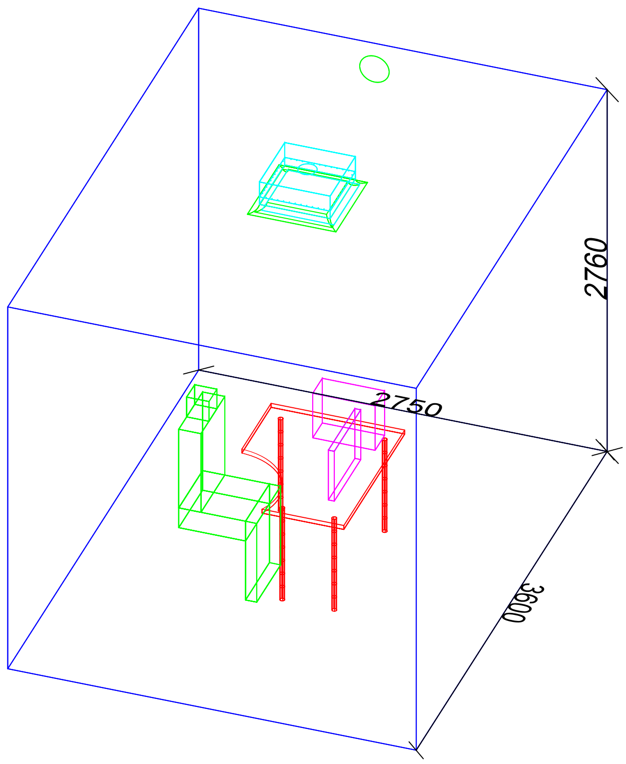

Figure 7.1. "Cube" geometry

7.1.2 Annex 20 Room

Four cases are considered for Annex 20 room. Geometries used for numerical simulations simulate office. In first case geometry consists of two tables, two manikins, two computers, two computer displays and two desk lamps, positioned centrally and active chilled beam (Lindab Plexus) at the level of ceiling, centrally positioned. Internal dimensions of room in both cases are 3,6x4,2x2,5 m (length, width, height respectively). Air is supplied through inlet surface (refer to section7.1.3 for beam details). Outlet is positioned at the bottom of a wall, in one of the corners, next to one of work stations. Figure 7.2 represents created model.

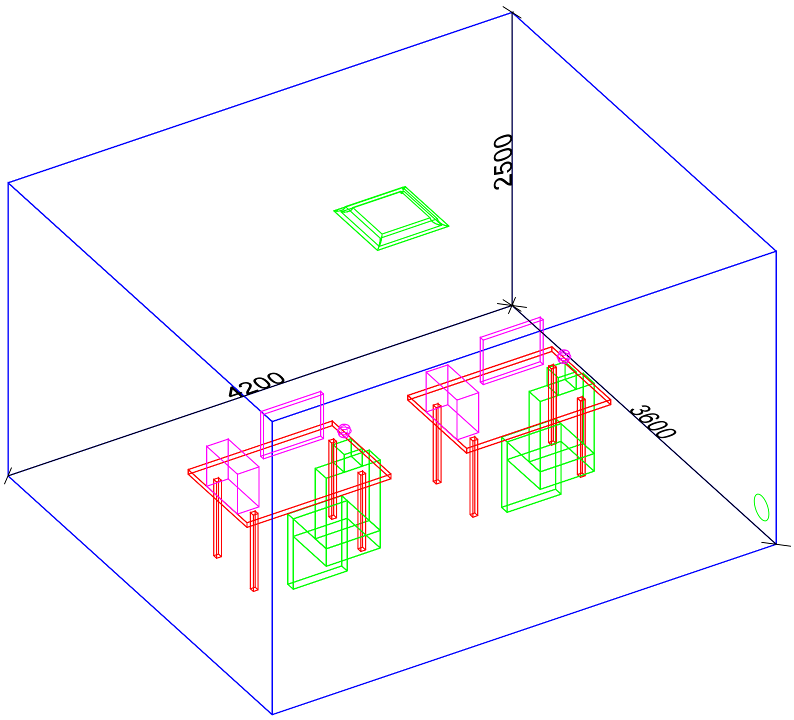

Figure 7.2. Geometry of test room, symmetric heat sources distribution [Nielsen and Jakubowska, 2009].

Second analyzed case consists of the same room and equipment, the same boundary conditions for inlet, outlet and heat sources, however heat load distribution in a room is different - work stations are shifted to one side of room and positioned one after another. Geometry of second case is presented in figure 7.4.

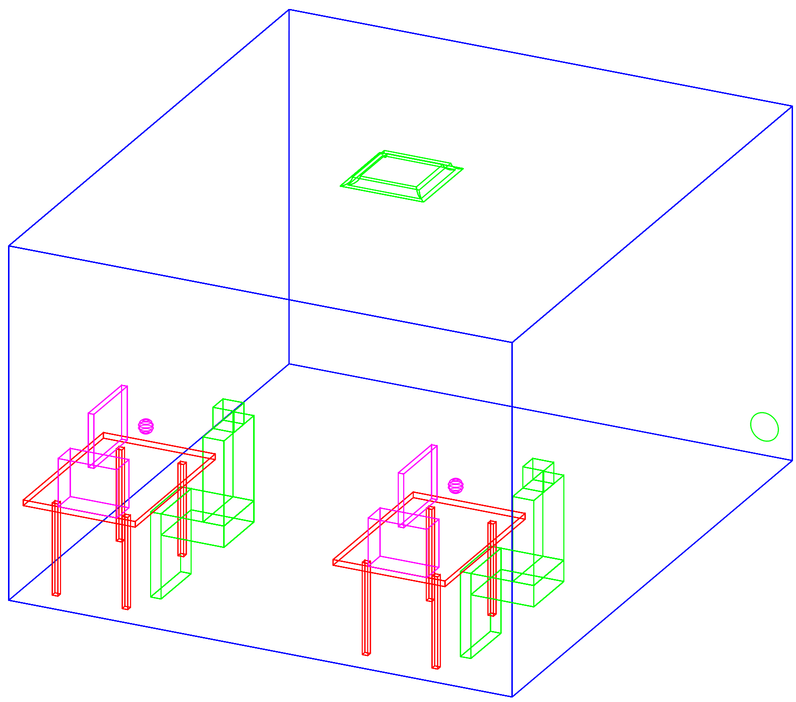

Figure 7.3. Geometry of test room, asymmetric heat sources distribution.

Third considered case is a personal ventilation. Two beams are placed inside the room, one over each of workstations. This way, supply rate required by IAQ requirements can be divided between two beams (each of beams supply half volume of air required). Such setup may limit draft around sitting person resulting in better performance in comparison to one, centrally positioned beam.

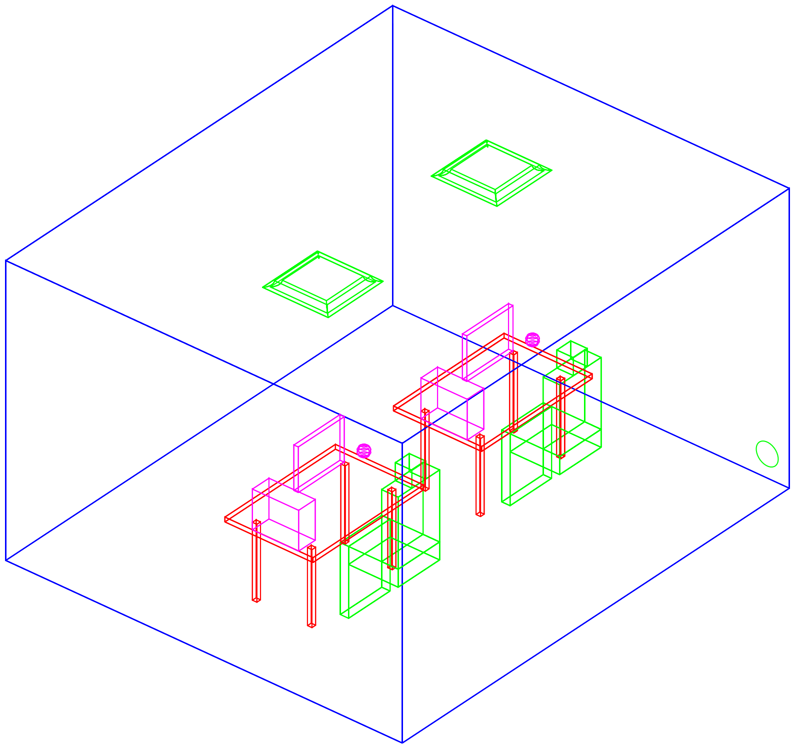

Figure 7.4. Geometry of test room, personal ventilation.

7.1.3 CFD Boundary conditions for a beam

Two beam models were analyzed in order to select best fitting to the task solution. Created beam models differ in amount of details and as such, more complex model is more computational-heavy than simplified model.

Complex model consits of full geometry of real beam with some minor simplifications - jetcones are reduced to circular holes (figure 7.6C) as well as cooling coil geometry is excluded from inside of the beam.

Simplified model is reduced to only bottom part. Inlet is changed from circular surface at the top of the beam to square surface at the top of curvature (blue surface, figure 7.8A). Inlet (velocity-inlet) with uniform magnitude across the boundary is defined in a way that it combines both primary and secondary air fluxes in terms of both temperature of air after mixing as well as it's volume. It means that the temperature set at inlet of the beam is resultant temperature that would occur after mixing primary and secondary air jets. As simplified beam model does not include mixing chamber, secondary air jet needs special handling. Red surface (figure 7.8A) is defined as an outlet (outflow) and is created in order to dispose warm air that floats to the ceiling and would normally be sucked inside the beam and mix with primary air. Outlet (outflow) replaces perforated plate of the beam which in real life conditions delivers secondary air to a mixing chamber of ACB (figure 7.5). Reason behind selecting outlet boundary condition as *outflow* instead of *outlet-vent* is to prevent backflow of air from beam outlet, as it requires backflow temperature definition which due to lack of experimental testing is unknown. Velocity-inlet boundary condition allows to define amount of air supplied to the room with respect to velocity parameter. Velocity magnitude is calculated with following equation:

$$V = Q/A \tag{7.1}$$

where

Q	Volumetric flow rate.	m^3/s
A	Area of inlet surface.	m^2

Both discussed beam models (full and simplified) are presented in figures 7.6 and 7.8.

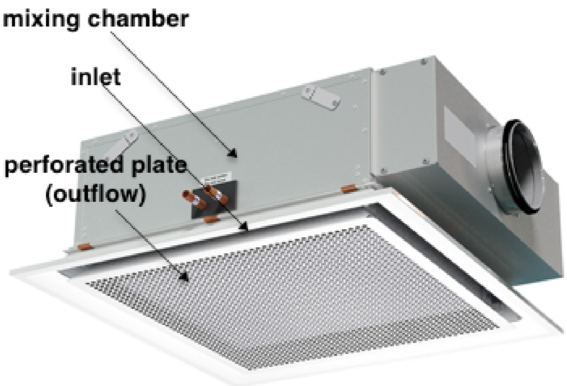

Figure 7.5. Lindab Plexus.

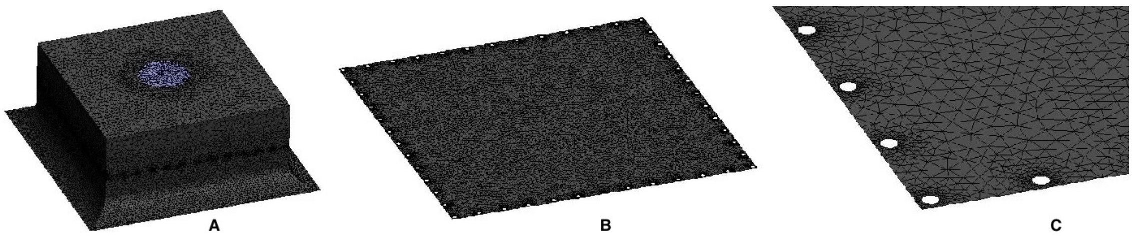

Figure 7.6. Complex (full) beam model. A - overview of model, B - inner plate with JetCone holes, C - close look at inner plate.

Simplified beam model has been created by slicing full beam model (red line). Top part of the beam (light blue part) has been removed. After simplification beam model is limited to only bottom curved part (green part).

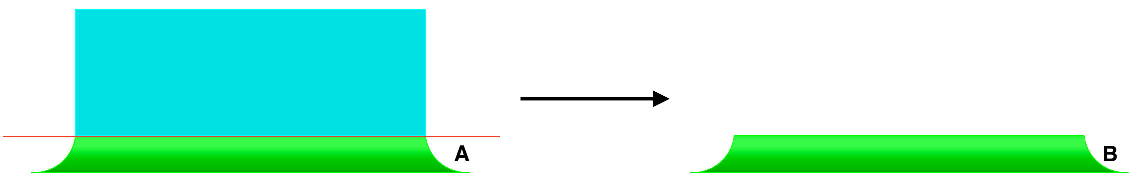

Figure 7.7. Beam model transition from full beam model (A) to simplified beam model (B).

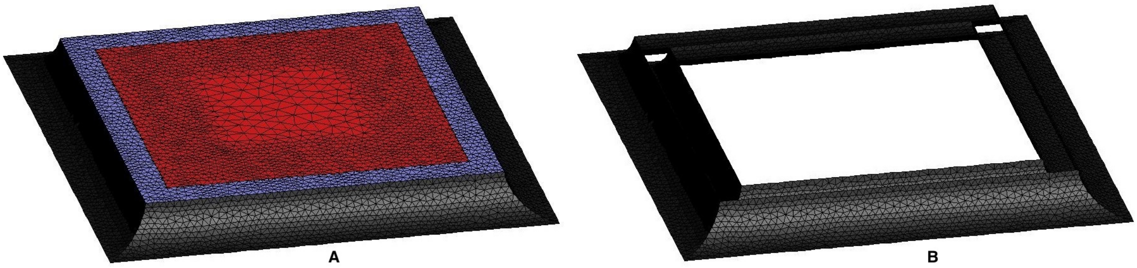

Figure 7.8. Simplified beam model. A - overview of simplified model, blue surface is inlet, red - outlet, B - model with inlet/outlet surfaces switched off.

Both models have been tested to verify which model would provide more reasonable results. Final selected model was simplified beam model as it can reproduce 360 spread pattern of Lindab Plexus, produce very similar velocity distribution at the same time being much less computational heavy (approximately 3 million cells for room model with simplified beam versus full beam model with approximately 7 million cells model).

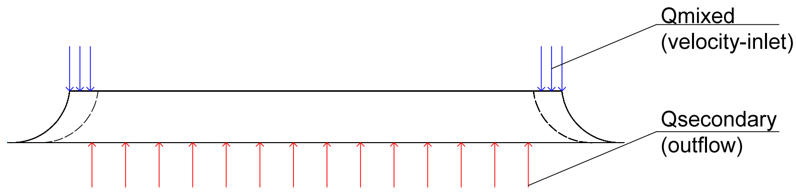

Figure 7.9. Boundary conditions - velocity vectors of supply and secondary airflows.

In order to further validate created CFD beam solution, a study concerning induction rate has been conducted. Using LindQST as a source of reference values, a volumetric flow rate surface monitor was set at beam outflow (red surface, see figure 7.8 for further details). Obtained comparison has been presented in table 7.1. Study showed that differences LindQST source and CFD estimations remain within acceptable limit.

CFD [l/s]	LindQST [l/s]
50	52
44,5	47
42	39

Table 7.1. Induction rate comparison between LindQST and CFD surface monitor.

7.2 Beam exit region

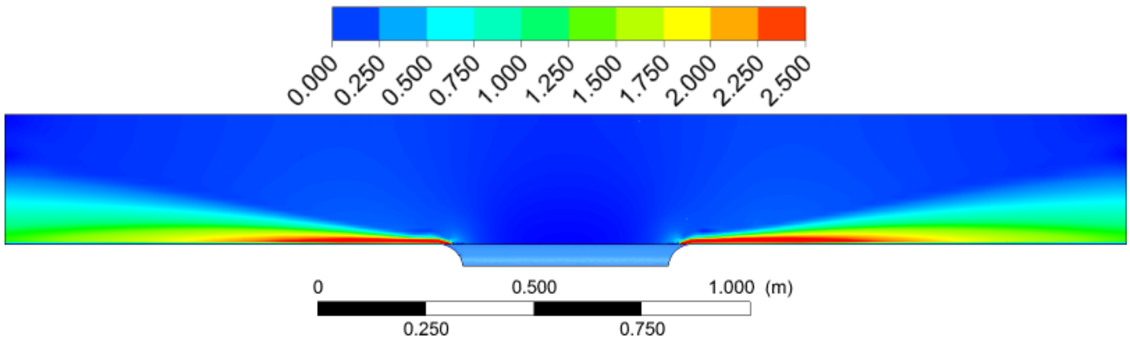

Figure 7.10. Beam exit region, primary air flow rate - 20l/s CFD reproduction of isothermal measurements (chapters 4 and 5).

In order to make simulation computational bearable, model had to be simplified. Lack of complex geometry leads to differences in velocity distribution in exit region. Lindab Plexus is equipped with JetCone system allows user to control throw length in the room. As such, differences in magnitude between wall jet measured in the laboratory and wall jet obtained within CFD simulations are visible. Due to that, focus has been limited only to room, excluding vicinity of the beam. Model was adjusted to obtain boundary conditions that would reflect velocity distribution within the room measured during full-scale experiments.

7.3 Heat sources

There are four different types of heat sources inside tested rooms: thermal manikins, computers. desktops and desk lamps. As radiation is not considered in simulations, values have to be adjusted. Convective part of heat release is presented in table 7.2.

Heat source	Convective part [%]	Nominal heat release [W]	Convective part [W]
Manikin	40	100	40
Computer	50	50	25
Screen	50	50	25
Desk Lamp	50	40	20

Table 7.2. Convective part of heat release [Carl Erik Hyldgård and Steen-Thode, 1997]

7.4 Mesh and surfaces definition

Mesh has been generated with use of Octree tetrahedral meshing method. Surface meshes have been varied in size depending on it's location and importance in the system. As such, inlet, outlet and beam parts were meshed with finer mesh while for walls defined mesh was coarsened.

Additionally, mesh size varies depending on it's location in 3D space, mesh that is closer the exit region of the beam is finer than the one close to the walls or in the middle of domain (in the middle of room height, between heat sources and beam).

Heat sources as well as beam elements have been meshed with addition of 5 prism layers.

Surfaces were meshed with quad dominant, autoblock method. Each surface had either surface temperature (walls) or heat release (heat sources) prescribed, based on measurements obtained in "The Cube".

7.5 Grid independence

In order to determine grid independence of analysed models, several mesh densities were created. Grid independence was stated once the changes in solution were insignificant or refining mesh did not change solution anymore. In order to determine grid independence, a maximum velocity across the model has been extracted for each case and values obtained were plotted.

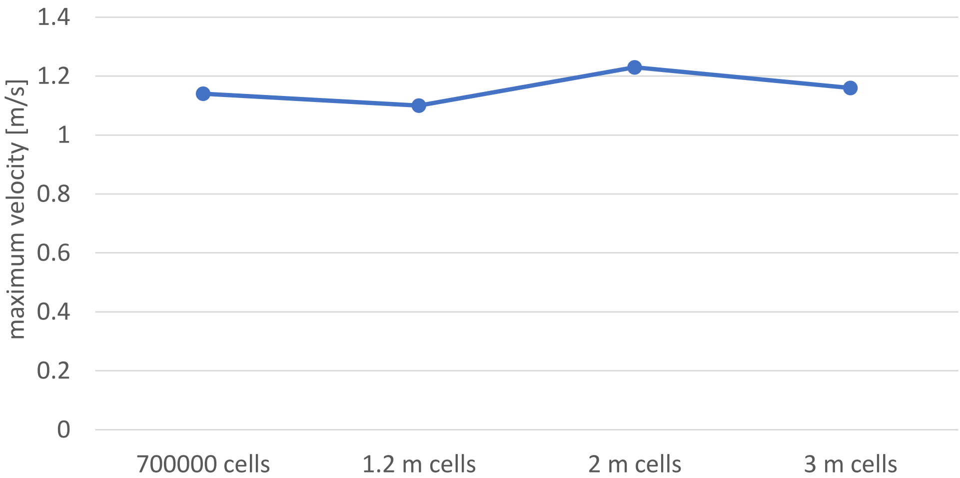

Figure 7.11. Grid study - symmetric heat sources.

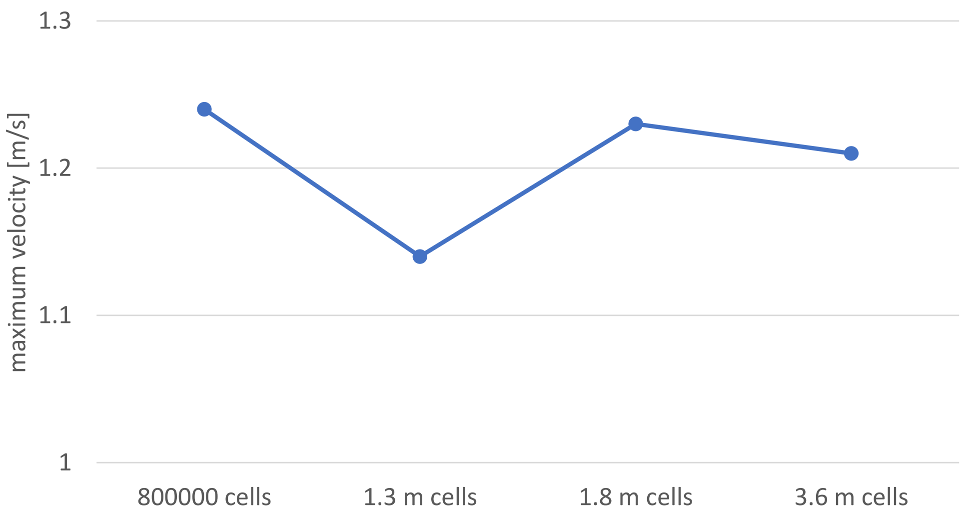

Figure 7.12. Grid study - asymmetric heat sources.

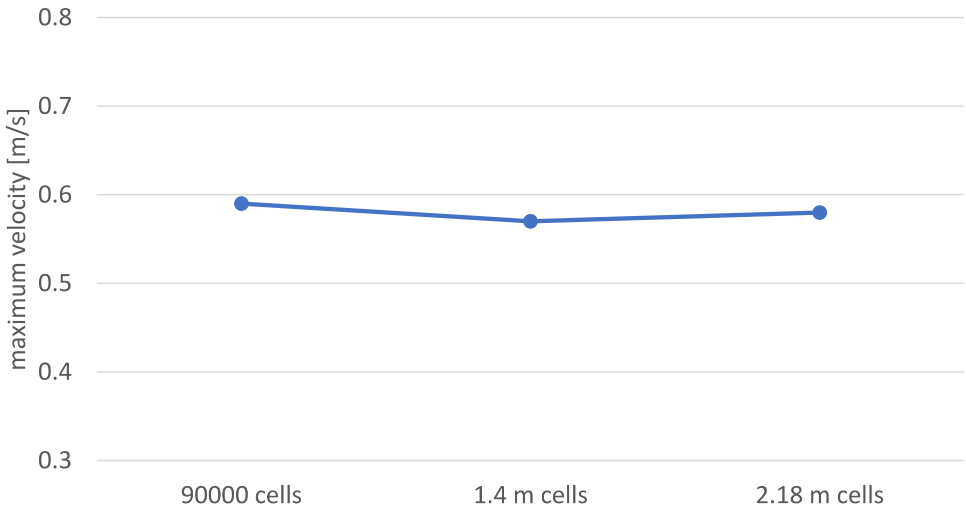

Figure 7.13. Grid study - personalized ventilation.

7.6 Validation

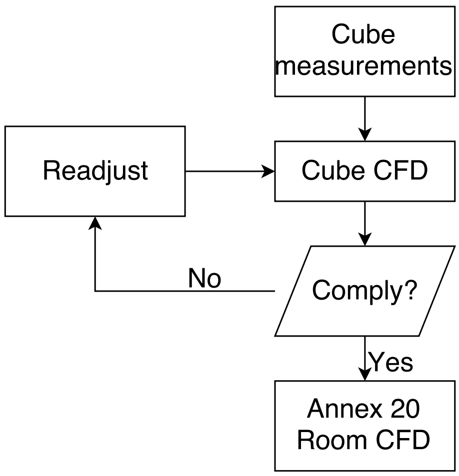

Figure 7.14. CFD validation procedure

Validation is required to specify how well can CFD simulation reflect real conditions obtained in the test room. The procedure consisted of several steps. First, isothermal measurements for the beam were conducted with use of PIV and hot-sphere anemometers systems. Afterwards, full-scale measurements in "Cube" facility were collected. Data from both isothermal jet measurements and full scale - "Cube" were combined for Cube CFD validation (setting up proper boundary conditions). Once the compliance between collected data and CFD was stated, boundary conditions were transfered to Annex 20 Room CFD.

7.7 Selection of turbulence model

In chapter 2. Literature review - Chilled Beam Systems short summary of the various turbulence models is made. RNG $k-\epsilon$ turbulence model is very popular among the indoor climate researchers, however each experimental setup may require different turbulence model. In order to determine best fitting model for simulation, four turbulence models were tested. Models taken into considerations were:

- Standard $k-\epsilon$
- RNG $k-\epsilon$
- Realizable $k-\epsilon$
- SST $k-\omega$

All analyzed models were tested with identical boundary conditions. Afterwards selected points matching regions measured in full scale experiment (figure 6.6 on page 46) were exported (Matlab script, Appendix E) and compared with each other. Comparison between models and measurements is presented below.

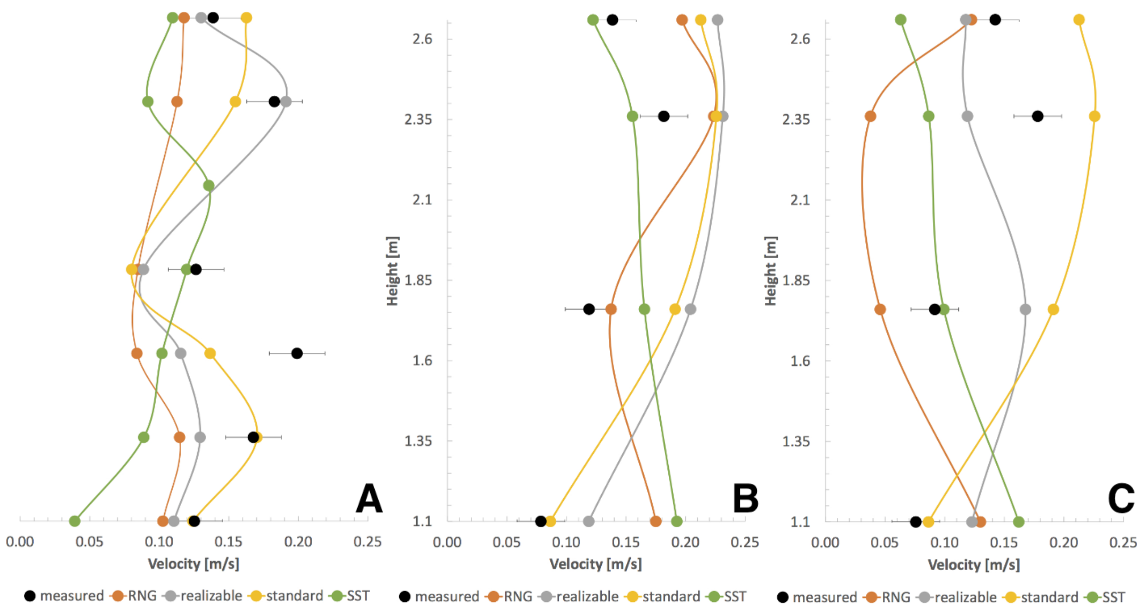

Figure 7.15. Comparison between measurements and turbulence models. A - ceiling grid, B - pole behind manikin, C - pole in front of manikin. Refer to Appendix G for all analyzed cases.

All obtained results have been analyzed. As no turbulence model fully covers measurements pattern, velocity magnitudes in most crucial areas have been compared instead. Comparison is presented in table 7.4. Probes used for experimental testing are burdened with measurement error equal approximately 0,02 m/s. As such, error bars were added to measured data sets in each of graphs as well as possible offset between measurement and CFD was taken into consideration when selecting best fitting model. Exact measurement error of probes with relation to velocity magnitude is presented in table 7.3.

Range	Error
0 - 1 m/s	±2% of reading and ±0,02 m/s
1 - 5 m/s	±5% of reading

Table 7.3. Accuracy of measurement, Dantec 54R10 probes, [Martin Heine Kristensen, 2015].

Turbulence model	Feet height [m/s]	Neck height [m/s]	Measured (feet/neck)±0,02 [m/s]
k-ϵ Standard	0,04	0,09	0,06/0,08
k-ϵ Realizable	0,17	0,07	0,06/0,08
k-ϵ RNG	**0,05**	**0,11**	**0,06/0,08**
k-ω SST	0,04	0,09	0,06/0,08

Table 7.4. Crucial parameters comparison, 10 l/s primary air flow rate.

Table 7.4 presents comparison between various turbulence models in comparison to measurements obtained within areas of feet and neck of manikin for 10 l/s of primary air supply case. Although table present only once case out offive analyzed, turbulence model which produced least offset from measurements was RNG k-ϵ which has been bolded in mentioned table. As such, RNG k-ϵ has been selected as a turbulence model used for Annex 20 Room simulations.

7.8 Fluent setup

For both CFD models (both "Cube" and Annex 20 room) same Fluent setup was used. Final selected turbulence model was RNG k-ϵ. Air has been defined with Boussinesq approach with values as follows: density - 1.225, Cp - 1006.43, thermal conductivity - 0.0242, viscosity - 1.7894e-05, thermal expansion coefficient 0.0034. Wall treatment has been resolved with scalable wall function. Boundary conditions were set as follows:

Boundary	Boundary type (Fluent)
inlet	velocity-inlet
outlet	outflow
walls	wall
table	wall
heat sources	wall
beam elements	wall

Table 7.5.

Solution methods used for simulations:

Variable	Solution method
Scheme	SIMPLE
Gradient	Least Squares Cell Based
Pressure	Second Order
Momentum	Second Order Upwind
Turbulent Kinetic Energy	Second Order Upwind
Turbulent Dissipation Rate	Second Order Upwind
Energy	Second Order Upwind

Table 7.6.

Used under relaxation factors are listed below.

URF	Value
Pressure	0.3
Density	0.7
Body Forces	0.7
Momentum	0.3
Turbulent Kinetic Energy	0.8
Turbulent Dissipation Rate	0.5
Turbulent Viscosity	0.8
Energy	0.8

Table 7.7.

Heat load distribution 8

This chapter describes the impact of heat load location on the performance of active chilled beam system. CFD simulation results of standard and shifted heat load distributions are presented.

In practice air distribution in a room is a combination of the ventilation air and thermal flows from the heat sources. Therefore the strength and location of the heat sources is significant factor that must be considered in the design phase. The change of furniture, workstation location, heat source number and strength can change the air distribution in the office. See the figure 8.1 with 3 different scenarios.

For example, when the thermal plumes from heat sources counteract the fresh ventilation air - this can prevent local discomfort. According to Müller et al. [2013] thermal plume above a sitting human body has an upward velocity of approx. 0,25 m/s. If the the thermal plume flow is weaker than the colliding airflow from the two diffusers that will cause discomfort, scenario A. In case of an asymmetric office layout discomfort can be caused by a large air circulation in the room, scenario B. Also the strength of each heat source and interaction between the thermal plumes can affect room air distribution. For example, in scenario C, the thermal plume from one side of room is merging with the airflow from the ventilation.

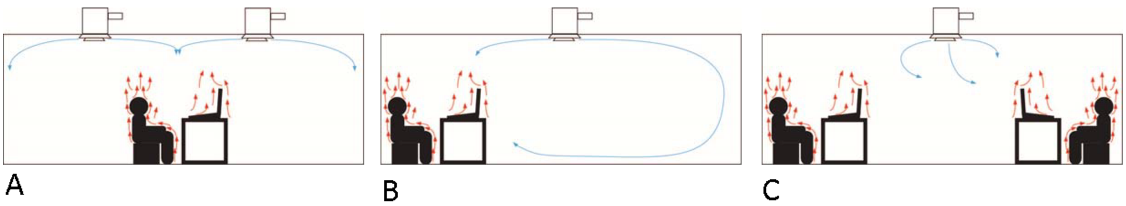

Figure 8.1. Airflow interaction: A - colliding airflow B - asymmetric heat load distribution C - effect of a stronger heat source. [Müller et al., 2013] Figure 8.5

Koskela et al. [2010] investigated asymmetric room layout for an office case where ventilation is delivered with ACBs. According to the research and CFD simulations two main causes of draught risk were found:

- downfall of colliding inlet jets
- large scale circulation caused by asymmetric room layout

Therefore, further the impact of the thermal load distribution on the room airflow pattern is considered for the symmetric and asymmetric work station scenarios. The standard cooling demand of 480 W with fresh air supply of 20 l/s in the geometry of Annex 20 room is simulated.

8.1 Symmetric work stations

Most desirable distribution of heat sources is a standard, symmetric heat load distribution. Study shows that velocity magnitude across regions of interest (around seated manikins) is the lowest out of considered cases, figure 8.2.

The effect of the attached flow and wall jet can be seen as the air moves from wall surface towards the seated occupants. Convective flow from the seated occupant is merged with the primary air, thus enhancing the local discomfort effect. On the other hand, thermal plume from right occupant goes into the induction area of ACB. This shows that the induction principle plays an important role for air distribution in a room with an active chilled beam system.

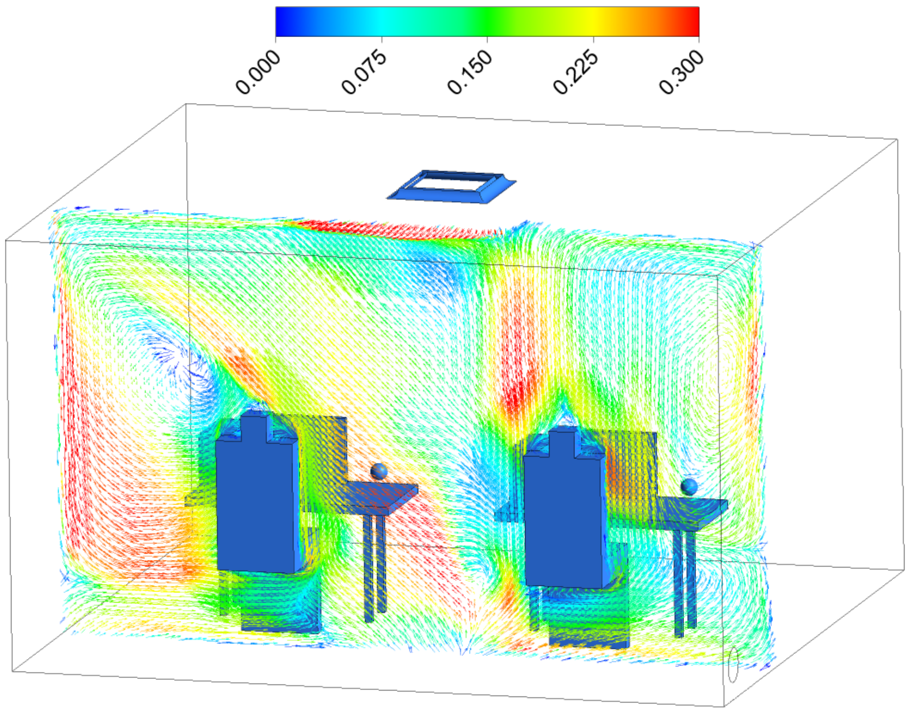

Figure 8.2. Symmetric heat load distribution. Cross section made trough thermal manikin. Fresh air supply - 20 l/s, mixed air flow rate - 74 l/s.

Additionally, the same observation can be seen in the figure 9.3 on page 67. Standard case (dark blue) shows highest capabilities of heat removal maintaining velocity magnitude within acceptable limit of 0,15 l/s.

8.2 Asymmetric work stations

Placing work stations in asymmetric manner causes the raise of velocity in the region around heat sources, see figure 8.3, compared to the previous scenario. Large scale circulation can be observed.

From the previous research it can be seen that the circulation across the space from the heat sources creates high air velocities at the ankle level of the seated occupants. However, with use of ACB, the air movement in the middle of the room, right before the seated occupants, is disrupted. The air is sucked upwards due to the induction principle of ACB.

Additionally, work stations close to wall will suffer from the downdraught from the wall surface. The airflow is merged with the thermal plume from heat sources.

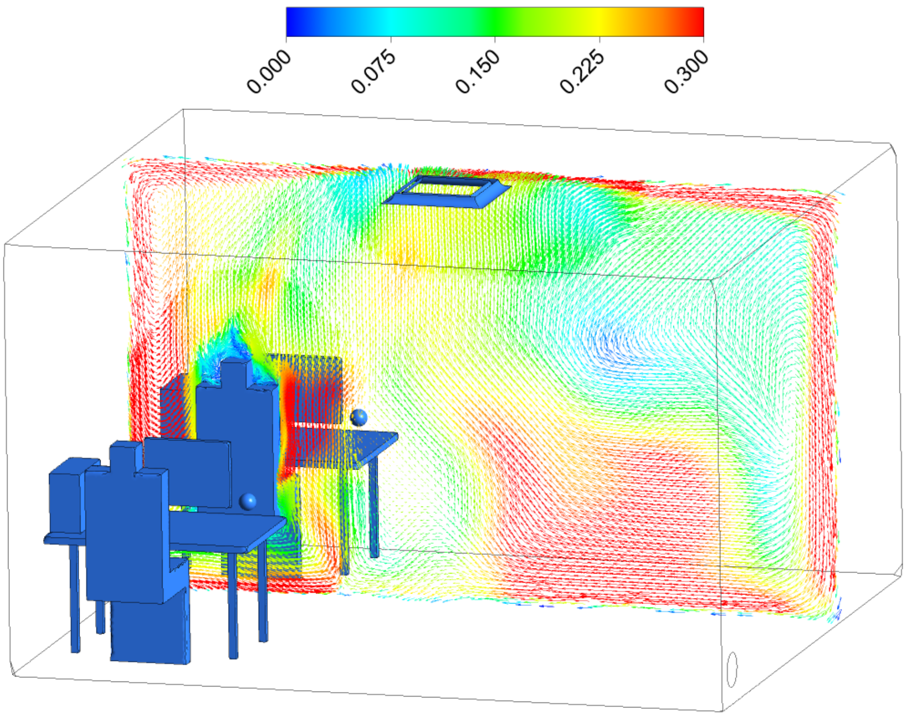

Figure 8.3. Asymmetric heat load distribution. Cross section made trough thermal manikin. Fresh air supply - 20 l/s, mixed air flow rate - 74 l/s.

According to Kosonen et al. [2007b] convective flow from opposing thermal load can cause the supply air wall jet to de-attach from the ceiling and fall into occupied zone before reaching the wall. However it is not clearly visible in this scenario even though the heat sources are very close to the wall.

Uneven heat sources distribution seem to perform slightly worse in comparison to even heat sources distribution in range of lower supply rates (up to approximatelly 55 l/s). For high supply rates however, both distribution seem to create conditions where ventilation system performs with the same efficiency.

8.3 Colliding airflow in scenario with two ACBs

Another scenario with two ACB is considered, see figure 8.4. Each chilled beam supply 10 l/s of fresh air. However, in this situation the total volumetric flow rate from fresh and induced air will be larger, namely 96 l/s (48 l/s + 48 l/s). This can cause higher air speed magnitudes in the room when comparing with standard scenario with the same heat load distribution.

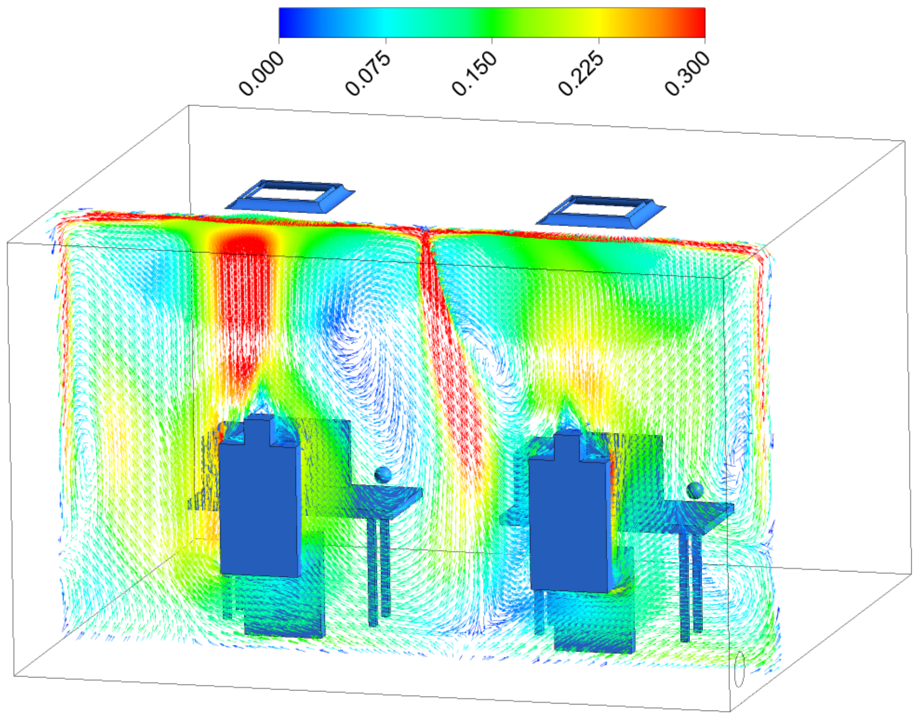

Figure 8.4. Colliding airflow with two ACBs. Cross section made trough thermal manikin. Fresh air supply - 20 l/s, mixed air flow rate - 96 l/s.

Colliding airflow of a cool ventilation air can be observed in the middle of the room. However, in this room setup it does not seem to cause any discomfort for occupants because the merged cold airflow falls downwards, not directly on the occupants. Also the convective flow from thermal manikin can neutralize it, or at least decrease the effect.

8.4 Summary of heat load distribution

REHVA guidebook by Müller et al. [2013] mentions that the use of RANS in CFD modelling fail to predict the interaction of thermal plumes and ventilation air. In these CFD predictions clear images of the thermal plumes can be observed in all presented airflow interaction scenarios. Airflow from the heat sources is merging with supply air. Some of the observations regarding air movement are summarized:

- The effect of the wall jet seem to be affecting local discomfort quite significantly, as it creates high velocity regions close to the occupants, for example in scenario with asymmetric work stations located very close to the wall.

- Interesting observation is that the induction flow rate is affecting the room air distribution quite significantly. In scenario with asymmetric work stations the induction of the warm air is stopping the flow of the large circulation. This creates a separate circulation region in the opposite side of the concentrated heat loads.

- Another observation is that the convective air flow from the heat sources is being drawn into the chilled beam. Therefore it can be predicted that the induction of the warm room air can increase the sensible cooling effects, when the heat sources are placed under the active chilled beam. However, this claim has to be investigated more closely, also with regards to IAQ and mixing efficiency of the room air. Basically this is the scenario with two ACBs - each above the one work station.

Design Chart - Annex 20 room 9

In this chapter the thermal comfort Design Chart for Annex 20 room is presented. All considered cases are plotted in the graph and compared with each other as well as original Design Chart is shortly introduced.

As mentioned before Annex 20 room is a room with specific dimensions and heat load distribution - single-cell room with two sitting occupants working at two workstations. In order to provide comparable results between systems, the same setup has to be used for each tested ventilation system.

After investigation of air movement around the ACB as well as velocity distribution within occupied zone of room in both isothermal and non-isothermal conditions, CFD-model was developed and validated based on the data collected during the full-scale testing.

9.1 Data acquisition

Not entire occupied zone was taken into consideration when creating the Design Chart, data acquisition has been limited to certain areas. Four areas (around legs and necks of both manikins) were selected in order to acquire data for Design Chart. Collected cell-center values belonging to mentioned spaces were filtered from solution, averaged and highest of four obtained magnitudes was selected as final result for a given case. In order to obtain 0,15 m/s limiting curve, linear interpolation has been used. Areas of interest (black squares) are presented in figure 9.1. Data points calculation methodology used for the Design Chart is described in Annex I.

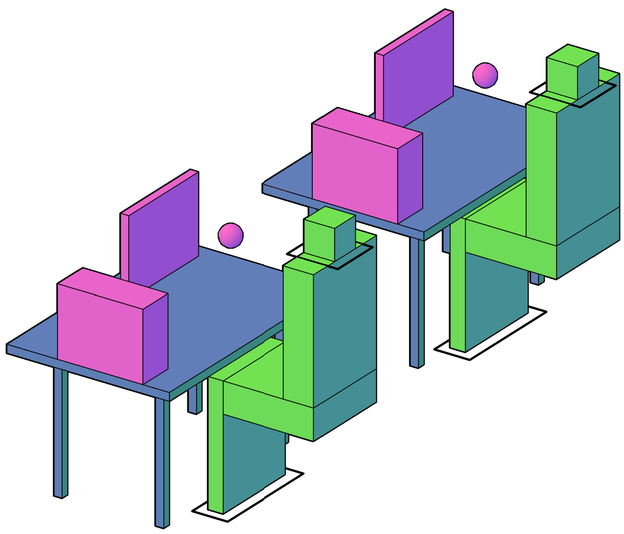

Figure 9.1. Areas used for data acquisition for chart (black squares).

9.2 Design Chart - original research

Design Chart shows capability of different ventilation systems to remove heat while conserving comfort conditions within occupied zone. Figure 9.2 shows previous experimental research on various ventilation systems with constant heat load conducted by [Nielsen and Jakubowska, 2009].

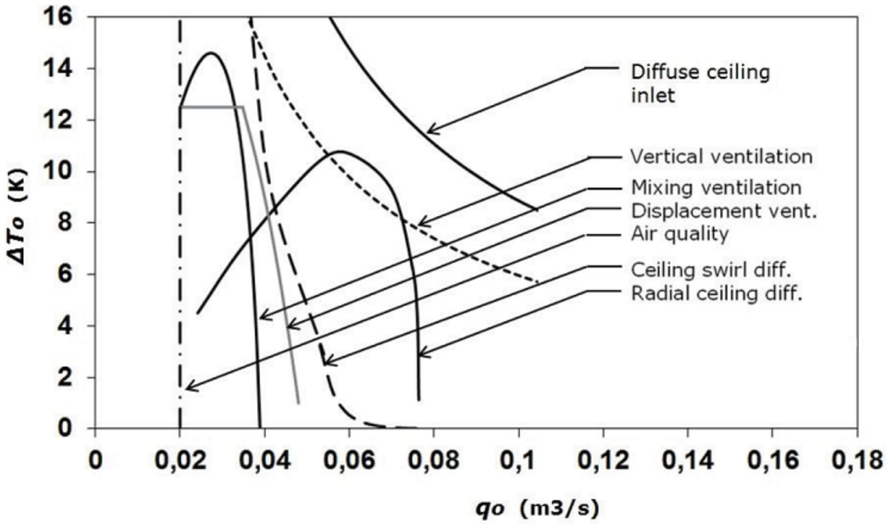

Figure 9.2. Design Chart for different ventilation systems. [Nielsen and Jakubowska, 2009].

Design Chart allows to compare six different air distribution systems. From figure 9.2 best performing ventilation systems are *Diffuse ceiling ventilation* (DCV) and *Vertical ventilation* systems. Vertical ventilation system is a ceiling-mounted low-impulse textile-based ventilation, Nielsen et al. [2005], produced by *KE Fibertec*. DCV also is a low-impulse air distribution system that supplies fresh air trough the whole celling area. Both systems can remove high amount of heat loads and do not produce draught with much higher air flow rates than other systems.

The research Nielsen et al. [2006] and Nielsen [2007] summarize that mixing ventilation (MV) with *Radial ceiling diffuser* and MV with *Ceiling swirl diffuser*, and *Displacement ventilation* (DV) in the Design Chart are limited due to the maximum supply air flow. This is because high volumetric flow rates will create high air velocities inside the occupied zone.

9.3 Design Chart - results

In this project the focus is set on air movement inside the room. The design limitation for acceptable air velocity inside the room is set to 0,15 m/s. Minimum air quality requirement of volumetric flow rate of fresh air is set to 10 l/s per person and thus 20 l/s for the Annex 20 room.

In the graph 9.3 *IAQ-1 beam* is a sum of the minimum fresh air requirement, 20 l/s, plus the induced air volumetric flow rate. Similarly, *IAQ-2 beams* is a sum of two ACB with the same flow rate, 10 l/s, plus the induced air volumetric flow rate.

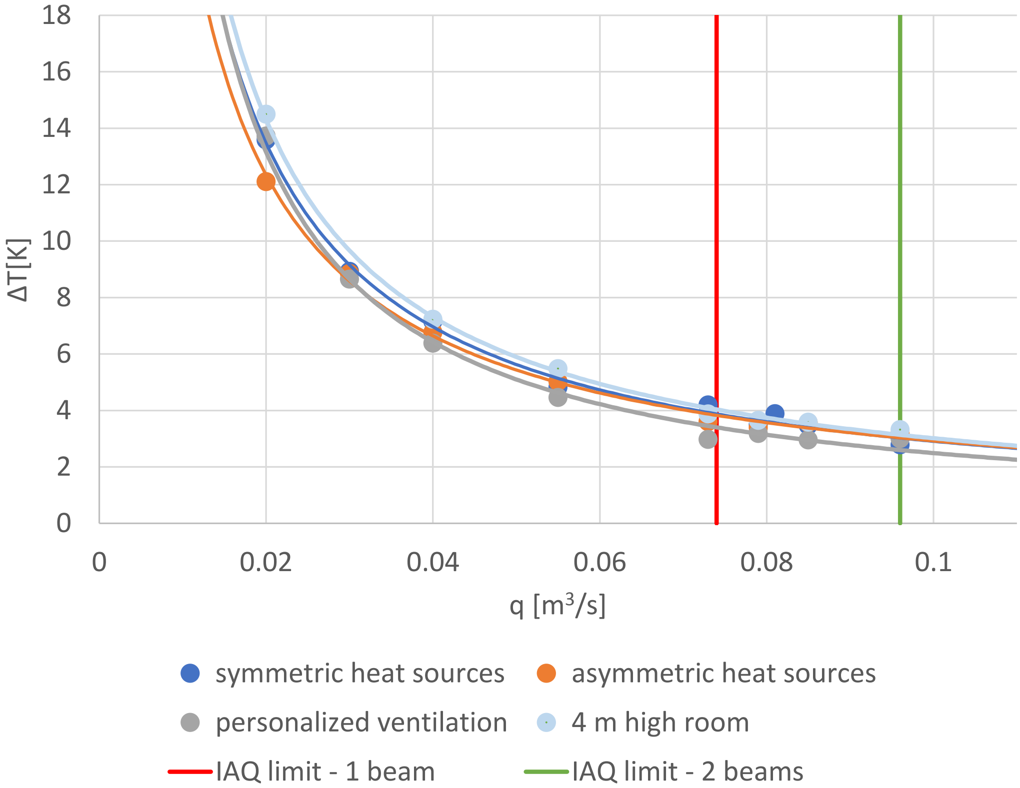

Figure 9.3. Design Chart for ACB, all considered cases.

Heat load distributions scenarios *symmetric heat sources* and *asymmetric heat sources* will create similar Design Chart. The scenario *personalized ventilation* with two ACB each 10 l/s moves the acceptable Design Chart area more to the higher flow rate side. Reason for that is induction ratio. For 10 l/s of fresh air supply, inducted air volume is approximately 38 l/s. Scenario with two beams assumes that each of the beams will supply 10 l/s of fresh air per second as such, IAQ limit has to be shifted to right side of graph (each beam then supplies 10 l/s of fresh air and 38 l/s of secondary air).

Comparison between ACB and other systems is presented in figure 9.4. Chart combines research earlier on various ventilation systems done by [Nielsen and Jakubowska, 2009] with recent work on active chilled beam system. Active chilled beam shows simmilar capacities in comparison to ceiling swirl and radial ceiling diffusers as well as displacement ventilation. Active chilled beam shows high potential of sustaining velocity magnitude below 0,15 m/s requirement in occupied zone in region of higher supply rates (over 60 l/s). Active chilled beam however, loses in comparison to both diffuse ceiling and vertical ventilation systems. Disadvantage of using active chilled beam system is inability to create conditions where sufficient amount of fresh air is being supplied to the room with full control of induction rate at the same time. Currently, setup does not allow to limit supply air volume below 74 l/s (summed volumes of inducted and primary air) with fresh air supply rate at 20 l/s. As such, direct comparison between systems is difficult as all other plotted systems meet IAQ requirement already at supply rate of 20 l/s in comparison to IAQ requirement of 74 l/s for ACB system.

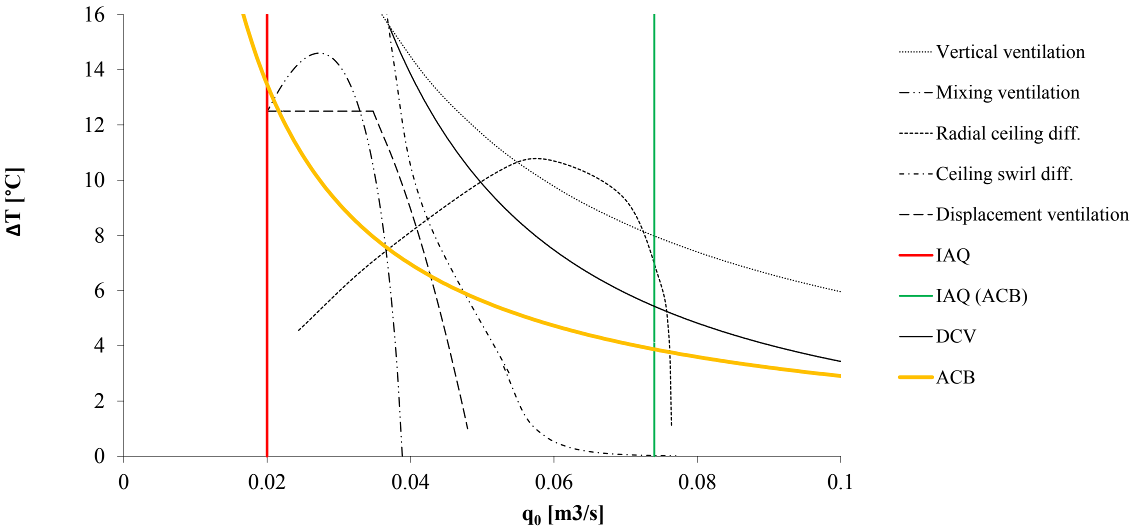

Figure 9.4. Design Chart [Nielsen and Jakubowska, 2009] with ACB system added to the graph.

Discussion 10

Isothermal velocity profile measurements

PIV-method was used to visualize the jet flow at the exit region of the active chilled beam. Even though the measurement results showed promising air distribution pattern, namely, showing clearly the room air entrainment and wall jet characteristics, the method still was regarded as not good for the current research. One of the few limitations was that the laser reflections limit the research area to the ceiling and chilled beam surfaces. Also PIV result precision proved to be dependant on many parameters that can be controlled by the PIV system operator. To mention few - 'the time between pulses' and window interrogation area size. Furthermore the seeding particle density straight affect acquired PIV image quality.

CFD

Two CFD predictions models of Lindab Plexus 60 chilled beam model were developed; simplified and full beam model. Simplified model was designed with precise outlet slot geometry. The simplification was made to the induction region of the ACB. It was set up as the - outlet. Mixed air flow rate was calculated using Lindab [c]. CFD simulation results proved to be sufficiently close to the hot-sphere anemometer readings in full-scale testing facility 'Cube'.

CFD simulation results of the Annex 20 room leave some level of uncertainty, mainly due to differences in size and heat load distribution in comparison to the full-scale testing facility "Cube" that was used for field measurements.

Design Chart

When comparing active chilled beam (ACB) with other conventional ventilation systems, the main difference is that ACB are based on the induction principle. This means that at the same primary air flow rates ACB will induce the warm room air, mix it with the primary air and thus the flow rate of mixed air supply flow rate will be much higher than in case with conventional ventilation air system.

Two methods can be used for obtaining the air flow rate value in the Design Chart. In first method only the volumetric flow rate of the primary air is used in the x-axis of the Design Chart. This value will show the same IAQ requirements as the other conventional ventilation systems. The second method would be to use the mixed primary and induced air flow rates. These flow rates will be much higher (approx. 5 times) than in the first method.

Conclusions 11

PIV

PIV measurement system has it's advantages and disadvantages. On one side PIV can show velocity measurements as a vector field which is really helpful in terms of CFD validation. Measurements provide both direction and magnitude, in contrast to hot-sphere anemometer system which is limited to magnitude only. On the other hand, PIV measurements show high level of uncertainty. Variation of parameters such as delay between frames may lead to wrong results and as such, has to be carefully adjusted, according to formulas or tools provided by acquisition software producer. Additionally, PIV system is very sensitive to seeding. Too dense or too scarce seeding can also lead to measurement error and needs to be adjusted accordingly. Study showed that in order to validate PIV analysis, measurements with another system should be conducted, for example hot-sphere anemometers and PIV can be used as a supplementary method.

Full-scale test

Full-scale testing was used only as a source of supplementary data for CFD modelling. Various distribution of anemometer probes resulted in vast amount of data that was later used. Obtaining data from full-scale testing resulted in more accurate (based on measurements and adjustments) boundary conditions for the CFD models.

CFD

In order to validate Annex 20 Room, data collected during "Cube" tests was compared with "Cube" CFD model. Once agreement was stated between CFD model and measurements, boundary conditions were transfered to Annex 20 Room. Two beam models (full and simplified) were developed and tested in order to state which approach will perform better. Simplified beam model has been used for CFD simulations. It has been verified that simplified model outlet can reproduce sufficiently close to reality flux through the surface, simulating induction rate that occurs for ACB. Several turbulence models were tested and RNG $k-\epsilon$ was selected as best matching to flow conditions obtained during the experiments. Four different Annex 20 Room cases were developed for the study, analysing different heat source distribution (symmetric and asymmetric) as well as personalized ventilation approach (diffusers above heads of occupants) and 4 meters high room. Study shows that best performing solution and as such, most optimal one is distributed heat sources. All cases, however show that differences in performance almost disappear in region of high supply rates (over 50 l/s).

Design Chart

Thermal comfort is evaluated in the the geometry and heat load distribution of Annex 20 Room model. This allows to compare the performance of the ACB system with other conventional ventilation systems. The results show that in order to provide air velocities below 0,15 m/s in this room set-up, ACB system is limited with regards to airflow rate. This is explained with the induction of the warm room air - as it magnifies the airflow rate from the ACB terminal and therefore can create draught risk in the room. Annex 20 room equipped with ACB terminal unit therefore perform worse than some other ventilation systems considered in previous research made by [Nielsen and Jakubowska, 2009]. Study shows that ACB performs better than mixing ventilation, radial ceiling and ceiling swirl diffusers in range of higher supply rates (more than 50 l/s). Although the difference between heat distribution does not significantly change capability of ACB to mantain comfortable indoor conditions, it was observed that symmetric heat distribution performed slightly better than other considered cases (asymmetric heat distribution and personalized ventilation with symmetric heat distribution).

Pratical approach

In practice following procedure is applied to configure the beam. Initially primary air flow rate at the indoor air quality requirement is set. In analyzed system (Lindab Plexus), primary air range depends on pressure and induction rate and is result of both primary air supply as well as pressure drop. In order to gain more control over induction rate, JetCone system can be adjusted (either pushed in or pulled out) to control pressure drop. As such, in order to have lowest possible induction rate, JetCones would be fully pulled out of the slots, while to obtain highest possible induction rate, JetCones would be pushed into the slots.

Bibliography

ASHRAE, 2007. ASHRAE. *2007 ASHRAE Journal. Chilled Beam Cooling.* ASHRAE, 2007.

ASHRAE, 2011. ASHRAE. *ASHRAE Handbook - HVAC Applications.* ASHRAE Handbook. American Society of Heating, Refrigerating and Air-Conditioning Engineers, 2011.

ASHRAE and REHVA, 2015. ASHRAE and REHVA. *Active and Passive Beam Application Design Guide.* ASHRAE Guide book. W. Stephen Comstock, 2015.

Cao et al., 2009. Guangyu Cao, Markku Sivukari, Jarek Kurnitski, Mika Ruponen and Olli Seppänen. *Particle Image Velocimetry (PIV) application in the measurement of indoor air distribution by an active chilled beam.* Elsevier: Building and Environment, 2009.

Cao et al., 2010. Guangyu Cao, Markku Sivukari, Jarek Kurnitski and Mika Ruponen. *Particle Image Velocimetry (PIV) application in the measurement of indoor air distribution by an active chilled beam.* Elsevier: International Journal of Heat and Fluid Flow, 2010.

Cao et al., 2013. Xiaodong Cao, Junjie Liu, Nan Jiang and Qingyan Chen. *Particle image velocimetry measurement of indoor airflow field. A review of the technologies and applicationsm.* Elsevier: Energy and Buildings, 2013.

Carl Erik Hyldgård and Steen-Thode, 1997. E.J. Funch Carl Erik Hyldgård and M. Steen-Thode. *Grundlaggende Klimateknik og Bygningsfysik.* I ISSN: 1395-8232 U9714, Handbook. Aalborg University, 1997.

Chen et al., 2015. Can Chen, Wenjian Cai, Youyi Wang and Chen Lin. *Further study on the heat exchanger circuitry arrangement for an active chilled beam terminal unit.* `https://goo.gl/yMGmSZ`, 2015.

CIBSE Journal and Tim Dwyer. CIBSE Journal and Tim Dwyer. *Module 65: Applying chilled beams to reduce building total carbon footprint.* `http://www.cibsejournal.com/cpd/modules/2014-06/`. last visited: 20-03-2017.

DantecDynamics. DantecDynamics. *Measurement principles of PIV.* `http://www.dantecdynamics.com/measurement-principles-of-piv`. last visited: 12-11-2016.

Dréau et al., 2014. Jérôme Le Dréau, Per Heiselberg and Rasmus Lund Jensen. *A full-scale experimental set-up for assessing the energy performance of radiant wall and active chilled beam for cooling buildings.* `https://goo.gl/2s5QWY`, 2014.

Dynamics, 2015. Dantec Dynamics. *DynamicStudio User's Guide.* User Manual. Dantec Dynamics, 2015.

Dynamics, 2011. Dantec Dynamics. *80x80 Light-sheet series. Installation and User's guide.* User Manual. Dantec Dynamics, 2011.

Filipsson et al., 2016. Peter Filipsson, Anders Truschel, Jonas Graslund and Jan-Olof Dalenback. *Induction ratio of active chilled beams - Measurement methods and influencing parameters.* `https://goo.gl/AZFGWj`, 2016.

Gericke and Scholz, 2014. Timo Gericke and Peter Scholz. *PIV compared to classical measurement techniques using the example of turbulent flow in the wake of an air outlet.* `https://goo.gl/bk6UPt`, 2014.

Guan and Wen, 2016. Zheming Guan and Changyun Wen. *Geometric optimization on active chilled beam terminal unit to achieve high entrainment efficiency.* `https://goo.gl/5AmXDF`, 2016.

Koskela et al., 2010. Hannu Koskela, Henna Haggblom, Risto Kosonen and Mika Ruponen. *Air distribution in office environment with asymmetric workstation layout using chilled beams.* https://goo.gl/XgKth8, 2010.

Kosonen et al., 2007a. Risto Kosonen, Arsen Melikov, Boryana Yordanova and Lyuben Bozkhov. *Impact of heat load distribution and strength on airflow pattern in rooms with exposed chilled beams.* https://goo.gl/u47fU53, 2007.

Kosonen et al., 2007b. Risto Kosonen, Maija Virta and Arsen Melikov. *The impact of thermal loads on indoor air flow.* https://goo.gl/FrGXy3, 2007.

Lindab, a. Lindab. *Lindab Plexus. Supply air beam.* https://goo.gl/kF0r8Q. last visited: 15-11-2016.

Lindab, b. Lindab. *Lindab Plexus. Supply air beam. Installation instructions.* https://goo.gl/MJQe2B. last visited: 26-04-2017.

Lindab, c. Lindab. *Lindab Quick Selection Tool. Waterborne selector.* https://goo.gl/s0kT4G. last visited: 13-03-2017.

LitronLasers, 2013. LitronLasers. *Nano PIV series. Laser System User Manual.* User Manual. Litron Lasers Ltd, 2013.

Markus Raffel and Christian E.Willert and Steve T.Wereley and Jürgen Kompenhans, 2007. Markus Raffel and Christian E.Willert and Steve T.Wereley and Jürgen Kompenhans. *Particle Image Velocimetry. A Practical guide. 2nd Edition.* ISBN: 978-3-540-72307-3. Berlin and Heidelberg: Springer-Verlag, 2007.

Martin Heine Kristensen, 2015. Rasmus Lund Jensen Martin Heine Kristensen, Jakob Søland Jensen. *Air Temperature Measurements Using Dantec Draught Probes.* http://goo.gl/w0WSPd, 2015.

Munson et al., 2013. Bruce R. Munson, Theodore H. Okiishi, Wade W. Huebsch and Alric P. Rothmayer. *Fundamentals of Fluid Mechanics-7th edition.* ISBN: 978-1-118-11613-5. John Wiley and Sons, Inc., 2013.

Mustakallio et al., 2016. Panu Mustakallio, Zhecho Bolashikov, Kalin Kostov, Arsen Melikov and Risto Kosonen. *Thermal environment in simulated offices with convective and radiant cooling systems under cooling (summer) mode of operation.* https://goo.gl/XFO59e, 2016.

Müller et al., 2013. Dirk Müller, Claudia Kandzia, Risto Kosonen, Arsen Krikor Melikov and Peter Vilhelm Nielsen. *Mixing Ventilation. Guide on mixing air distribution design.* REHVA guide book. Federation of European Heating, Ventilation and Air-conditioning Associations, 2013.

Nielsen, 2007. Peter Vilhelm Nielsen. *Analysis and Design of Room Air Distribution Systems.* http://goo.gl/jU8ZCS, 2007.

Nielsen and Jakubowska, 2009. Peter Vilhelm Nielsen and Ewa Jakubowska. *The Performance of Diffuse Ceiling Inlet and other Room Air Distribution Systems.* http://goo.gl/wHWNwC, 2009.

Nielsen et al., 2005. Peter Vilhelm Nielsen, Claus Topp, Mads Sennichsen and Heine Andersen. *Air Distribution in Rooms Generated by a Textile Terminal - Comparison with Mixing and Displacement Ventilation.* https://goo.gl/tK16yS, 2005.

Nielsen et al., 2006. Peter Vilhelm Nielsen, Thomas Heby and Bertil Moeller-Jensen. *Air Distribution in a Room with Ceiling-Mounted Diffusers - Comparison with Wall-Mounted Diffuser, Vertical Ventilation, and Displacement Ventilation.* https://goo.gl/w6xlxJ, 2006.

Rhee et al., 2015. Kyu-Nam Rhee, Mi-Su Shin and Sun-Ho Choi. *Thermal uniformity in an open plan room with an active chilled beam system and conventional air distribution systems.* https://goo.gl/BtEimq, 2015.

Sadrizadeh and Holmberg, 2006. Sasan Sadrizadeh and Sture Holmberg. *Evaluation of various turbulence models for indoor airflow prediction: a comparison study with experimental data.* https://goo.gl/sCczvO, 2006.

Sandberg, 2007. Mats Sandberg. *Whole-Field Measuring Methods in Ventilated Rooms.* https://goo.gl/s7ZdVt, 2007.

Sattari, 2015. Amir Sattari. *Investigations of Flow Patterns in Ventilated Rooms Using Particle Image Velocimetry.* https://goo.gl/bnbKhU, 2015.

Virta et al., 2007. Maija Virta, David Butler, Jonas Gräslund, Jaap Hogeling, Erik Lund Kristiansen, Mika Reinikainen and Gunnar Svensson. *Chilled Beam Application Guidebook.* REHVA guide book. Federation of European Heating, Ventilation and Air-conditioning Associations, 2007.

Zhang et al., 2007. Zhao Zhang, Wei Zhang, Zhiqiang (John) Zhai and Qingyan (Yan) Chen. *Evaluation of Various Turbulence Models in Predicting Airflow and Turbulence in Enclosed Environments by CFD. Part 2-Comparison with Experimental Data from Literature.* https://goo.gl/QkOQQj, 2007.

Part IV

Appendix

Plexus 60 - Lindab Quick Selection Tool

A

lindab | we simplify construction

Plexus - Active chilled beams

Project: Master Thesis: Active Chilled Beams - Air Distribution and Efficiency

2017-03-15

Requirements:

Primary airflow rate	qa	10	l/s
Room attenuation	Dr	4	dB
Static nozzle pressure loss	Δpstat	60	Pa
		Cooling	
Room air temperature	tr	22	°C
Temperature gradient in room	tg	0	K
Primary air temperature	tai	18	°C
Water inlet temperature	twi	14	°C
Temperature difference water circuit	Δtw	1.5	K

Results

Temp. difference between room air temp. and mean water temp.	Δtrw	7.23	K
Nominal water capacity	Pnom	246	W
Water flow rate	qw	0.0380	l/s
Corrected water capacity	Pw	245	W
Capacity air	Pa	48	W
Total Capacity	**P**	**293**	**W**
Pressure loss in water circuit	Δpw	2.9	kPa
Added pressure loss in connection	ΔPa	1	
Total air pressure loss in duct	ΔPt	61	Pa
Sound power	LwA	<20	dB(A)
Sound pressure level	LpA	<20	dB(A)
Penetration length, horizontal (min)	Xlp, min	1.1	m
Penetration length, horizontal (max)	Xlp, max	1.1	m
JetCone setpoint's		1+1+1+1	
Air volume / active meter	qa/Lact	4.2	l/s/m
Water capacity / active meter		102	W/m
Induction ratio	qai/qa	4.4	
Induction air volume	qai	44	l/s
Mixed air volume	qam	54	l/s
Mixed air temperature	tam	17.5	°C

Hz	63	125	250	500	1K	2K	4K	8K
Kok [dB]	12	-3	-4	-4	-4	-8	-11	-16
ΔL [dB]	15	14	6	10	7	6	9	17

Plexus - Active chilled beams

Plexus gives many placement possibilities since it fits into the false ceiling 600 x 600 alternative 1200 x 600. Plexus is provided with fixed lamellas which controls the primary air into non-parallel jets in a 360 degree air pattern. The 360 degree air pattern results in shorter air throws (30%) and a draft free indoor climate. Plexus can be used for both cooling, heating and ventilation. Plexus can be equipped with the functions Drypac condensation protection, Regula Secura condensation guard, down fold battery for better accessibility, and pre-mounted valves and actuators. The possibilities are many and the flexibility large.

- Unique 360° diffusion pattern
- Flexible JetCone technology
- Revolutionary heating solution
- Eurovent certified

Order code

Plexus IS60-12-125-B5-10-60

Distribution profile	Radial
Nominal length	0.6
Type	Supply
Function	Cooling 2-pipe system

5.0.0.170314 (Global)
3/15/2017 11:01:43 AM

We reserve the right to make changes without prior notice

PIV setup B

B.1 Time between pulses

In order to estimate 'time between pulses' the following values from figure B.1 were used. This is an example from Dantec Dynamic Studio 2015 with in-plane velocity of 1,0 m/s gives value 1036 μs. Time between pulses was recalculated for each of the flow rates used in experiment.

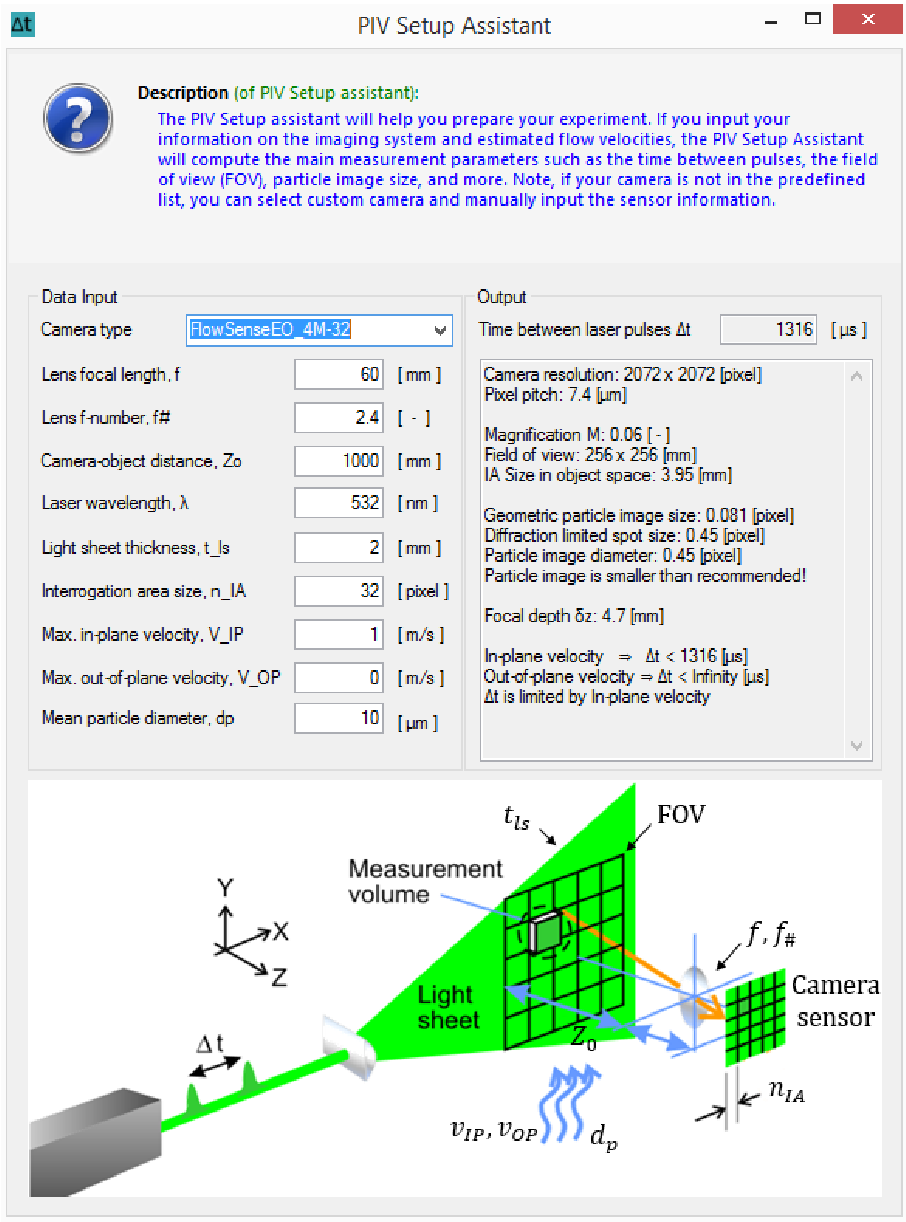

Figure B.1. Estimation of 'time between pulses' using PIV Assistant. [Dynamics, 2015]

B.2 System description

Timer Box

Timing devices that is used together DynamicStudio is TimerBox, model 80N77. See the connection diagram of the system with FlowSense EO camera and Laser in figure B.2.

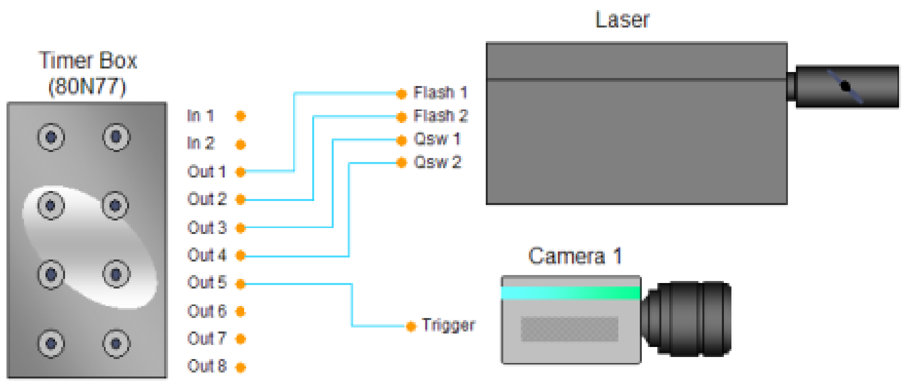

Figure B.2. Cabling of the synchronizing device - Timer box - 80N77. [Dynamics, 2015]

Laser Nano-PIV series

Double-pulsed NdYag laser, Nano-PIV series, model Nano L 200-15 PIV figure B.4. The Nano PIV series utilise an integrated PIV power supply (LPU550). It has built in all the control, power and cooling requirements for the two laser oscillators and 532 nm wavelength generation. Air to water cooling section is using deionized water.

Figure B.3. Nano-PIV Laser, model Nano L 200-15 PIV. LitronLasers [2013]

Laser head positions in figure B.4, option 1 is used in these experiments.

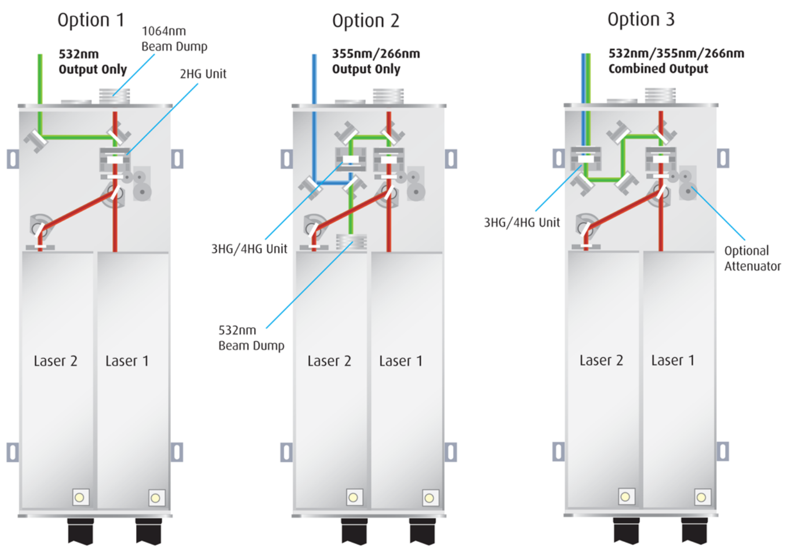

Figure B.4. PIV Laser Head Output Options. LitronLasers [2013]

Light sheet optics

Dantec 80x80 High power light-sheet series generates laser light sheet. Standard light sheet configuration consisting of entrance module, spacer ring, variable focus module, angle module and end ring is used in this project. It can be seen in the figure B.5 below.

Figure B.5. Dantec 80x80 High power light-sheet series. Standard configuration with variable focus module.

Focal length is adjustable continuously with the variable focus module, which is a Galilean like beam expander. Light-sheet divergence angle can be adjusted by changing cylindrical lens with the angle module. [Dynamics, 2011]

Traversing mechanism

3D Traversing mechanism with ISEL controller, figure B.7 and B.6, is used to position the camera with respect to the flow field measurement plane.

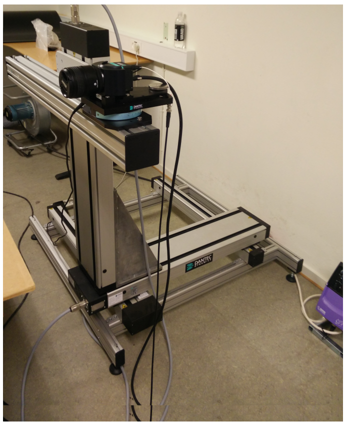

Figure B.6. Dantec Dynamics 3D Traversing mechanism.

Figure B.7. ISEL controller for 3D Traverse mechanism.

B.3 Calibration - calibration target

Camera calibration is performed by recording the images of a calibration target. It defines the co-ordinate system. Calibration target must be aligned with the light sheet and installed in the centre of the flow field that is measured.

Calibration target has a miniature traverse, which allows to translate the target perpendicular to the calibration-plane. If the traverse direction is not perpendicular, the calibration will produce smaller or larger errors depending on the angle.

CFD setup C

C.1 ICEM surface setups

Part	Max. size	Height r.	Num lay.	Tet. size ratio	Min. size	Prism limit
beaminside	10	1.1	5	1.1	5	1.1
beamoutside	10	1.1	5	1.1	5	1.1
ceiling	100	1.1	5	1.1	5	1.1
floor	100	1.1	5	1.1	5	1.1
inlet	20	1.1	5	1.1	5	1.1
lamp	20	1.1	5	1.1	5	1.1
manikin	50	1.1	5	1.1	5	1.1
monitor	50	1.1	5	1.1	5	1.1
outlet	20	1.1	5	1.1	5	1.1
PC	50	1.1	5	1.1	5	1.1
table	100	1.1	5	1.1	5	1.1
wall1	100	1.1	5	1.1	5	1.1
wall2	100	1.1	5	1.1	5	1.1
wall3	100	1.1	5	1.1	5	1.1
wall4	100	1.1	5	1.1	5	1.1

Table C.1. ICEM surfaces setup.

C.2 ICEM global settings

Global mesh size

Maximum element size: 80
All other settings default

Shell meshing parameters

Mesh type: quad dominant
Mesh method: Autoblock
Shell meshing parameters: Autoblock
Ignore size: 3
Surface blocking method: some mapped
Merge mapped blocks: ON

Volume meshing parameters

Mesh type: Tetra/Mixed
Mesh method: Robust (Octree)
All other settings default

Prism meshing parameters

Growth rate: exponential
Initial height: 5
Height ratio: 1.1
Number of layers: 5
Fix marching direction: ON
All other settings default

PIV Velocity Profile Measurements

D

All obtained PIV measurements are presented below. Values of flow rate refer to primary air flow rate used during measurements. Presented figures show velocity vector field with different primary air flow rates (20, 25, 30, 35, 40 l/s).

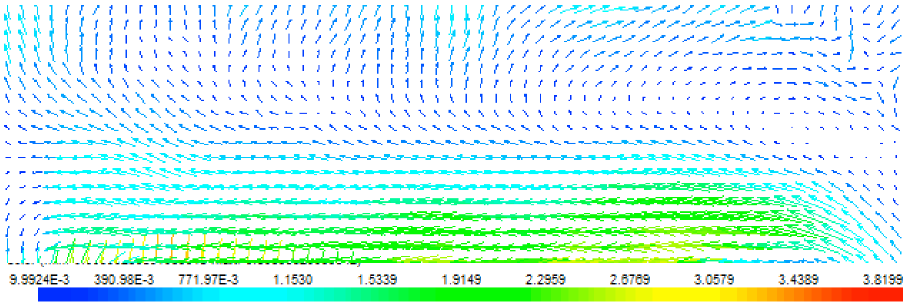

Figure D.1. 20 l/s

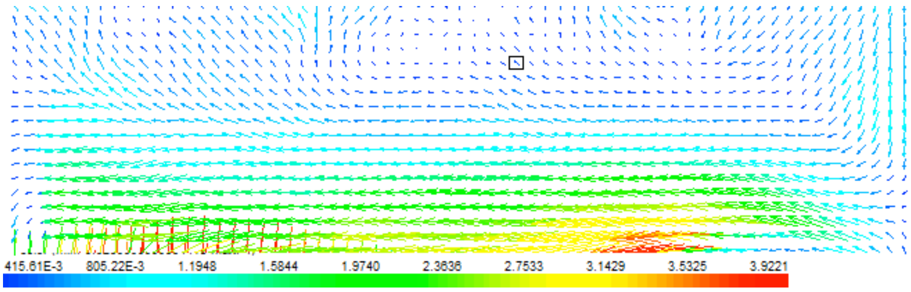

Figure D.2. 25 l/s

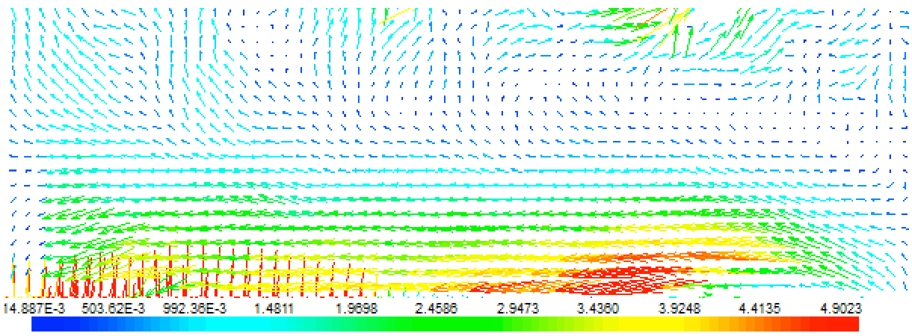

Figure D.3. 30 l/s

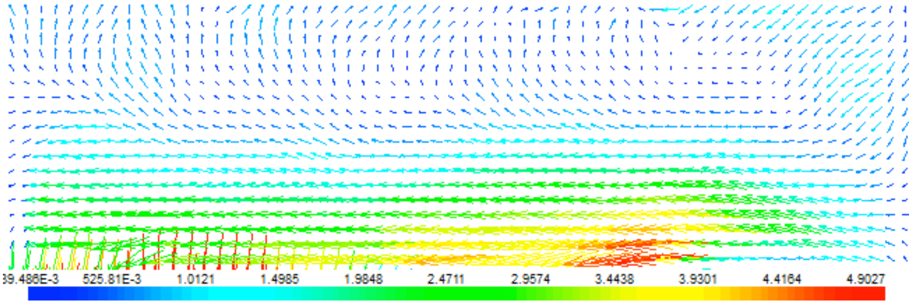

Figure D.4. 35 l/s

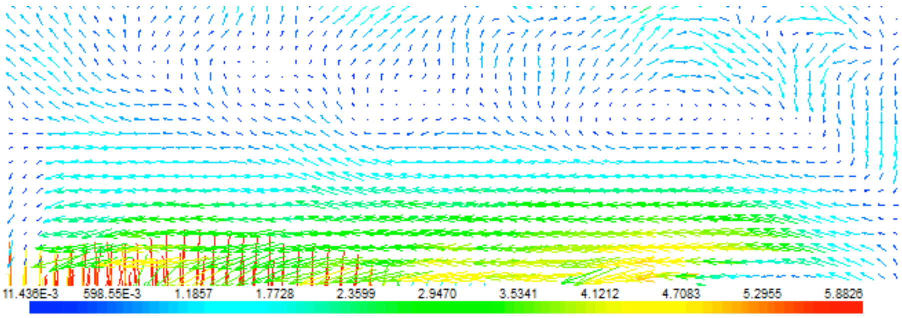

Figure D.5. 40 l/s

Matlab scripts E

Occupied zone filter

```
clear all
%OZ coordinates
xmin=;
xmax=;
ymin=-;
ymax=;
zmin=-;
zmax=;
%Import data
import=importdata('data.txt');
%extract from structure
data=import.data;
%select only OZ (logicals)
selection=data(:,2)>=xmin & data(:,2)<=xmax & data(:,3)>=ymin & data(:,3)<=ymax
& data(:,4)>=zmin & data(:,4)<=zmax;
%import all velocities as numeric values
allvelocities=data(:,5);
%select only velocities within OZ
velocities=allvelocities(selection);
%show max velocity in OZ
MAXVELOCITY=max(velocities)
```

Probes measurement-simulation comparison

```
clear all
clc
disp('Wait...')
results=xlsread('coordinates', 'A:A');
coordinates=xlsread('coordinates', 'B:G');
%import data
clc
disp('Data gets imported now...')
import=importdata('data.txt');
%extract from structure
data=import.data;
%import all velocities as numeric values
```

```
allvelocities=data(:,5);
i=1;
size=size(results,1)
for i=1:size
xmin=coordinates(i,1);
xmax=coordinates(i,2);
ymin=coordinates(i,3);
ymax=coordinates(i,4);
zmin=coordinates(i,5);
zmax=coordinates(i,6);
selection=data(:,2)>=xmin & data(:,2)<=xmax & data(:,3)>=ymin & data(:,3)<=ymax
& data(:,4)>=zmin& data(:,4)<=zmax;
%select only velocities within requirements
velocities=allvelocities(selection);
results(i,2)=max(velocities);
results(i,3)=mean(velocities);
clc
disp(sprintf('Analyzed probe:  %d', results(i,1)))
end
clc
clear xmin xmax ymin ymax zmin zmax import data allvelocities selection velocities
iteration i coordinates size
disp('Obtained results [column 1 - probe number, column 2 - max velocity, column
3 - mean velocity]:')
results
```

Design Chart, the "Cube" F

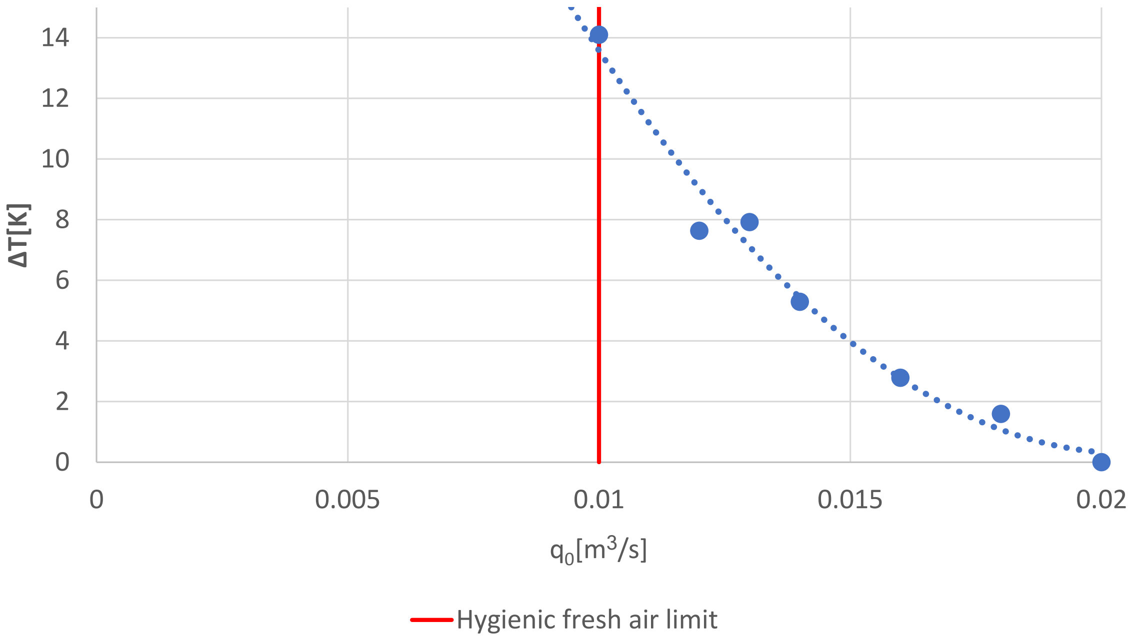

Figure F.1. Design Chart - $Q_0/\Delta T$(inlet-outlet)

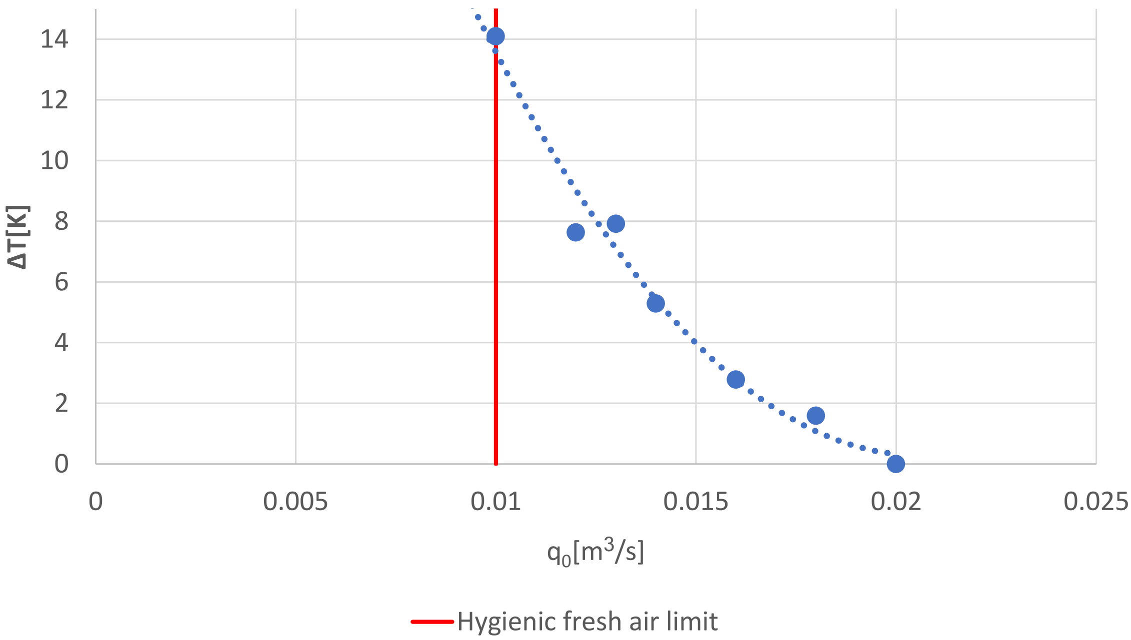

Figure F.2. Design Chart - $Q_0/\Delta T$(beam-outlet)

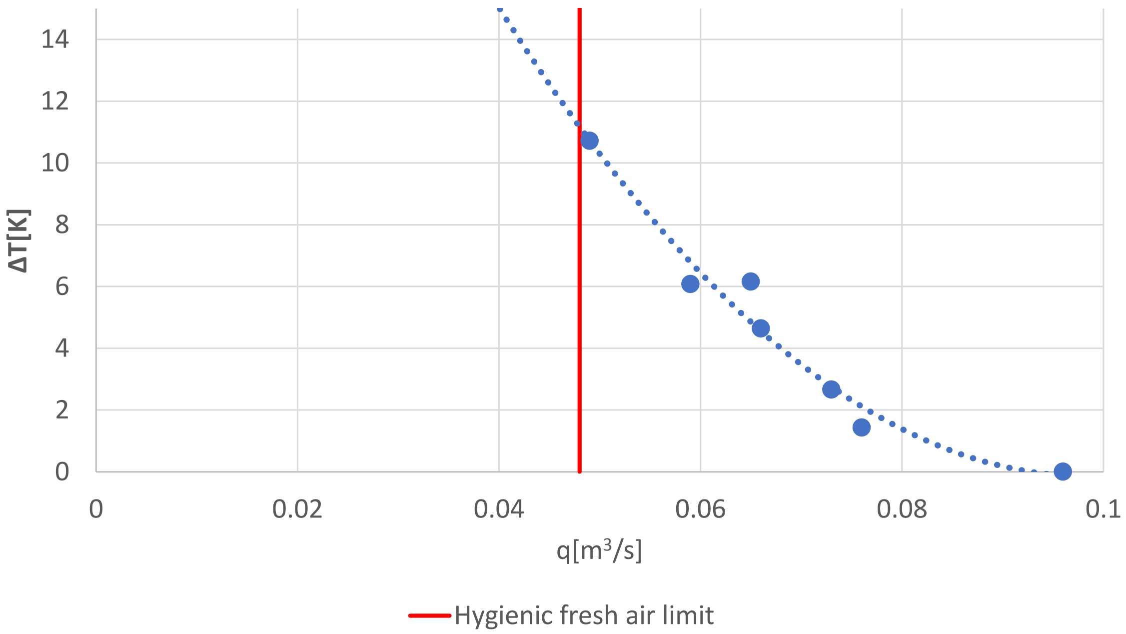

Figure F.3. Design Chart - $Q_{mixed}/\Delta T$(inlet-outlet)

Turbulence models comparison graphs G

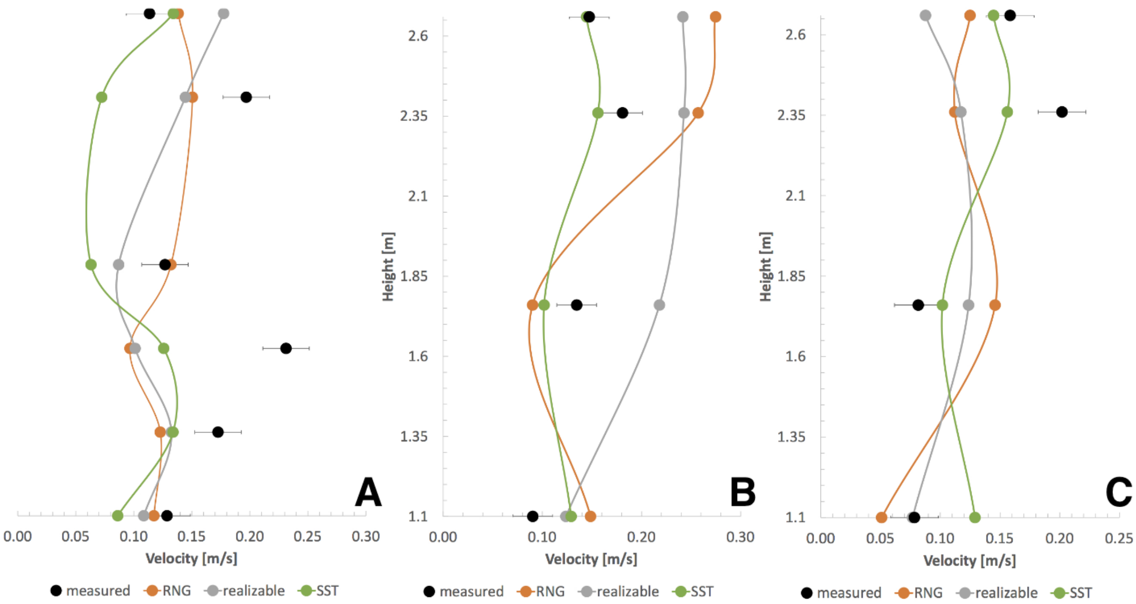

Figure G.1. 11 l/s primary air supply. Comparison between measurements and turbulence models. A - ceiling grid, B - pole behind manikin, C - pole in front of manikin.

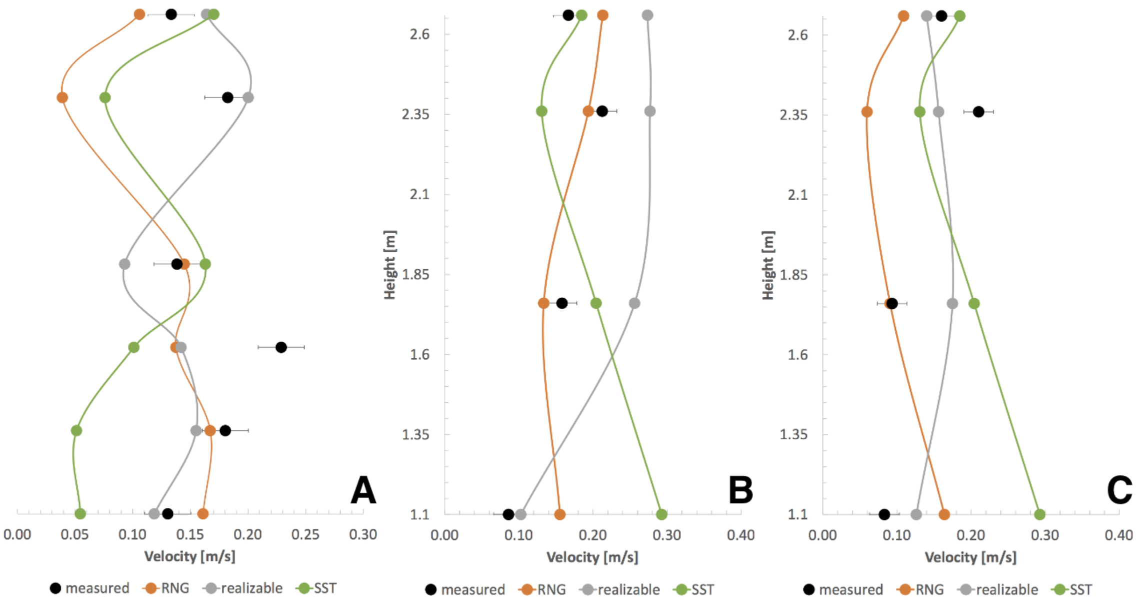

Figure G.2. 12 l/s primary air supply. Comparison between measurements and turbulence models. A - ceiling grid, B - pole behind manikin, C - pole in front of manikin.

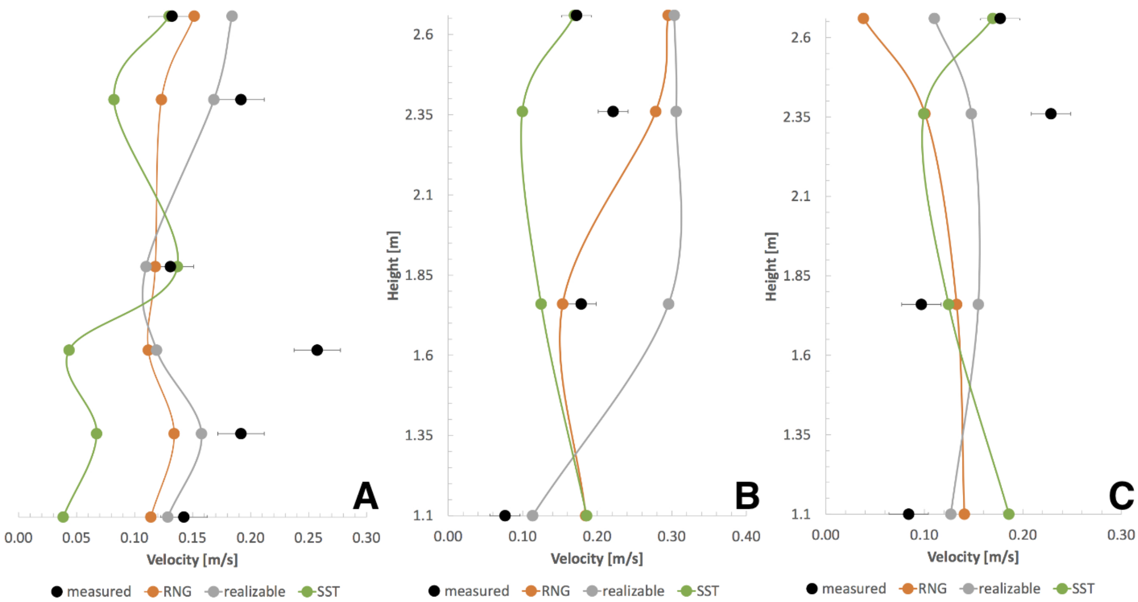

Figure G.3. 13 l/s primary air supply. Comparison between measurements and turbulence models. A - ceiling grid, B - pole behind manikin, C - pole in front of manikin.

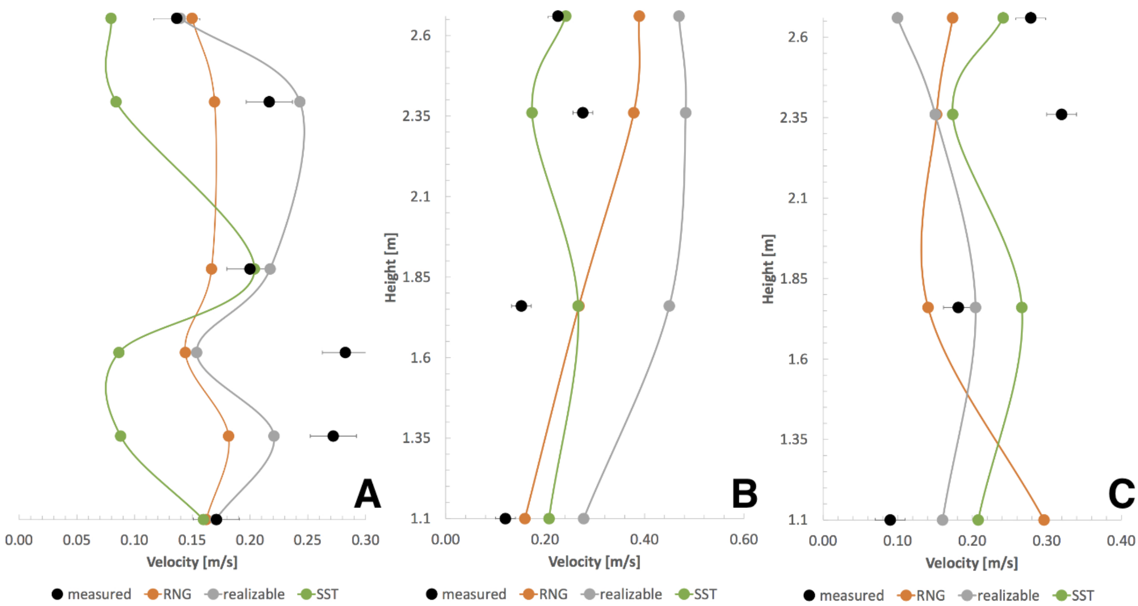

Figure G.4. 20 l/s primary air supply. Comparison between measurements and turbulence models. A - ceiling grid, B - pole behind manikin, C - pole in front of manikin.

Dimension data for CFD models H

H.1 The "Cube" testing facility

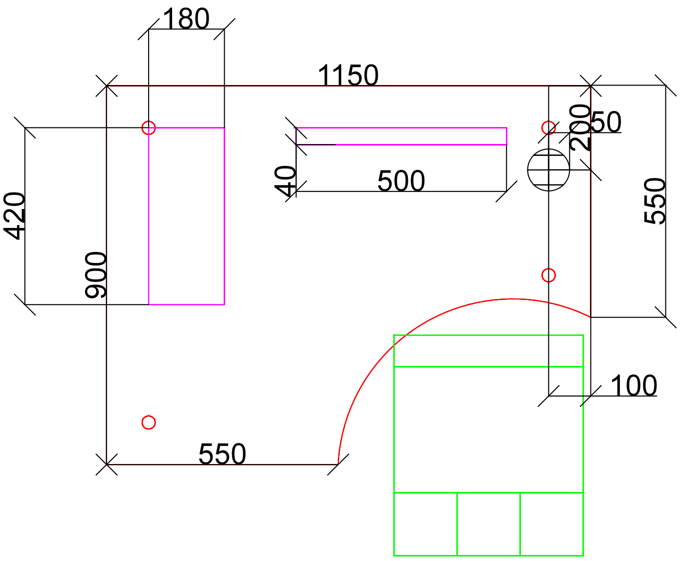

Figure H.1. Workstation, top view. Thermal manikin (green), PC and monitor (purple), table (red), lamp (black).

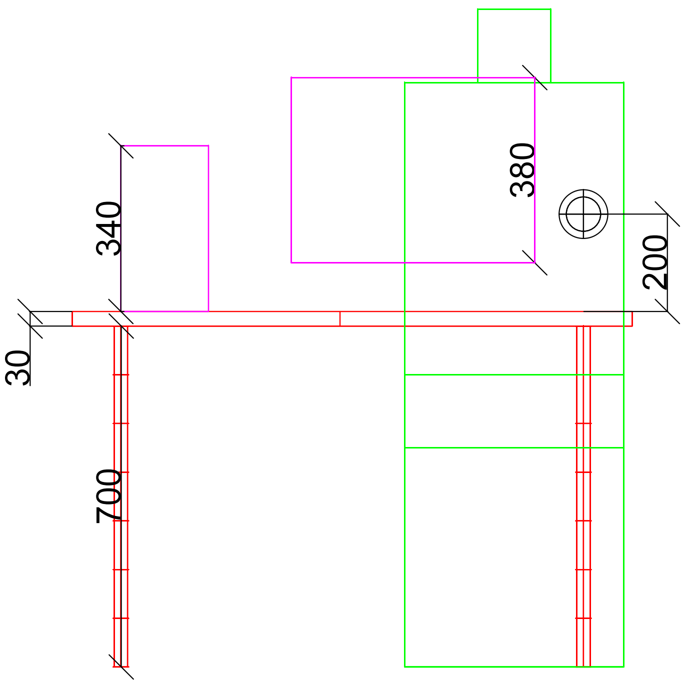

Figure H.2. Work station, front view. Thermal manikin (green), PC and monitor (purple), table (red), lamp (black).

H.2 Annex 20 room

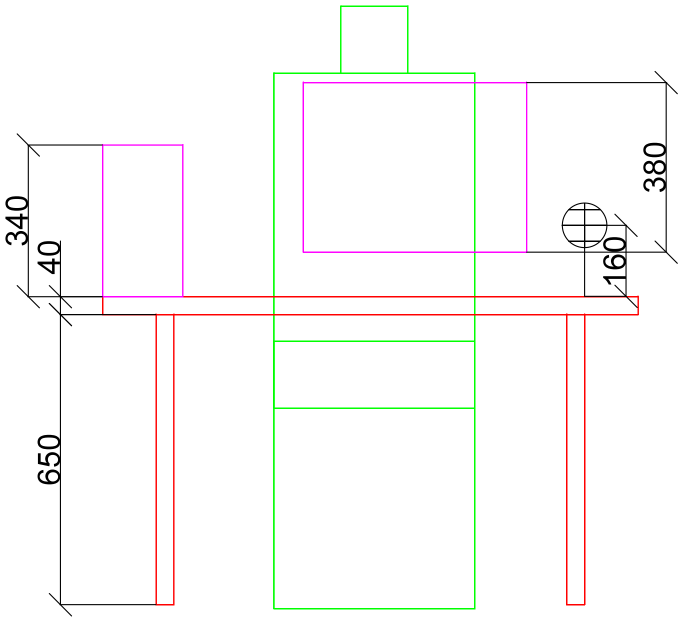

Figure H.3. Work station, front view. Thermal manikin (green), PC and monitor (purple), table (red), lamp (black).

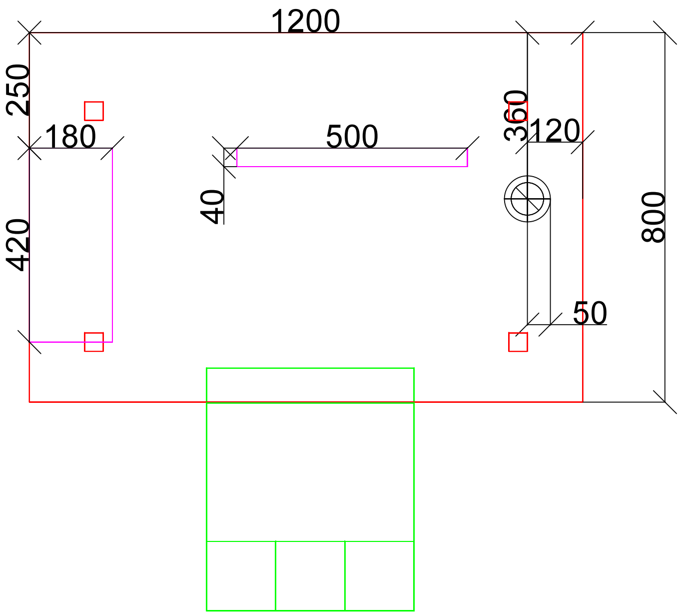

Figure H.4. Work station, top view. Thermal manikin (green), PC and monitor (purple), table (red), lamp (black).

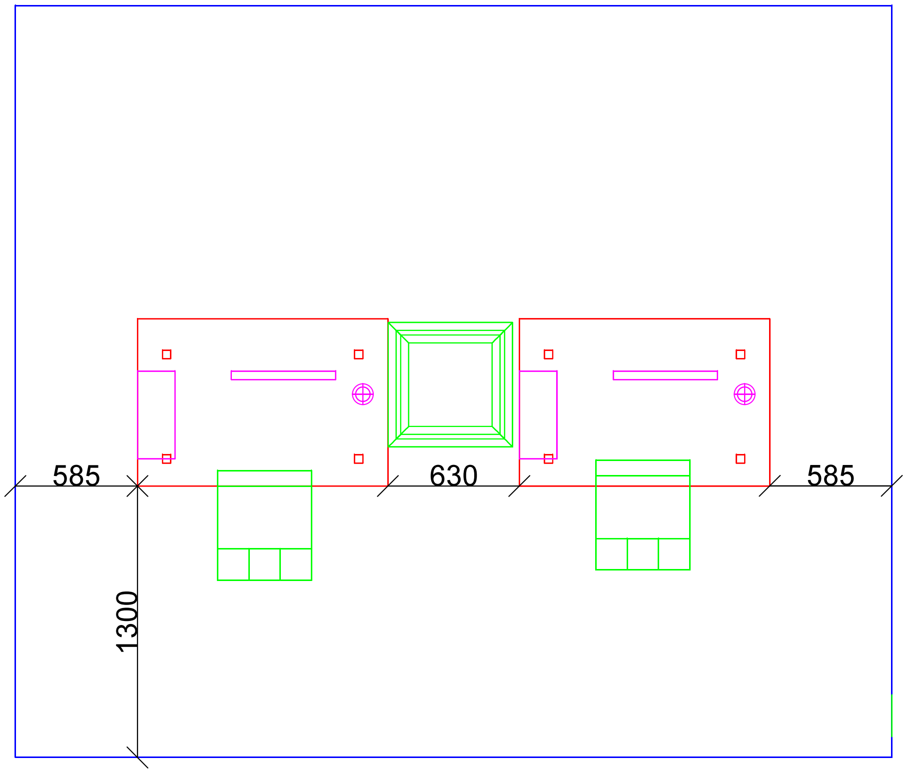

Figure H.5. Location of work stations in the room, symmetric heat sources distribution case

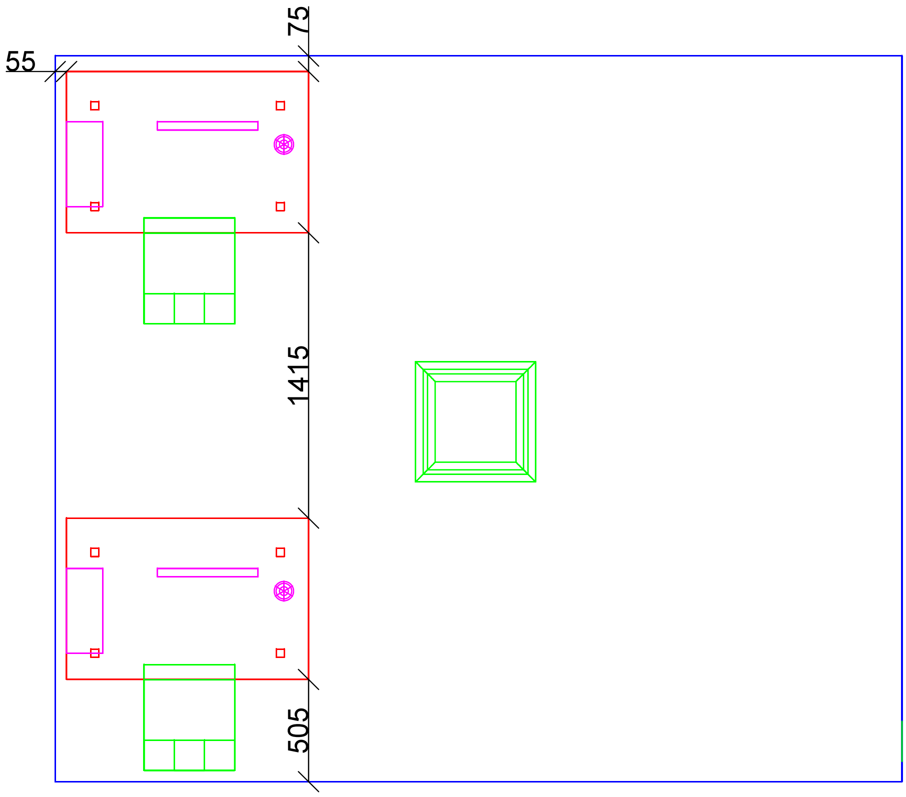

Figure H.6. Location of work stations in the room, asymmetric heat sources distribution case

Design Chart I

I.1 Design Chart calculations

Obtained simulations were assumed to occur in fully developed flow conditions. This means that every obtained point is Reynolds number (Re) independent. As such, obtained data points depend only on Archimedes number (Ar).

Archimedes number is calculated based on following equation:

$$Ar = \frac{\beta g l_0 \Delta T_0}{u_0^2} \tag{I.1}$$

where

β	the thermal expansion coefficient	1/K
g	the gravitational acceleration	m/s^2

Parameters β, g and l_0 are constant, equation I.2 is used instead.

$$constant = \frac{\Delta T_0}{q_0^2} \tag{I.2}$$

Every point which was later plotted in Design Chart was calculated based on two points with the same (similar) Ar number. In order to obtain a point on 0,15 m/s limiting curve, linear interpolation is used, equation I.3.

$$Y = ((X - X1)(Y2 - Y1)/(X2 - X1)) + Y1 \tag{I.3}$$

where

$X1, Y1$	first point's coordinates
$X2, Y2$	second point's coordinates
X	target velocity magnitude (0,15)
Y	interpolated value (q_0, ΔT)

I.2 Reynolds number independency study

Re independent flow regions in the test room has to be investigated. Re is calculated by equation I.4, where a special attention is given to the characteristic length, l_0, and the inlet air velocity, u_0.

$$Re = \frac{\rho u_0 l_0}{\mu} \tag{I.4}$$

where

ρ	is the density of air [kg/m^3]
u_0	is the inlet air velocity [m/s]
l_0	is the characteristic length [m]
μ	is the dynamic viscosity of air [kg/(m·s)]

From Munson et al. [2013], air's density and dynamic viscosity at 20 °C are 1204 kg/m^3 and $1.82 \cdot 10^{-5}$ kg/(m·s), respectively.

Active chilled beam involves some difficulties when evaluating the parameters used in Re calculations. Firstly, estimation of l_0 is complicated due to the complex geometry of the air terminal device. The characteristic length for the experiments is calculated as $\sqrt{a_0}$, where a_0 is the summed nozzle area of the ACB through which primary air is supplied.

Further, calculation of velocity u_0 can be done either using primary air flow rate or the mixed air flow rate with the induced room air.

Re independency is evaluated for the "Cube" test room measurements.

I.2.1 Re independency - primary airflow rate

The primary air flow rate, Q_1, is varied from 14 l/s to 20 l/s. The velocity at the measurement points is normalized with u_0. Re independent flow would mean that by increasing the Re, dimensionless velocity at some specific Re value will stop changing.

The dimensionless velocity u_x/u_0 - Re graphs are presented below. Pole 2 and 6 have the lowest relative difference from average value - below 1 %, the rest of the poles reach up to 20 %.

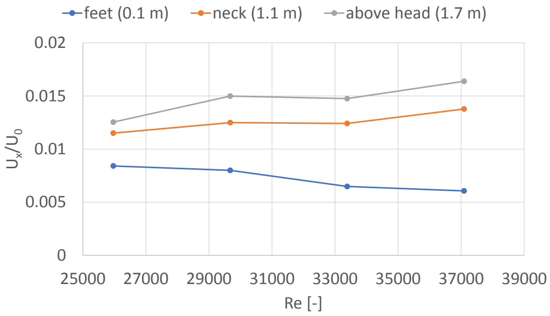

Figure I.1. Pole 1

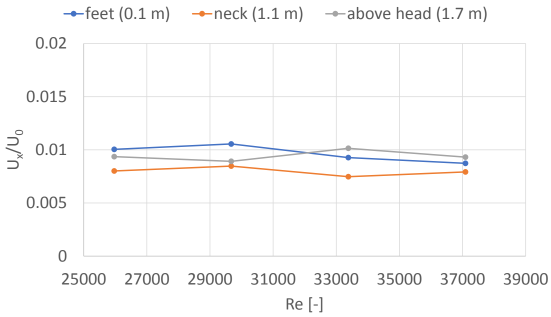

Figure I.2. Pole 2

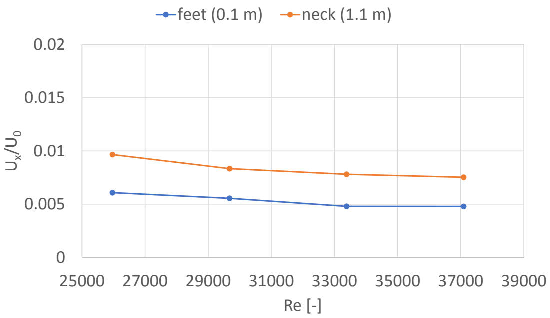

Figure I.3. Pole 3

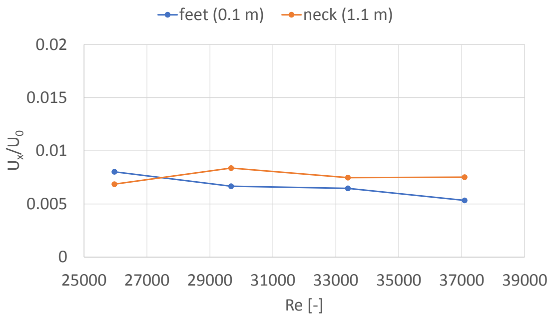

Figure I.4. Pole 4

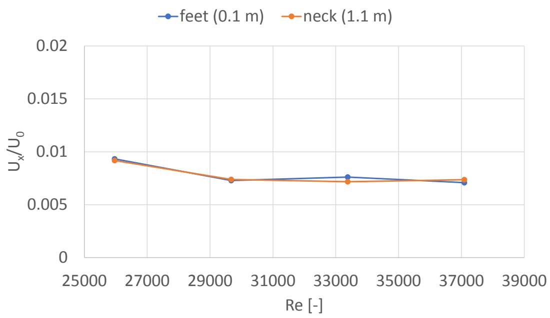

Figure I.5. Pole 5

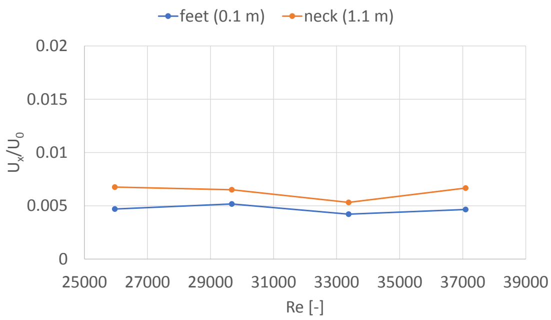

Figure I.6. Pole 6

I.2.2 Re independency - mixed airflow rate

Q_1 is varied from 14 l/s to 20 l/s. However, i this approach mixed air flow rate, Q_3, including secondary air flow rate is used to calculate velocity u_0. Q_3 varies from 66 l/s to 96 l/s.

The dimensionless velocity u_x/u_0 - Re graphs are presented below. Pole 2 and 6 have the lowest relative difference from average value - below 4 %, the rest of the poles reach up to 7 %.

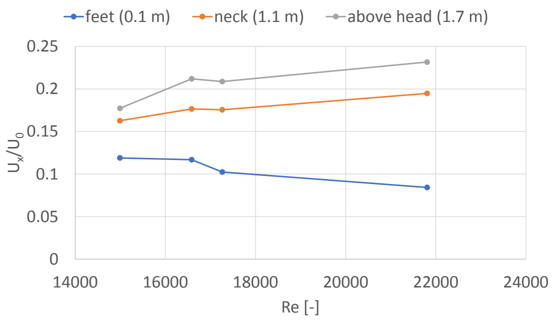

Figure I.7. Pole 1

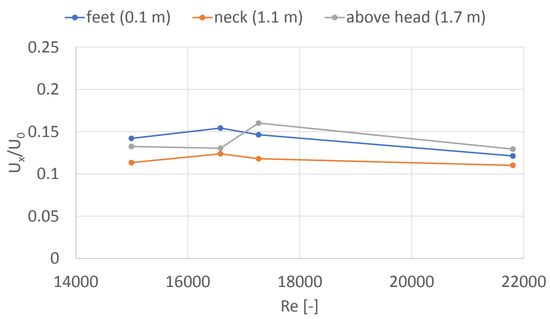

Figure I.8. Pole 2

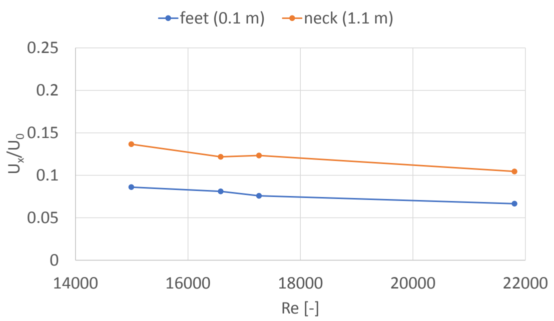

Figure I.9. Pole 3

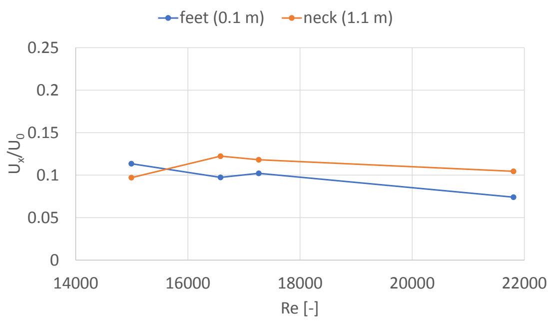

Figure I.10. Pole 4

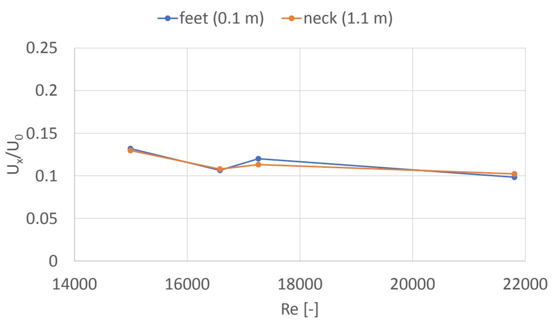

Figure I.11. Pole 5

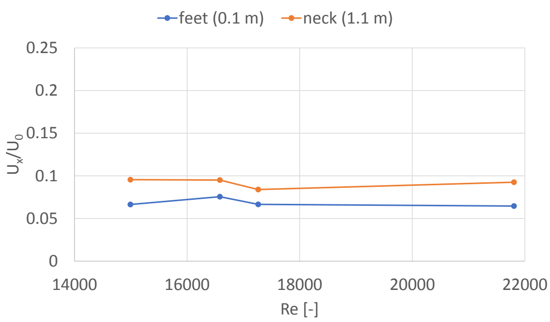

Figure I.12. Pole 6